

## Abstract

Lithium ion batteries have dominated the portable electronics market and have the potential to dominate large-scale battery applications including hybrid and electric vehicles, as well as grid storage, because of their high energy and power densities<sup>1,2</sup>. It is well known that conventional electrolytes show poor anodic stabilities above 4.5 V versus Li/Li<sup>+</sup>.<sup>3</sup> As a result, high voltage electrolytes are essential for the development of next generation high energy lithium ion batteries. Both fluorinated electrolytes and additives can be introduced into the electrolyte system.<sup>4</sup> In this work, fluorinated electrolytes were used in both graphite-LiNi<sub>0.5</sub>Co<sub>0.2</sub>Mn<sub>0.3</sub>O<sub>2</sub> (NCM523) (operated between 3.0 - 4.6 V) and graphite- LiNi<sub>0.5</sub>Mn<sub>1.5</sub>O<sub>4</sub> (LNMO) (operated between 3.5 - 4.9 V) full cell systems. The baseline electrolyte for all cells (referred to as Gen2) was composed of 1.2M LiPF<sub>6</sub> dissolved in a mixture of EC and EMC (3:7 in weight ratio). After a series of electrochemical tests, compared to the baseline electrolyte, the fluorinated electrolytes displayed significantly enhanced performance under both high cut off voltage and high temperature (55 °C). The post test analysis results showed that the cycled electrode can not only reach a much more stable interface but also overcome the crystal structure change after long term cycling when the fluorinated electrolyte system was used. In addition to changing the solvent, a series of additives were designed, synthesized and evaluated for high-voltage Li-ion battery cells using a Ni-rich layered cathode materials LiNi<sub>0.5</sub>Co<sub>0.2</sub>Mn<sub>0.3</sub>O<sub>2</sub> (NCM523). The repeated charge/discharge cycling for NCM523/graphite full cells using Gen2 with 1 wt % of these additives as electrolytes was performed. Electrochemical performance testing and post analysis result demonstrated that our as selected or designed cathode additives could passivate the cathode and prevent the cathode from side reactions. The developed methodology could provide

fundamental direction in the design and investigation of better electrolytes for the next generation lithium ion batteries

## Acknowledgement

I would like to express my sincere gratitude to my advisor Professor Yan Wang in WPI for always guiding, supporting and encouraging me into the field of battery research. He has offered me invaluable opportunities to pursue my research interest and conduct intriguing projects. I also want to thank Dr. Zhengcheng Zhang, my co-advisor from Argonne National Laboratory, for his sharing of in-depth knowledge about electrolyte. His unlimited knowledge and sharp insight in organic chemistry and electrochemistry was a constant inspiration and motivating factor in my research. Nothing could be accomplished without his guidance in these three years at Argonne National Laboratory.

I also want to thank Professor Richard D. Sisson Jr, Professor Jianyu Liang and Professor Chrysanthe Demetry for not only being my committee members, but also providing excellent suggestions and teaching me valuable knowledge of thermodynamic, crystallographic, physic chemistry and material science. I would like to thank Rita Shilansky, our department secretary, for her kindly help all the way.

In Argonne, I would like to acknowledge Dr. Libo Hu for his sharing of in-depth knowledge about the electrolyte and Dr. Chicheung Su for his intensive support with the NMR, GC-MS and organic synthesis experiments. I am very grateful to Dr. Cameron Peebles for sharing me with his ample knowledge of organic chemistry. I also want to thank Dr. Adam Tornheim for his help with the electrochemical measurement and our division secretary Brittany Spears. Many thanks to my talented and supportive lab members when I were in WPI, especially Dr. Qina Sa, Dr. Eric Gratz, Ms. Ruolin Zhou and Mr. Jin Liu who have been helping me out when I was experiencing

difficulties in graduate school study. It is so fortunate for me to work in both Professor Yan Wang and Dr. Zhengcheng Zhang's group.

This research is supported by the U.S. Department of Energy, Vehicle Technologies Office. I would like to thank the Cell Analysis, Modeling, and Prototyping (CAMP) Facility of Argonne's Chemical Sciences and Engineering Division for providing the electrode materials.

Finally, I am very indebted to all of my family members for their understanding, support, and encouragement all these years.

## Table of Contents

Abstract-----	I
Acknowledgement -----	III
Table of Contents-----	V
Executive Summary-----	1
Chapter 1. Introduction-----	5
Chapter 2. Probing voltage stability of electrolytes with floating test-----	26
Chapter 3. Systematically study of fluorinated cyclic carbonates as the SEI former-----	46
Chapter 4. Mechanistic Study of Fluorinated Electrolytes for High Voltage $\text{LiNi}_{0.5}\text{Co}_{0.2}\text{Mn}_{0.3}\text{O}_2$ Cathode of Lithium ion Batteries-----	84
Chapter 5. Mechanistic Insight in the Function of Phosphite Additives for Protection of $\text{LiNi}_{0.5}\text{Co}_{0.2}\text{Mn}_{0.3}\text{O}_2$ Cathode in High Voltage Li-ion Cells-----	118
Chapter 6. Design and Synthesis of Novel Phosphates Additives for High Voltage Lithium-ion Battery -----	150
Chapter 7. Conclusion and Future Work-----	175
Appendices-----	179

## Executive Summary

In Phase I, we reported a method using constant potential electrolysis with a slightly overcharged LNMO cathode as the working electrode, abbreviated as an “electrochemical floating test”, where the cell potential is allowed to “float” (or held) at different values to evaluate the stability of the electrolyte. Firstly, different fluorinated cyclic carbonate, asymmetric fluorinated linear carbonate and symmetric fluorinated linear carbonates were designed and synthesized by wet chemical process. The new electrolyte was made by dissolving  $\text{LiPF}_6$  salt into the as prepared cyclic carbonate and linear carbonate. For an ideal electrolyte with no impurities and no oxidation at the working electrode, the only current observed when a potential is applied is the capacitance current, which should decline to zero when the equilibrium is reached. The effects of cyclic carbonate and linear carbonate on the stability of the electrolyte under room temperature and high temperature (55 °C) was investigated.

In Phase II, fluorinated cyclic carbonates with different substituents including fluoroethylene carbonate (FEC), difluoroethylene carbonate (DFEC), trifluoropropylene carbonate (TFPC), 4-((2,2,3,3-tetrafluoropropoxy)methyl)-1,3-dioxolan-2-one (TFP-PC-E) and 4-(2,2,3,3,4,4,5,5,5-nonafluoropentyl)-1,3-dioxolan-2-one (NFPEC) were synthesized and evaluated. The graphite/ $\text{LiNi}_{0.5}\text{Co}_{0.2}\text{Mn}_{0.3}\text{O}_2$  full cell performance using various fluorinated cyclic carbonates with fixed linear fluorinated carbonate as electrolyte components was evaluated. A conductivity cell was designed to test the conductivity of the electrolytes with different cyclic carbonates under the temperature range from 10 °C to 60 °C. Additionally, the oxidation stability was tested using a 3 electrode Swagelok cell with a Pt working electrode. The effects of the substituent

groups were also investigated by probing their performance in graphite/NCM523 full cell chemistry.

In Phase III, The capacity fading mechanism in different electrolyte system was studied. A novel fluorinated electrolyte containing 1.0 M  $\text{LiPF}_6$  dissolved in a mixture of FEC and HFDEC solvent with 1wt % LiDFOB as the additive was utilized in a graphite- $\text{LiNi}_{0.5}\text{Co}_{0.2}\text{Mn}_{0.3}\text{O}_2$  full cell, which was operated between 3.0 - 4.6 V. Compared with the conventional EC and EMC based electrolyte, fluorinated electrolytes showed excellent cycling performance under a 4.6V cut off voltage. Synchrotron X-Ray Diffraction (SXRD) and X-ray absorption near edge structure (XANES) were conducted to investigate and compare the cycled bulk cathode electrode in different electrolytes. It was found that the cathode cycled in the fluorinated electrolyte can maintain the crystal structure of NCM523 better than the baseline electrolyte. Furthermore, the transition metal can be charged to a higher valence state under high cutoff voltage when fluorinated electrolytes were employed.

In Phase IV, the effects of triethylphosphite (TEP) and Tris(2,2,2-trifluoroethyl) phosphite (TTFP) as electrolyte additives in a  $\text{LiPF}_6$ -ethylene carbonate (EC)-ethyl methyl carbonate (EMC) electrolyte were evaluated. Compared to the baseline electrolyte, both TEP and TTFP showed a lower oxidation potential and as a result, a decomposition layer on the surface of the cathode should be formed. However, only the cell with TTFP demonstrated an improvement in both the capacity retention and Coulombic efficiency. Therefore, our tests showed that TEP is not an effective electrolyte additive for use in this cell chemistry. However, fluorination of the

ethyl groups (yielded TTFP) of the additive leads to the enhancement of the electrochemical stability and significant improvement of the cycling performance of NCM523-graphite cells.

In Phase V, taken together the advantages of different additives tested before, fluorinated cyclic phosphates were introduced as novel additives for high voltage Li-ion battery using graphite/LiNi<sub>0.5</sub>Co<sub>0.2</sub>Mn<sub>0.3</sub>O<sub>2</sub> (NCM523) cell. Cyclic fluorinated phosphates with various chemical structures were designed, synthesized and characterized by NMR. Full cells (graphite/NCM523) using the state-of-the-art electrolyte with 1 wt% phosphate additive added demonstrated significant improvement in the cycling performance compared to the cell without additive. Based on results from comprehensive electrochemical testing, theoretical calculations and post test analysis, we were able to identify the benefits of using fluorinated electrolytes and new additives in LIBs. For the first part, a series of fluorinated cyclic and linear carbonates were designed, synthesized and evaluated. Most of the fluorinated carbonates exhibit higher anodic stability than the traditional carbonates, such as ethylene Carbonate (EC), ethyl methyl carbonate (EMC) or dimethyl carbonate (DMC). Two of the formulated fluorinated carbonate based electrolytes showed better electrochemical performance and thermostability than the conventional EC/EMC based electrolyte. Based on the post test analysis and simulation results, different capacity fading mechanisms exist between the baseline electrolyte and the fluorinated electrolyte. Our results show that for cells cycled in the baseline electrolyte the capacity fading comes from: i) transition metal (TM) dissolution from the cathode and TM plating on the anode, ii) the phase change of NCM523 on the cathode surface, iii) the impedance arisen from the anode, iv) electrolyte decomposition reaction, and v) the losing of active lithium from the cathode. On

the other hand, capacity fading of the cell cycled in the fluorinated electrolyte comes from i) the active lithium lose from the cathode materials and ii) the impedance arisen from the cathode.

Also, the effect of additives for conventional electrolyte was also studied in this work. Initially we compared the effectiveness of TEP and TTFP as cathode electrolyte additive in a  $\text{LiNi}_{0.5}\text{Co}_{0.2}\text{Mn}_{0.3}\text{O}_2$ -graphite 4.6V system. Our results showed that the additive with fluorinated groups can passivate the cathode surface and reduce parasitic, unwanted surface side reactions. Moreover, with the understanding of the relationship between the structural factors and electrochemical performance of various additives, we designed and synthesized a new cathode additive for HEHV battery system, 2-(2,2,2-trifluoroethoxy)-1,3,2-dioxaphospholane 2-oxide (TFPOP), which combines the advantages of fluorinated alkyl group, five member ring and phosphate. The new additive exhibits significant improvement on the HEHV battery.

## Chapter 1 Introduction

### 1.1 Li-ion batteries technologies

Li-ion batteries technology has become increasingly important in recent years<sup>1, 14-17</sup>. Lithium is both one of the most electropositive elements and one of the highest electrochemically active metals ( $-3.04$  V versus standard hydrogen electrode). These traits enable Li-ion batteries to have higher energy density than other types of rechargeable batteries. Despite their extensive use, there is still continued commercial interest in developing next generation Li-ion batteries that would lead to remarkably higher energy density and longer cycle life. The ultimate goal is to enable the wide adoption of hybrid and electric vehicles and decrease the dependence of mass transportation on non-sustainable fossil fuels. Figure 1.1a<sup>6</sup> summarizes the design and operation of various EVs. There are several levels at which EVs can be operated, categorized by the depth of pure electrical propulsion and hence, the size of the battery pack that should be used. Figure 1.1b<sup>6</sup> tabulates three main options for EV operation, indicating the appropriate numbers: total battery capacity needed, energy density available, battery weight, driving distance between charges and average speed.

a						
Modes of operation		battery capacity needed, kWh	Energy density, Wh/kg	Weight of battery, Kg	Speed, kilometres per hour	Distance on one charge, kilometres
	Hybrid	<3	40-50 (Ni-MH)	60 (Ni-MH)	100+	15
	Plug in Hybrid	5.6-18	90-100 (Li-ion)	60-200 (Li-ion)	100+	10-60
	Full EV	35-54	90-100 (Li-ion)	450 (Li-ion)	>100	150-200

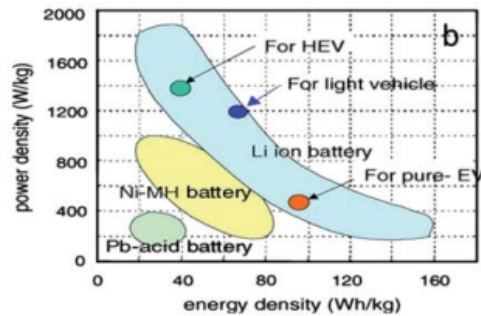


Figure. 1.1 (a) Characterization of the main three kinds of EVs: light EV (hybrid), PHEV and full EV, in terms of performance and battery properties. (b) Ragone plot.

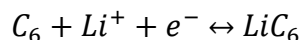
### 1.1.1 Li-ion battery components

There are four key components in a lithium-ion batteries system: cathode, anode, electrolyte and separator.

#### i) Anode:

Due to the dendrite issue of using lithium as a pure metal anode, the primary choice of anode material for lithium-ion batteries is graphite because of its reasonable specific capacity (374mAh/g), long cycle life, abundant materials supply and relatively low cost. Graphite

intercalates reversibly with lithium to form  $\text{LiC}_6$  as the final product according to the following reaction (Eq 1)



The intercalation of lithium into graphite occurs in stages such as  $\text{LiC}_{24}$ ,  $\text{LiC}_{27}$  and  $\text{LiC}_{12}$  via first-order phase transition reactions between the various stages.

Despite its extensive application, the traditional carbon-based anode materials, such as graphite<sup>18</sup>, graphene<sup>19</sup>, and carbon nanotubes<sup>20</sup>, cannot meet the demand for high capacity and energy. Meanwhile, there are a lot of researchers working on the alloy type anodes such as Si, Sn and Se due to their high specific capacity and enhanced safety.<sup>21-24</sup> For example, Si can alloy with Li and form  $\text{Li}_{4.4}\text{Si}$ , which can reach a theoretical capacity as high as  $4200 \text{ mAh/g}^{25}$ , and this is more than ten times higher than that of commercial graphite anodes. However, the short cycle life of the Si electrode prevents it from being widely used.<sup>26</sup> Two main reasons have been widely accepted to explain the short cycle life. First, when the lithium ions diffuse into the Si anode, the volume of the anode will expand to almost 300%–400% of its initial size. Since the morphology of Si plays an important role in determining its capacity and cyclability, such a huge volume change causes significant capacity loss. Moreover, lithium ion intercalation/deintercalation causes tremendous stress in the Si lattice and thus leads to cracking and crumbling of the Si particles. Second, the cycling performance of the Si electrode can also be influenced by the interfacial property that originate from the formation of a solid electrolyte interphase (SEI) layer which would have a negative effect on the specific capacity because of Li ion consuming<sup>27-28</sup>. The SEI layer becomes thicker and thicker during cycling, leading to a decreased capacity and low Coulombic efficiency.

## ii) Cathode

The cathode (positive electrode) is the major factor that determines the energy density and cost of Li-ion batteries<sup>13, 29</sup>. One of the most common commercialized cathode materials is lithium cobalt oxide  $\text{LiCoO}_2$ . The structure of layered compound  $\text{LiMO}_2$  (M indicate transition metal) is shown in Figure 1.2<sup>30</sup>. In this structure, the oxygen anions have a close-packed arrangement in ABCABC stacking sequence. The oxygen anions, which form a close-packed FCC lattice with cations located in the 6 coordinated octahedral crystal site. The slabs and Li layer are stacked alternatively. And then the lithium ions can be diffused in a two-dimensional plane. Goodenough first recognized that  $\text{LiCoO}_2$  had a structure similar to the layered structures of the dichalcogenides and showed that the lithium could be removed electrochemically, thus making it a viable cathode material<sup>31</sup>. The first commercialized lithium ion battery cathode is  $\text{LiCoO}_2$  from SONY Company<sup>32</sup>. SONY combined the  $\text{LiCoO}_2$  cathode with a carbon anode to make the first successful Li-ion battery, which now dominates the lithium battery market. The layered structure cathode material can reach a comparable high capacity when charged to a high voltage. However, there is a limited availability of cobalt, which causes it to have a high price. This price limits its use to small cells, such as those used in computers, cell phones, and cameras. Not only is this material very expensive, but it suffers from limited practical capacity ( $< 140\text{mAh/g}^{-1}$ ), poor thermostability and bad rate performance<sup>33</sup>. An alternative cathode will be needed for large-scale applications, as envisioned in HEV or for load leveling.

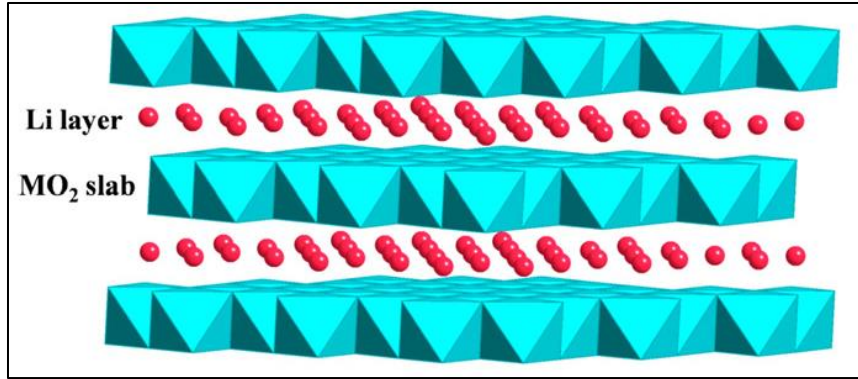


Figure 1.2. Crystal structure of LiCoO<sub>2</sub>

Consequently, intensive works on new cathode materials for Li-ion batteries have been carried out recently (as shown in Table 1). In 1997, a new cathode revolution comes with the discovery of the electrochemical properties of the olivine phase, in particular LiFePO<sub>4</sub>, by Padhi et al<sup>34</sup>. This is the first cathode material with potentially low cost and plentiful elements and also environmentally benign that could have a major impact in electrochemical energy storage. The structure of LiFePO<sub>4</sub> is shown in Figure 1.3<sup>35</sup>. It contains slightly distorted hcp anion oxygen arrays with half of the octahedral sites occupied by Fe and one eighth by Li. The LiO<sub>6</sub> octahedra are edge-shared while the FeO<sub>6</sub> octahedra are corner-shared<sup>35</sup>. However, this material has a low conductivity at room temperature. It could only reach its theoretical capacity under low rate due to the low lithium diffusion at the interface.<sup>22</sup> Even the modification on the surface may improve this issue, such as a conductive carbon coating<sup>23</sup>, it will increase the cost of that cathode material a lot.

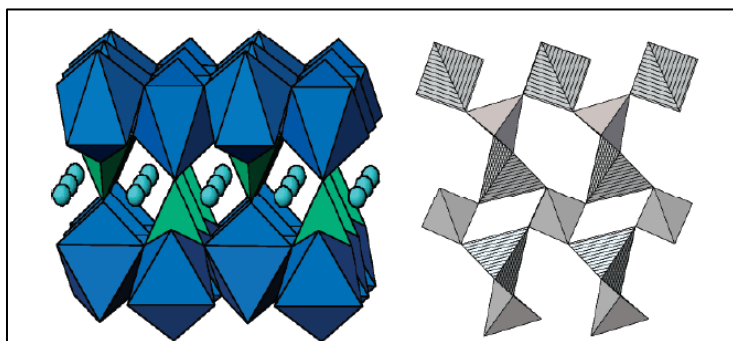


Figure 1.3. Structures of orthorhombic  $\text{LiFePO}_4$  and trigonal quartz-like  $\text{FePO}_4$ .

The first spinel structure cathode material,  $\text{LiMn}_2\text{O}_4$  was proposed by Thackeray et al. in 1983<sup>31</sup> shown in Figure 1.4a, even this material can be charged to a comparable high voltage without safety issue, however, it still have the capacity fading problem due to the transition metal dissolution and phase transformation. After that, multiple efforts have been made to improve it. Doping a new element tend to be one of the most effective ways to resolve this problem. Multiple dopants including inactive ions such as Mg, Al, and Zn, first row transition metal ions such as Ti, Cr, Fe, Co, Ni, and Cu and rare earth metal ions such as Nd and La have been investigated<sup>30</sup>. And  $\text{LiNi}_{0.5}\text{Mn}_{1.5}\text{O}_4$ , Figure 1.4b<sup>16</sup>, shows the best overall electrochemical performances among the above.

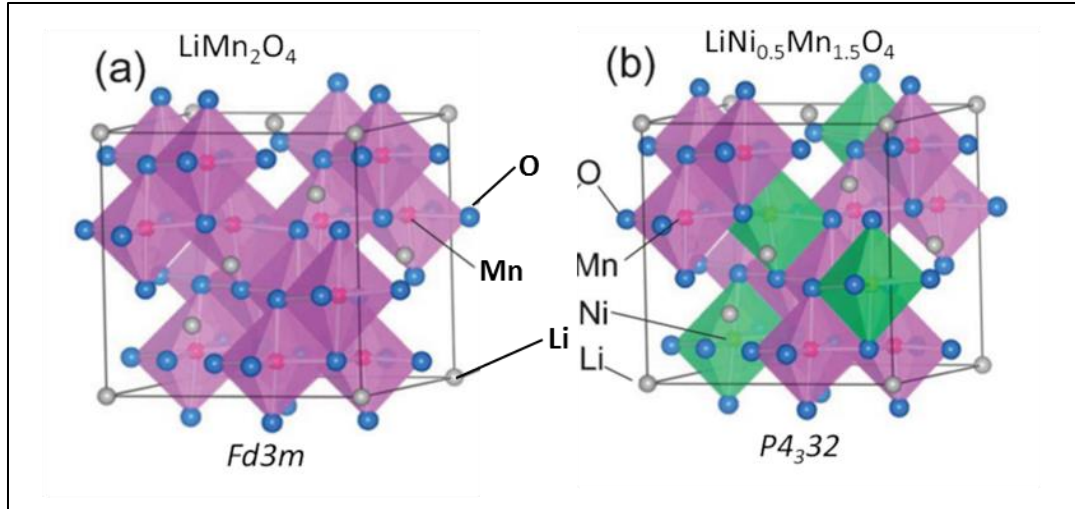


Figure 1.4. Crystal structure of (a)LMO (b)LNMO spinel cathode with lithium insertion.

In the year of 2000, the first lithium nickel manganese cobalt oxide,  $\text{LiNi}_{1/3}\text{Co}_{1/3}\text{Mn}_{1/3}\text{O}_2$  (NCM333), was synthesized by Ohzuku's group<sup>36</sup>. After that, extensive research on the development and improvement of new Ni-rich layered  $\text{LiNi}_x\text{Co}_y\text{Mn}_z\text{O}_2$  materials has been conducted.<sup>36-45</sup>  $\text{LiNi}_x\text{Co}_y\text{Mn}_{(1-x-y)}\text{O}_2$  (NCM) materials have been selected as one of the primary battery materials for commercial applications such as EV, laptops and mobile phones. One of the most promising advantages of NCM cathode materials is its high practical capacity under high cutoff voltages. The most promising part of this cathode material is we can adjust the ratio of different transition metal to reach different requirements. For example, a high Ni concentration will donate a high specific capacity and a high Co will leads to better high voltage stability due to a compact crystal structure, moreover, a high Mn will give a better thermostability. For example, for the NCM523 material, a specific capacity of 220mAh/g can be reached when it is charged up to 4.7 V

Vs  $\text{Li}/\text{Li}^+$ . This is almost twice that of some other conventional cathode materials such as  $\text{LiFePO}_4$  (LFP),  $\text{LiMnO}_2$  (LMO) and  $\text{LiNi}_{0.5}\text{Mn}_{1.5}\text{O}_4$  (LNMO) as shown in Table 1.

Table1 Summary of SOA cathode material

Material	Group space	Specific Capacity(mAh/g)	Midpoint V vs. Li at C/20	Pros	Cons
$\text{LiCoO}_2$	$R\bar{3}m$	155	3.9	Most common cathode	Co is expensive and toxic, low thermo stability
$\text{LiNi}_{1-x-y}\text{Co}_y\text{Mn}_x\text{O}_2$ (NCM)	$R\bar{3}m$	140-180	3.8	Capacity depends on upper voltage cutoff, safer and low cost	Transition metal dissolution and plating issue
$\text{LiNi}_{0.8}\text{Co}_{0.15}\text{Al}_{x0.05}\text{O}_2$ (NCA)	$C\bar{2}m$	200	3.73	Safer and less expensive. high capacity	Transition metal dissolution, Surface Oxygen loss
$\text{LiMn}_2\text{O}_4$ (Spinel)	$Fd\bar{3}m$	100-120	4.05	Safer and less expensive than LCO	Poor high temperature stability
$\text{LiFePO}_4$ (LFP)	$Pmnb$	160	3.45	Very safe	Low volumetric energy, poor rate performance
$\text{Li}[\text{Li}_{1/9}\text{Ni}_{1/3}\text{Mn}_{5/9}]\text{O}_2$	$R\bar{3}m$	275	3.8	High specific capacity	Low rate capacity and 1 <sup>st</sup> Coulombic efficiency
$\text{LiNi}_{0.5}\text{Mn}_{1.5}\text{O}_2$	$P4_332$	130	4.6	Up to 5V high cutoff voltage	Requires an electrolyte that is stable ate high voltage

### iii) Separator

A conventional lithium-ion battery separator is made of polymers including polypropylene (PP), polyethylene (PE), *etc.*, because of their desirable mechanical strength and electrochemical stability<sup>16</sup>. Due to their nonpolar property, polymer separators suffer from poor wettability. Additionally, the low melting point and glass transition temperature of those polymers may result

in thermal shrinkage.<sup>46</sup> It is well-known that both shrinking and melting of the separator in a lithium-ion battery would lead to physical contact between the electrodes causing a short circuit. This would not only result in the failure of the cell but also generate heat and cause serious safety problems. Therefore, many researches are underway to explore separators with high thermal-resistance and good wettability<sup>16, 46</sup>. One possible solution is to develop an inorganic particle based separator, in which a fine porous structure is combined with ultrafine inorganic particles, such as Al<sub>2</sub>O<sub>3</sub>, SiO<sub>2</sub>, and MgO.<sup>47-49</sup> Inorganic particle based separators have good wettability and very high surface area due to the fine ceramic particles as well as good high temperature performance. However, they are very brittle and can easily crack during cell winding and assembling. The cracks will lead to a direct contact between the anode and cathode and thus, the failure of the cell. To solve the problems associated with inorganic particle based separators, composite separators combining ceramic particles and polymers, which are more flexible and stronger, are being developed. For example, Lee *et al.* developed an Al<sub>2</sub>O<sub>3</sub> coated polyimide nanofiber separator<sup>50</sup>; Wang *et al.* synthesized a porous Al<sub>2</sub>O<sub>3</sub> particle-PVDF composite separator to solve the brittle problem<sup>51</sup>; Shinet *et al.* use polyethylene to improve the performance of the ceramic particle based separator<sup>51</sup>; Degussa *et al.* developed a series of Separion (a trade name) separators by combining the characteristics of polymeric nonwoven and ceramic nanoparticles<sup>16</sup>.

#### **iv) Electrolyte**

The conventional lithium-ion battery employs organic carbonate esters as the electrolyte solvent, in particular, mixtures of ethylene carbonate (EC) with dimethyl carbonate (DMC), diethyl

carbonate (DEC), and/or ethyl methyl carbonate (EMC) are dissolved in  $\text{LiPF}_6$  salt (shown in Figure 1.5)<sup>2-3</sup>. However, this electrolyte continuously decomposes above 4.5 V vs.  $\text{Li}^+/\text{Li}$ , limiting its application to a cathode chemistry that delivers capacity at a high charging voltage. Therefore, the demand for a better electrolyte has become a high priority for the development of lithium-ion batteries with high energy density.

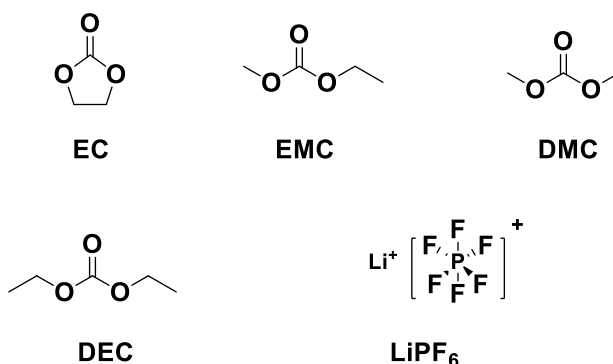


Figure 1.5. Chemical structure of the baseline carbonate EC, EMC, DMC, DEC and the  $\text{LiPF}_6$  salt.

An ideal electrolyte should have a higher lowest unoccupied molecular orbital (LUMO) energy level than that of the anode and a lower highest occupied molecular orbital (HOMO) energy level than that of the cathode side.<sup>9</sup> In other words, the electrolyte should be neither oxidized at the cathode nor reduced at the anode side during cycling as shown in Figure 1.6a. However, during cycling, the anode is stabilized around 0.1V vs  $\text{Li}^+/\text{Li}$ , as a result, the carbonate based electrolyte will be reduced continuously<sup>2-3</sup>. Thus, a solid electrolytes interphase (SEI) is needed to kinetically stabilize the anode and enable further cycling without continual solvent decomposition. The conventional electrolyte is well known in not only forming a stable SEI, but also remaining stable at upper cutoff voltages of the earlier generation cathode such as  $\text{LiCoO}_2$

(LCO) or  $\text{LiFePO}_4$  (LFP), which have an upper cutoff voltage below 4.0V vs  $\text{Li}^+/\text{Li}$  as shown in Figure 1.6b.<sup>10</sup> However, it cannot match the new generation high operation voltage cathode materials such as  $\text{LiNi}_{0.5}\text{Mn}_{1.5}\text{O}_4$  (LNMO) and  $\text{LiNi}_x\text{Co}_y\text{Mn}_{(1-x-y)}\text{O}_2$  (NCM) materials, which have a cutoff voltage up to 4.9V and 4.6V respectively<sup>11</sup>. As the result, new electrolyte designs are still needed to enable the new generation high energy and high voltage batteries. There are two design principles current being researched: i) create a new electrolyte system, which has a higher oxidation potential than the traditional carbonate based electrolyte, and as shown in Figure 1.6d ii) introduce additive/additives into the conventional electrolyte as shown in Figure 1.6c. The former principle utilizes the introduction of fluorine (F) and/or fluorinated alkyl groups ( $\text{R}_f$ ) to organic solvents including cyclic and linear carbonates, sulfones, cyclic and linear esters, and ethers to increase the voltage stability of electrolyte due to the high electronegativity of F species. The latter principle uses additives that can form a protective layer on the electrode and protect the cathode material from dissolution and overcharge<sup>12</sup>. However, although adding additive is cheaper and can passivate the electrode surface furthermore, protect the electrolyte from side reactions, it still cannot change the properties of the entire electrolyte, such as the HOMO and LUMO energy level or flammability and flash point. As a result, the fluorinated electrolyte is still essential.

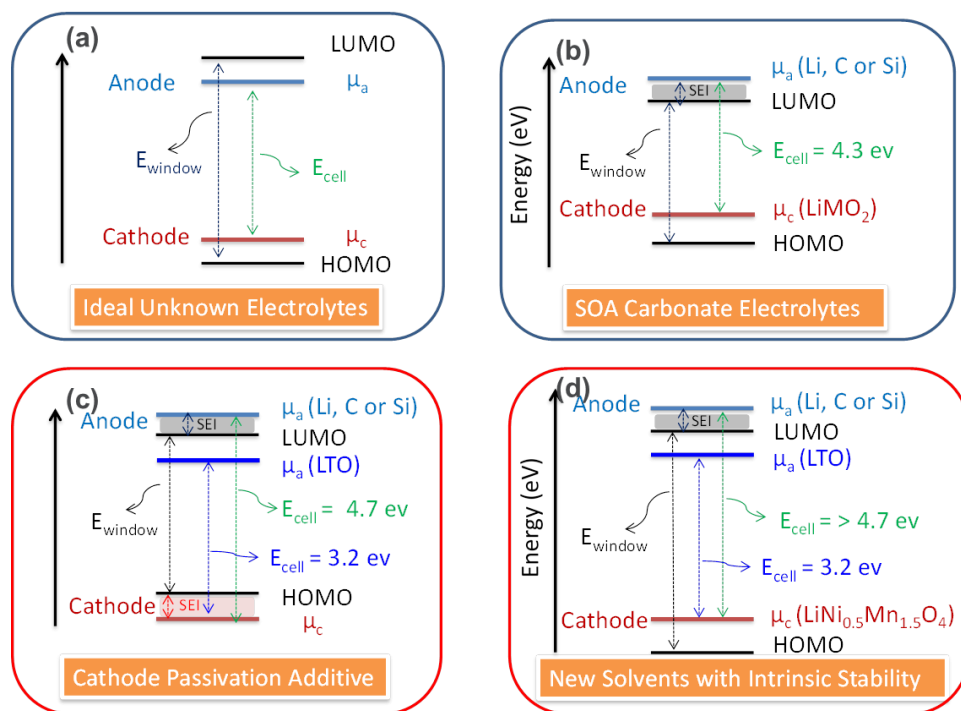


Figure 1.6 HOMO and LUMO energy level schematic diagram of (a). ideal electrolyte system, (b). SOA carbonate electrolyte (c) electrolyte with additive (d) fluorinated electrolyte with intrinsic stability

Several studies have been dedicated to the development of high voltage electrolytes such as sulfones,<sup>52-53</sup> ionic liquids<sup>54</sup>, and dinitriles<sup>55</sup>, as well as electrolyte additives<sup>12</sup> that stabilize the charged cathode surface to afford a reversible  $\text{Li}^+$  intercalation chemistry in the coveted 5-V region. These electrolyte materials can provide high anodic stability, but they suffer from their intrinsic high viscosity, low dielectric constant, and low conductivity. More importantly, they do not form a solid-electrolyte interphase (SEI) on carbonaceous anode material. Therefore, it continues to be a major challenge to develop an electrolyte additive for these new electrolytes

that will provide the SEI formation required for extended cycling performance, especially under heavily abusive conditions.

Due to their high conductivity, excellent solubility with lithium salts, and ability to form a stable SEI, carbonates are still an excellent choice as the solvent for electrolyte systems. However, traditional carbonates like EC and EMC have a low potential limit, which makes them unstable in high voltage cells. As a result, focus has shifted to fluorinated carbonates which are expected to have higher oxidation potentials according to density functional theory (DFT) calculations<sup>56</sup>.

### **1.1.2 Li-ion battery working principle**

For today's commercialized lithium-ion battery system, both cathode and anode materials are intercalation materials. The transition metal oxides in the cathode, and the graphite in anode, constitute a large unchangeable host with specific sites for lithium ion intercalation. All lithium ions are in the cathode side initially (therefore a 0% SOC) and the battery system is assembled in 'discharged' status.

While charging, lithium ions are extracted from the cathode host, moved through the non-aqueous electrolyte and intercalated into the anode host. Meanwhile, electrons move from the cathode to the anode through the outside current collectors forming an electric circuit as shown in Figure 1.7<sup>13</sup>.

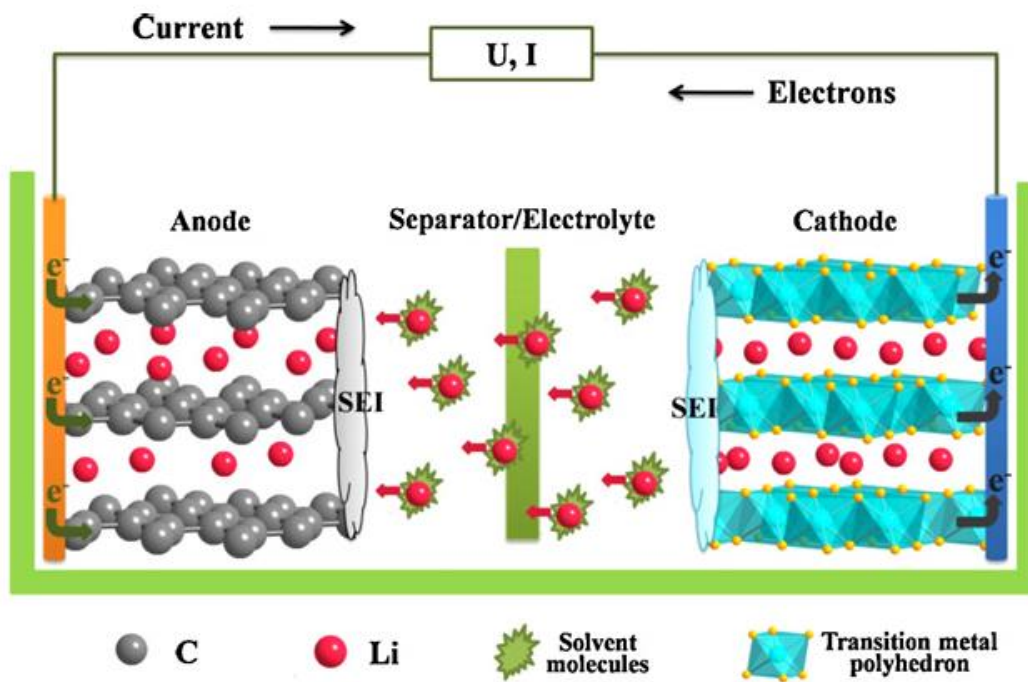


Figure 1.7. Working principle of SOA Li-ion battery

## 1.2 New electrolyte design for HEHV Li ion batteries

To accommodate these next-generation electrode materials, massive research efforts have been devoted into two separate directions of electrolyte development<sup>2-3</sup>. The first direction is to develop additives that passivate the electrode surface so that the well-established conventional electrolyte can still be used in the novel systems. In this case, additives are not only targeting the anode surface, but also the cathode surface because of the high working potential of the high energy cathode materials. For example, Lee *et al.*<sup>57</sup> reported that the addition of 5 wt% methyl(2,2,2-trifluoroethyl) carbonate to the conventional carbonate electrolyte can significantly improve cycling performance. Dahn and co-workers<sup>58</sup> and others<sup>4, 59</sup> revealed the improved oxidation stability of the conventional electrolyte when tris(trimethylsilyl)phosphate and/or

tris(trimethylsilyl) phosphite were used as electrolyte additives in NCM333/graphite cell operated at 4.2 V cutoff voltage at 40°C. Zuo *et al.*<sup>60</sup> presented that the addition of 1 wt% LiBF<sub>4</sub> enhanced cycling performance for LiNi<sub>0.5</sub>Co<sub>0.2</sub>Mn<sub>0.3</sub>O<sub>2</sub>/graphite cell at 4.5 V. Xu *et al.*<sup>61</sup> reported that the lithium borate can be used as an additive to modify the surface of LiNi<sub>0.5</sub>Mn<sub>1.5</sub>O<sub>4</sub> for better capacity retention. Wang *et al.*<sup>62</sup> reported triethylborate as an electrolyte additive for high voltage NCM cathode and the capacity retention improved both at 25 °C and 55 °C. Other cathode additives were also reported by Chen *et al.*,<sup>63</sup> Mai *et al.*,<sup>64</sup> and Chen *et al.*<sup>65</sup>

The second direction is to completely abandon conventional electrolyte and develop a totally new electrolyte system that utilize novel salts, new carbonate solvents or non-carbonate solvents and the corresponding additives. Of the novel solvents, fluorinated organic solvents are of wide interest due to possible application in high voltage<sup>40,66</sup>, high capacity<sup>6</sup>, low temperature lithium-ion batteries. Based on theoretical calculations, fluorinated organic solvents generally have higher oxidation and reduction potentials than their non-fluorinated versions. In most cases, fluorinated carbonates show 0.2 V to 1.0 V increases in oxidation potential and 0.2 to 0.4 V increases in reduction potential compared with non-fluorinated carbonates. The increase in redox potential has several types of effect in electrolyte formulated with fluorinated solvents. First of all, the overall voltage stability on the positive electrode is expected to increase considerably with fluorinated solvents. Second, due to the increased reduction potential, fluorinated electrolyte formulations may need additives that decompose at even higher reduction potentials to form an effective SEI. Lastly, fluorinated solvent that are capable of forming SEI alone may be used as additives in conventional electrolyte formulations due to their high reduction potential.

Based on such calculations, fluorinated solvents, especially carbonates are suitable candidates for Li-ion batteries electrolyte solvents that require high working potential. Indeed, testing of fluorinated electrolyte in high voltage Li-ion batteries has taken place widely in both academia and industry.

### **1.3 Research Objective and Technic Targets**

#### **1.3.1 Project objectives**

- i). To develop a new advanced electrolyte system with outstanding stability at high voltage and high temperature. It should also demonstrate improved safety characteristics consisting of a high voltage  $\text{LiNi}_{0.5}\text{Mn}_{1.5}\text{O}_4$  (LNMO) or  $\text{LiNi}_{0.5}\text{Co}_{0.2}\text{Mn}_{0.3}\text{O}_2$  (NCM523) cathode and graphite anode.
- ii). To systematically study different fluorinated electrolyte additives and Co-solvents by various electrochemical method. We envisioned this by figuring out the effect of the substitution group on the performance of electrolyte, and then by introducing this new electrolyte in next generation Li-ion batteries.
- iii). To gain a fundamental understanding of the interaction between electrolyte and electrode materials, the dependence of Solid Electrolyte Interface (SEI) functionality on electrolyte composition, and the effect of high temperature on full Li-ion cells using the advanced electrolyte system.

#### **1.3.2 Technical targets**

- i). Design and synthesize new fluorinated linear and cyclic carbonates.

- ii). Develop a screening method for oxidation stability of the synthesized F-solvents.
- iii). Develop the fluorinated electrolyte formulations that not only showed improved oxidation stability, but also stable cycling performance in LNMO/graphite or NCM523/graphite full cells.
- iv). Achieve stable charge/discharge cycling performance with the optimal electrolyte in full cells at both room and high temperature (55 °C).
- v). Performed the diagnosis analysis of the surface morphology and chemical composition of the cycled anode and cathode electrodes with fluorinated/baseline electrolyte by SEM/TEM, XPS, ICP-MS, FT-IR, XRD.
- vi). Fundamental understanding of the interaction between the electrolyte and the high voltage electrode.

## Reference

1. Lu, L.; Han, X.; Li, J.; Hua, J.; Ouyang, M., A Review on the Key Issues for Lithium-Ion Battery Management in Electric Vehicles. *Journal of power sources* **2013**, *226*, 272-288.
2. Xu, K., Nonaqueous Liquid Electrolytes for Lithium-Based Rechargeable Batteries. *Chemical reviews* **2004**, *104*, 4303-4418.
3. Xu, K., Electrolytes and Interphases in Li-Ion Batteries and Beyond. *Chemical reviews* **2014**, *114*, 11503-11618.
4. Mai, S.; Xu, M.; Liao, X.; Hu, J.; Lin, H.; Xing, L.; Liao, Y.; Li, X.; Li, W., Tris(Trimethylsilyl)Phosphite as Electrolyte Additive for High Voltage Layered Lithium Nickel Cobalt Manganese Oxide Cathode of Lithium Ion Battery. *Electrochim. Acta* **2014**, *147*, 565-571.
5. Goodenough, J. B.; Park, K.-S., The Li-Ion Rechargeable Battery: A Perspective. *Journal of the American Chemical Society* **2013**, *135*, 1167-1176.
6. Etacheri, V.; Marom, R.; Elazari, R.; Salitra, G.; Aurbach, D., Challenges in the Development of Advanced Li-Ion Batteries: A Review. *Energy & Environmental Science* **2011**, *4*, 3243-3262.
7. Xu, K.; Zhang, S.; Jow, T. R.; Xu, W.; Angell, C. A., Liobob as Salt for Lithium-Ion Batteries: A Possible Solution for High Temperature Operation. *Electrochemical and Solid-State Letters* **2002**, *5*, A26-A29.
8. Zhang, S.; Ding, M. S.; Xu, K.; Allen, J.; Jow, T. R., Understanding Solid Electrolyte Interface Film Formation on Graphite Electrodes. *Electrochemical and Solid-State Letters* **2001**, *4*, A206-A208.
9. Xu, K.; von Cresce, A., Interfacing Electrolytes with Electrodes in Li Ion Batteries. *Journal of Materials Chemistry* **2011**, *21*, 9849-9864.
10. Chikkannanavar, S. B.; Bernardi, D. M.; Liu, L., A Review of Blended Cathode Materials for Use in Li-Ion Batteries. *Journal of Power Sources* **2014**, *248*, 91-100.
11. Pelosato, R.; Cordaro, G.; Stucchi, D.; Cristiani, C.; Dotelli, G., Cobalt Based Layered Perovskites as Cathode Material for Intermediate Temperature Solid Oxide Fuel Cells: A Brief Review. *Journal of Power Sources* **2015**, *298*, 46-67.
12. Zhang, S. S., A Review on Electrolyte Additives for Lithium-Ion Batteries. *Journal of Power Sources* **2006**, *162*, 1379-1394.
13. Aurbach, D.; Markovsky, B.; Salitra, G.; Markevich, E.; Talyossef, Y.; Koltypin, M.; Nazar, L.; Ellis, B.; Kovacheva, D., Review on Electrode–Electrolyte Solution Interactions, Related to Cathode Materials for Li-Ion Batteries. *Journal of Power Sources* **2007**, *165*, 491-499.
14. Zhang, J.; Lee, J., A Review on Prognostics and Health Monitoring of Li-Ion Battery. *Journal of Power Sources* **2011**, *196*, 6007-6014.
15. Verma, P.; Maire, P.; Novák, P., A Review of the Features and Analyses of the Solid Electrolyte Interphase in Li-Ion Batteries. *Electrochimica Acta* **2010**, *55*, 6332-6341.
16. Zhang, S. S., A Review on the Separators of Liquid Electrolyte Li-Ion Batteries. *Journal of Power Sources* **2007**, *164*, 351-364.
17. Malini, R.; Uma, U.; Sheela, T.; Ganesan, M.; Renganathan, N., Conversion Reactions: A New Pathway to Realise Energy in Lithium-Ion Battery—Review. *Ionics* **2009**, *15*, 301-307.
18. Peled, E.; Menachem, C.; Bar-Tow, D.; Melman, A., Improved Graphite Anode for Lithium-Ion Batteries Chemically Bonded Solid Electrolyte Interface and Nanochannel Formation. *Journal of The Electrochemical Society* **1996**, *143*, L4-L7.

19. Wu, Z.-S.; Ren, W.; Xu, L.; Li, F.; Cheng, H.-M., Doped Graphene Sheets as Anode Materials with Superhigh Rate and Large Capacity for Lithium Ion Batteries. *ACS nano* **2011**, *5*, 5463-5471.
20. Wu, H.; Chan, G.; Choi, J. W.; Yao, Y.; McDowell, M. T.; Lee, S. W.; Jackson, A.; Yang, Y.; Hu, L.; Cui, Y., Stable Cycling of Double-Walled Silicon Nanotube Battery Anodes through Solid-Electrolyte Interphase Control. *Nature nanotechnology* **2012**, *7*, 310-315.
21. Liu, N.; Wu, H.; McDowell, M. T.; Yao, Y.; Wang, C.; Cui, Y., A Yolk-Shell Design for Stabilized and Scalable Li-Ion Battery Alloy Anodes. *Nano letters* **2012**, *12*, 3315-3321.
22. Mao, O.; Dunlap, R.; Dahn, J., Mechanically Alloyed Sn-Fe (-C) Powders as Anode Materials for Li-Ion Batteries: I. The Sn<sub>2</sub>Fe-C System. *Journal of The Electrochemical Society* **1999**, *146*, 405-413.
23. Wang, H.; Cui, L.-F.; Yang, Y.; Sanchez Casalongue, H.; Robinson, J. T.; Liang, Y.; Cui, Y.; Dai, H., Mn<sub>3</sub>O<sub>4</sub>- Graphene Hybrid as a High-Capacity Anode Material for Lithium Ion Batteries. *Journal of the American Chemical Society* **2010**, *132*, 13978-13980.
24. Cui, L.-F.; Yang, Y.; Hsu, C.-M.; Cui, Y., Carbon- Silicon Core- Shell Nanowires as High Capacity Electrode for Lithium Ion Batteries. *Nano letters* **2009**, *9*, 3370-3374.
25. Li, H.; Huang, X.; Chen, L.; Wu, Z.; Liang, Y., A High Capacity Nano Si Composite Anode Material for Lithium Rechargeable Batteries. *Electrochemical and Solid-State Letters* **1999**, *2*, 547-549.
26. Li, H.; Huang, X.; Chen, L.; Zhou, G.; Zhang, Z.; Yu, D.; Mo, Y. J.; Pei, N., The Crystal Structural Evolution of Nano-Si Anode Caused by Lithium Insertion and Extraction at Room Temperature. *Solid State Ionics* **2000**, *135*, 181-191.
27. Xin, X.; Zhou, X.; Wang, F.; Yao, X.; Xu, X.; Zhu, Y.; Liu, Z., A 3d Porous Architecture of Si/Graphene Nanocomposite as High-Performance Anode Materials for Li-Ion Batteries. *Journal of Materials Chemistry* **2012**, *22*, 7724-7730.
28. Sim, S.; Oh, P.; Park, S.; Cho, J., Critical Thickness of SiO<sub>2</sub> Coating Layer on Core@ Shell Bulk@ Nanowire Si Anode Materials for Li-Ion Batteries. *Advanced Materials* **2013**, *25*, 4498-4503.
29. Yi, T.-F.; Zhu, Y.-R.; Zhu, X.-D.; Shu, J.; Yue, C.-B.; Zhou, A.-N., A Review of Recent Developments in the Surface Modification of LiMn<sub>2</sub>O<sub>4</sub> as Cathode Material of Power Lithium-Ion Battery. *Ionics* **2009**, *15*, 779-784.
30. Xu, B.; Qian, D.; Wang, Z.; Meng, Y. S., Recent Progress in Cathode Materials Research for Advanced Lithium Ion Batteries. *Materials Science and Engineering: R: Reports* **2012**, *73*, 51-65.
31. Mizushima, K.; Jones, P.; Wiseman, P.; Goodenough, J., Li<sub>x</sub>CoO<sub>2</sub> (0 < x < 1): A New Cathode Material for Batteries of High Energy Density. *Materials Research Bulletin* **1980**, *15*, 783-789.
32. Yoshio, M.; Brodd, R. J.; Kozawa, A., *Lithium-Ion Batteries*; Springer, 2009; Vol. 1.
33. Cho, J.; Kim, Y. J.; Park, B., Novel LiCoO<sub>2</sub> Cathode Material with Al<sub>2</sub>O<sub>3</sub> Coating for a Li Ion Cell. *Chemistry of Materials* **2000**, *12*, 3788-3791.
34. Zhou, X.; Wang, F.; Zhu, Y.; Liu, Z., Graphene Modified LiFePO<sub>4</sub> Cathode Materials for High Power Lithium Ion Batteries. *Journal of Materials Chemistry* **2011**, *21*, 3353-3358.
35. Whittingham, M. S., Lithium Batteries and Cathode Materials. *Chemical reviews* **2004**, *104*, 4271-4302.
36. Ohzuku, T.; Makimura, Y., Layered Lithium Insertion Material of LiCo<sub>1/3</sub>Ni<sub>1/3</sub>Mn<sub>1/3</sub>O<sub>2</sub> for Lithium-Ion Batteries. *Chem. Lett.* **2001**, *7*, 642-643.

37. Xu, K., Nonaqueous Liquid Electrolytes for Lithium-Based Rechargeable Batteries. *Chem. Rev.* **2004**, *104*, 4303-4418.
38. Zhang, S.; Ding, M. S.; Xu, K.; Allen, J.; Jow, T. R., Understanding Solid Electrolyte Interface Film Formation on Graphite Electrodes. *Electrochem. Solid State Lett.* **2001**, *4*, A206-A208.
39. Xu, B.; Qian, D.; Wang, Z.; Meng, Y. S., Recent Progress in Cathode Materials Research for Advanced Lithium Ion Batteries. *Mater. Sci. Eng. Reports* **2012**, *73*, 51-65.
40. Lin, F.; Markus, I. M.; Nordlund, D.; Weng, T.-C.; Asta, M. D.; Xin, H. L.; Doeff, M. M., Surface Reconstruction and Chemical Evolution of Stoichiometric Layered Cathode Materials for Lithium-Ion Batteries. *Nat. Commun.* **2014**, *5*, 3529 (9 pages).
41. Mohanty, D.; Kalnaus, S.; Meisner, R. A.; Rhodes, K. J.; Li, J.; Payzant, E. A.; Wood III, D. L.; Daniel, C., Structural Transformation of a Lithium-Rich  $\text{Li}_{1.2}\text{Co}_{0.1}\text{Mn}_{0.55}\text{Ni}_{0.15}\text{O}_2$  Cathode During High Voltage Cycling Resolved by in Situ X-Ray Diffraction. *J. Power Sources* **2013**, *229*, 239-248.
42. Abe, K.; Yoshitake, H.; Kitakura, T.; Hattori, T.; Wang, H.; Yoshio, M., Additives-Containing Functional Electrolytes for Suppressing Electrolyte Decomposition in Lithium-Ion Batteries. *Electrochim. Acta* **2004**, *49*, 4613-4622.
43. Sa, Q.; Gratz, E.; He, M.; Lu, W.; Apelian, D.; Wang, Y., Synthesis of High Performance  $\text{LiNi}_{1/3}\text{Mn}_{1/3}\text{Co}_{1/3}\text{O}_2$  from Lithium Ion Battery Recovery Stream. *J. Power Sources* **2015**, *282*, 140-145.
44. Chikkannanavar, S. B.; Bernardi, D. M.; Liu, L., A Review of Blended Cathode Materials for Use in Li-Ion Batteries. *J. Power Sources* **2014**, *248*, 91-100.
45. Huang, Z.-D.; Liu, X.-M.; Oh, S.-W.; Zhang, B.; Ma, P.-C.; Kim, J.-K., Microscopically Porous, Interconnected Single Crystal  $\text{LiNi}_{1/3}\text{Co}_{1/3}\text{Mn}_{1/3}\text{O}_2$  Cathode Material for Lithium Ion Batteries. *J. Mater. Chem.* **2011**, *21*, 10777-10784.
46. Cho, T.-H.; Tanaka, M.; Onishi, H.; Kondo, Y.; Nakamura, T.; Yamazaki, H.; Tanase, S.; Sakai, T., Battery Performances and Thermal Stability of Polyacrylonitrile Nano-Fiber-Based Nonwoven Separators for Li-Ion Battery. *Journal of Power Sources* **2008**, *181*, 155-160.
47. Kim, M.; Shon, J.-Y.; Nho, Y. C.; Lee, T.-W.; Park, J. H., Positive Effects of E-Beam Irradiation in Inorganic Particle Based Separators for Lithium-Ion Battery. *Journal of The Electrochemical Society* **2010**, *157*, A31-A34.
48. Fu, D.; Luan, B.; Argue, S.; Bureau, M. N.; Davidson, I. J., Nano SiO<sub>2</sub> Particle Formation and Deposition on Polypropylene Separators for Lithium-Ion Batteries. *Journal of Power Sources* **2012**, *206*, 325-333.
49. Huang, X., Separator Technologies for Lithium-Ion Batteries. *Journal of Solid State Electrochemistry* **2011**, *15*, 649-662.
50. Lee, J.; Lee, C.-L.; Park, K.; Kim, I.-D., Synthesis of an Al<sub>2</sub>O<sub>3</sub>-Coated Polyimide Nanofiber Mat and Its Electrochemical Characteristics as a Separator for Lithium Ion Batteries. *Journal of Power Sources* **2014**, *248*, 1211-1217.
51. He, M.; Zhang, X.; Jiang, K.; Wang, J.; Wang, Y., Pure Inorganic Separator for Lithium Ion Batteries. *ACS applied materials & interfaces* **2014**, *7*, 738-742.
52. Sun, X.; Angell, C. A., Doped Sulfone Electrolytes for High Voltage Li-Ion Cell Applications. *Electrochemistry Communications* **2009**, *11*, 1418-1421.
53. Sun, X.-G.; Angell, C. A., New Sulfone Electrolytes for Rechargeable Lithium Batteries.: Part I. Oligoether-Containing Sulfones. *Electrochemistry communications* **2005**, *7*, 261-266.

54. Kuboki, T.; Okuyama, T.; Ohsaki, T.; Takami, N., Lithium-Air Batteries Using Hydrophobic Room Temperature Ionic Liquid Electrolyte. *Journal of power sources* **2005**, *146*, 766-769.
55. Nagahama, M.; Hasegawa, N.; Okada, S., High Voltage Performances of Li<sub>2</sub>NiPO<sub>4</sub>F Cathode with Dinitrile-Based Electrolytes. *Journal of The Electrochemical Society* **2010**, *157*, A748-A752.
56. He, M.; Hu, L.; Xue, Z.; Su, C. C.; Redfern, P.; Curtiss, L. A.; Polzin, B.; von Cresce, A.; Xu, K.; Zhang, Z., Fluorinated Electrolytes for 5-V Li-Ion Chemistry: Probing Voltage Stability of Electrolytes with Electrochemical Floating Test. *Journal of The Electrochemical Society* **2015**, *162*, A1725-A1729.
57. Lee, Y.-M.; Nam, K.-M.; Hwang, E.-H.; Kwon, Y.-G.; Kang, D.-H.; Kim, S.-S.; Song, S.-W., Interfacial Origin of Performance Improvement and Fade for 4.6 V LiNi<sub>0.5</sub>Co<sub>0.2</sub>Mn<sub>0.3</sub>O<sub>2</sub> Battery Cathodes. *J. Phys. Chem. C* **2014**, *118*, 10631-10639.
58. Sinha, N. N.; Burns, J. C.; Dahn, J. R., Comparative Study of Tris(Trimethylsilyl)Phosphate and Tris(Trimethylsilyl)Phosphite as Electrolyte Additives for Li-Ion Cells. *J. Electrochem. Soc.* **2014**, *161*, A1084-A1089.
59. Han, Y.-K.; Yoo, J.; Yim, T., Why Is Tris(Trimethylsilyl) Phosphite Effective as an Additive for High-Voltage Lithium-Ion Batteries? *J. Mater. Chem.* **2015**, *3*, 10900-10909.
60. Zuo, X.; Fan, C.; Liu, J.; Xiao, X.; Wu, J.; Nan, J., Lithium Tetrafluoroborate as an Electrolyte Additive to Improve the High Voltage Performance of Lithium-Ion Battery. *J. Electrochem. Soc.* **2013**, *160*, A1199-A1204.
61. Xu, M.; Zhou, L.; Dong, Y.; Chen, Y.; Demeaux, J.; MacIntosh, A. D.; Garsuch, A.; Lucht, B. L., Development of Novel Lithium Borate Additives for Designed Surface Modification of High Voltage LiNi<sub>0.5</sub>Mn<sub>1.5</sub>O<sub>4</sub> Cathodes. *Energy & Environ. Sci.* **2016**, DOI 10.1039/C5EE03360H.
62. Wang, Z.; Xing, L.; Li, J.; Xu, M.; Li, W., Triethylborate as an Electrolyte Additive for High Voltage Layered Lithium Nickel Cobalt Manganese Oxide Cathode of Lithium Ion Battery. *J. Power Sources* **2016**, *307*, 587-592.
63. Chen, J.; Zhang, H.; Wang, M.; Liu, J.; Li, C.; Zhang, P., Improving the Electrochemical Performance of High Voltage Spinel Cathode at Elevated Temperature by a Novel Electrolyte Additive. *J. Power Sources* **2016**, *303*, 41-48.
64. Mai, S.; Xu, M.; Liao, X.; Xing, L.; Li, W., Improving Cyclic Stability of Lithium Nickel Manganese Oxide Cathode at Elevated Temperature by Using Dimethyl Phenylphosphonite as Electrolyte Additive. *J. Power Sources* **2015**, *273*, 816-822.
65. Chen, R.; Liu, F.; Chen, Y.; Ye, Y.; Huang, Y.; Wu, F., An Investigation of Functionalized Electrolyte Using Succinonitrile Additive for High Voltage Lithium-Ion Batteries. *J. Power Sources* **2016**, *306*, 70-77.
66. Hu, L.; Zhang, Z.; Amine, K., Fluorinated Electrolytes for Li-Ion Battery: An FeC-Based Electrolyte for High Voltage LiNi<sub>0.5</sub>Mn<sub>1.5</sub>O<sub>4</sub>/Graphite Couple. *Electrochemistry Communications* **2013**, *35*, 76-79.

## Chapter 2. Fluorinated Electrolytes for 5-V Li-ion Chemistry: Probing Voltage Stability of Electrolytes with Electrochemical Floating Test

### Abstract

A series of electrolyte formulations containing fluorinated cyclic carbonates and fluorinated linear carbonates with LiPF<sub>6</sub> has been evaluated as electrolyte solvents for high-voltage Li-ion batteries. The anodic stability of the new electrolytes on fully charged spinel LiNi<sub>0.5</sub>Mn<sub>1.5</sub>O<sub>4</sub> (LNMO) cathode was examined by electrochemical floating tests. The effects of fluorine substitution on the cyclic and linear carbonate, ratio of cyclic vs. linear carbonate, and LiPF<sub>6</sub> concentration on the electrolyte oxidation stability were investigated. Based on this study, the floating test proved to be an effective tool for identification of stable electrolyte materials.

**Keywords:** Fluorinated electrolyte; oxidation stability; electrochemical floating test; 5-V LiNi<sub>0.5</sub>Mn<sub>1.5</sub>O<sub>4</sub> cathode; high voltage lithium-ion batteries

### 2.1 Introduction

High-energy lithium-ion (Li-ion) batteries that operate at high voltage have been attracting considerable attention because of their potential application in electric vehicles <sup>1</sup>. To increase the energy density of Li-ion batteries, researchers have developed high capacity cathodes such as the lithium-rich “layered-layered” composite  $x\text{Li}_2\text{MnO}_3 \cdot (1-x)\text{LiMO}_2$  (M=Ni, Co, Mn) <sup>2</sup> and high voltage cathodes such as the spinel LiNi<sub>0.5</sub>Mn<sub>1.5</sub>O<sub>4</sub> (LNMO) <sup>3-4</sup> and LiCoPO<sub>4</sub> <sup>5</sup>. Of these, the

high-voltage spinel LNMO is particularly popular. While providing high energy density, such high voltage cathodes impose a strongly oxidative environment on the organic electrolyte during charging, resulting in rapid decomposition of conventional electrolytes<sup>6-7</sup>. To accommodate these high voltage cathodes, a lot of novel electrolyte systems based on fluorinated carbonates<sup>8-9</sup>, sulfones<sup>10-11</sup>, nitriles<sup>12</sup>, and ionic liquids<sup>13</sup> have been proposed. Because of the large number of candidates for high-voltage electrolyte solvents, screening the voltage stability of each solvent would be very labor-intensive. Traditional methods of measuring the oxidation potential of organic solvents usually involves linear/cyclic voltammetry using an inert electrode such as platinum and glassy carbon. However, such measurements are in many cases misleading, because interactions of these organic solvents with actual electrode materials are usually more complicated and may happen at a much lower potential due to the catalytic effect of the cathode material lowering the kinetic barrier of oxidation. Unfortunately, using active cathode material to run voltammetry measurement has a drawback in that the material itself is redox active and can interfere with the observation of electrolyte oxidation. Thus, developing a fast and effective method to screen the voltage stability of electrolyte solvents on actual cathode materials is of vital importance.

Herein, we report a method using constant potential electrolysis with a slightly overcharged LNMO cathode as the working electrode, abbreviated as an “electrochemical floating test”, where the cell potential is allowed to “float” at different values to evaluate the voltage stability of the electrolyte. For an ideal electrolyte with no impurities and no oxidation at the working electrode, the only current observed when a potential is applied is the capacitance current, which should decline to zero when the equilibrium is reached. However, in reality, the electrolytes are oxidized, and the current intensity measured corresponds to the severity of oxidation. As a result,

the leakage currents of each electrolyte at different potentials can be compared to produce a voltage stability profile of a given solvent. The effect of different ratios of mixed solvents and lithium salt concentrations can also be probed.

## **2.2. Material and methods**

### *2.2.1. Theoretical calculations*

The Gaussian 09 code was used for all calculations<sup>14</sup>. Oxidation and reduction potentials were calculated by optimizing the geometries of the neutral and ionic species at the B3LYP/6-31G\* level, followed by frequency calculations to determine gas-phase free energies. Solvation effects were taken into account by using a single-point B3LYP/6-31+G\* PCM calculation with the default (water) solvent and a dielectric constant of 55.725, representing an electrolyte composed of 25% ethylene carbonate (EC), 25% ethyl methyl carbonate (EMC), and 50% propylene carbonate (PC). Finally, basis set effects were taken into account with a single-point B3LYP/6-311+G(3df,2p) calculation. From these results, the total free energy of each species was calculated as electronic energy plus gas-phase free energy plus solvation free energy. The free energies of the neutral and ionic species were then subtracted to obtain an absolute free energy difference. During this process the electron affinity (reduction potential) or ionization potential (oxidation potential) was calculated. Absolute free energy changes were converted to standard hydrogen electrode potentials by subtracting 4.5 V and then to Li<sup>+</sup>/Li potentials by adding 3.04 V. Further details on reduction potential calculations can be found in Ref.<sup>15</sup> and on oxidation potentials in Ref.<sup>8</sup>.

## 2.2.2. Synthesis of fluorinated solvents

2.2.2.1. *Fluorinated cyclic carbonate.* Fluorinated cyclic carbonates such as tetrafluoropropyl-propylene carbonate-ether (TFP-PC-E) were synthesized along with corresponding fluorinated epoxides and carbon dioxide (CO<sub>2</sub> gas) according to a procedure in the literature <sup>16</sup>. In a typical procedure for TFP-PC-E, glycidyl 2,2,3,3-tetrafluoropropyl ether (Sigma-Aldrich, 7.52 g, 40 mmol, 1 equiv) and methyltriphenylphosphonium iodide (Sigma-Aldrich, 0.812 g, 2 mmol, 5 mol%) were dissolved in 8 mL of 1-methoxy-2-propanol and stirred at room temperature under a CO<sub>2</sub> atmosphere (1 atm). The reaction mixture was stirred at ambient condition for 4 days, until the conversion reached 96%, as detected by gas chromatography-mass spectrometry. The reaction solvent was then removed by a rotary evaporator. The crude product was dried over 4 Å molecular sieves, decanted, and purified by fractional distillation under reduced pressure. Pure product (99.8% by gas chromatography) was obtained as fractions (90-100 °C/0.2 mm Hg) with an isolated yield of 37% and 10 ppm water content as measured by Karl-Fischer titration. Fractions containing trace amounts (<0.5%) of starting materials were combined for further purification.

2.2.2.2. *Asymmetric fluorinated linear carbonate.* The asymmetric fluorinated linear carbonates were synthesized from the corresponding fluorinated alcohols with methyl or ethyl chloroformate following a procedure in the literature <sup>17</sup>. In a typical procedure for trifluoroethyl methyl carbonate (F-EMC), 2,2,2-trifluoroethanol (Sigma-Aldrich, 50.02 g, 0.5 mol, 1 equiv), triethylamine (Sigma-Aldrich, 55.65 g, 0.55 mol, 1.1 equiv), and 4-dimethylaminopyridine (Sigma-Aldrich, 0.61 g, 5 mmol, 1% mol) were mixed together in a round-bottom flask and

cooled to 0 °C. Methyl chloroformate (Sigma-Aldrich, 47.25 g, 0.5 mol, 1 equiv) was added into the mixture dropwise via a syringe pump over the course of 6 h. The mixture was then allowed to warm up to ambient temperature and stirred for 24 h. The reaction was then quenched with 1N HCl solution, and the product was washed further with HCl and then brine solution. After being dried with 4 Å molecular sieves, the crude product was fractional distilled twice to obtain pure product (99.7% by gas chromatography) with an isolated yield of 50% and 15 ppm water content as measured by Karl-Fischer titration.

*2.2.2.3. Symmetric fluorinated linear carbonate.* The symmetric fluorinated linear carbonates were synthesized from the corresponding fluorinated alcohols with triphosgene. In a typical procedure for di-trifluoroethyl carbonate (HF-DEC), 2,2,2-trifluoroethanol (18.5 g, 0.185 mol, 6.17 equiv), triethylamine (20.2 g, 0.2 mol, 6.67 equiv), and 4-dimethylaminopyridine (Sigma-Aldrich, 36 mg, 0.3 mmol, 1% mol) were mixed together in a round-bottom flask and cooled to 0 °C. A solution of triphosgene (8.9 g, 0.03 mol, 1 equiv) in CH<sub>2</sub>Cl<sub>2</sub> was added into the mixture dropwise via a syringe pump over the course of 8 h. The mixture was then allowed to warm up to ambient temperature and stirred for 48 h. The reaction was then quenched with 1N HCl, and the product was extracted with CH<sub>2</sub>Cl<sub>2</sub> and washed further with HCl and then with brine solution. The crude product was distilled to remove CH<sub>2</sub>Cl<sub>2</sub>, dried with 4 Å molecular sieves, and then fractional distilled twice to afford the pure product (99.1% by gas chromatography) with an isolated yield of 39% and 15 ppm water content as measured by Karl-Fischer titration.

*2.2.3. Electrode and electrochemical floating test*

The cathode was made of 84 wt%  $\text{LiNi}_{0.5}\text{Mn}_{1.5}\text{O}_4$  (LNMO), 8 wt% Super P-Li, and 8 wt% Solvey 5130 polyvinylidene fluoride (PVDF) binder coated on aluminum foil. The active material loading averaged  $12.5 \text{ mg cm}^{-2}$ . The graphite anode was made of 89.8 wt% Conoco Phillips CGP-A12, 4 wt% Super P-Li, 6 wt% Kureha 9300 PVDF binder, and 0.2 wt% oxalic acid coated on copper foil. The active material loading averaged  $5.3 \text{ mg cm}^{-2}$ .

The electrochemical floating test used 2032 coin cells with LNMO as the cathode, Li metal as the anode, and microporous polypropylene/polyethylene/polypropylene (PP/PE/PP) as the separator. The effective electrode area was  $1.6 \text{ cm}^2$ . The LNMO/Li cell was charged to 4.9 V at a rate of C/13 and then maintained at 4.9 V, 5.0 V, 5.1 V, and 5.2 V for 10 h with the current monitored by Maccor battery and cell testing equipment.

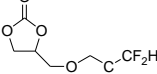
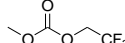
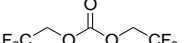
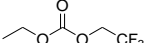
The charge-discharge cycling performance was determined with 2032 coin cells having LNMO as the cathode, graphite as the anode, and microporous PP/PE/PP as the separator. The effective electrode area was  $1.6 \text{ cm}^2$ . A two-cycle formation was performed with a rate of C/10 between 3.5 and 4.9 V, followed by 50 cycles at a rate of C/3 (0.67 mA) between 3.5 and 4.9 V.

### **2.3. Results and discussion**

We previously used the electrochemical floating test to compare the voltage stability of different fluorinated electrolyte formulations, and the results corresponded well with cell test data using LNMO and  $\text{Li}_4\text{Ti}_5\text{O}_{12}$  (LTO) as electrodes (8). However, we did not conduct a systematic study

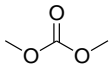
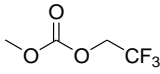
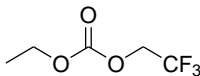
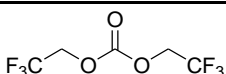
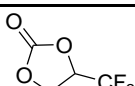
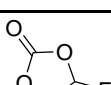
with this method because we did not have a variety of fluorinated solvents to screen at the time. In this study, three fluorinated cyclic carbonates (FEC, TFPC, and TFP-PC-E) and three fluorinated linear carbonates (F-EMC, HF-DEC and TF-DEC) were screened in comparison with their non-fluorinated counterparts (EC and DMC for voltage stability. The structures of all the solvents tested are depicted in Table 2.1.

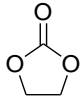
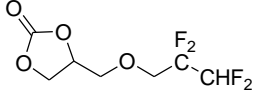
**Table 2.1.** Fluorinated cyclic and linear carbonates and their non-fluorinated counterparts used in the electrochemical floating test.

Cyclic carbonate				
	EC	FEC	TFPC	TFP-PC-E
Linear carbonate				
	DMC	F-EMC	HF-DEC	TF-DEC

Note: EC = ethylene carbonate; FEC = fluoroethylene carbonate; TFPC = trifluoropropylene carbonate; TFP-PC-E = tetrafluoropropyl-propylene carbonate-ether; DMC = dimethyl carbonate; F-EMC = trifluoroethyl methyl carbonate; HF-DEC = di-trifluoroethyl carbonate; TF-DEC = ethyl trifluoroethyl carbonate.

**Table 2.2.** Oxidation and reduction potentials of the solvents in Table 2.1 calculated by DFT computation.

Molecular Structure	Oxidation Potential ( $P_{ox}/V$ )	Oxidation Potential with Anion Effect ( $P_{ox}/V$ )
 (DMC)	6.71	7.06 ( $PF_6^-$ ), 6.07 ( $PF_6^-$ , transfer H); 5.93, 5.78 (TFSI $^-$ ), 5.16 (TFSI $^-$ , transfer H)
 (F-EMC)	7.10	6.26 ( $PF_6^-$ , HF forms spontaneously); 5.79 (TFSI $^-$ )
 (TF-DEC)	6.89	7.10 ( $PF_6^-$ ), 6.04 ( $PF_6^-$ , HF forms spontaneously); 6.01, 5.83, 5.81, 5.74 (TFSI $^-$ ), 5.17 (TFSI $^-$ , transfer H)
 (HF-DEC)	7.25	7.35 ( $PF_6^-$ )
 (TFPC)	7.30	6.21 ( $PF_6^-$ ); 5.33, 5.44, 5.87 (TFSI $^-$ )
 (FEC)	7.24	6.44 ( $PF_6^-$ ); 5.80 (TFSI $^-$ )

 (EC)	6.95	6.17 (PF <sub>6</sub> <sup>-</sup> , HF forms spontaneously); 5.83 (TFSI <sup>-</sup> ), 5.04 (transfer H)
 (TFP-PC-E)	6.24	6.05 (PF <sub>6</sub> <sup>-</sup> ); 5.90, 5.19, 5.22 (TFSI <sup>-</sup> )

To provide a theoretical guideline, we conducted a computational study of the synthesized solvents listed in Table 2.1. The oxidation and reduction potentials calculated by density functional theory (DFT) are summarized in Table 2.2. Based on the calculated results, the theoretical oxidative stabilities of the cyclic carbonates are in the order TFPC > FEC > EC >> TFP-PC-E, while the linear carbonates are in the order HF-DEC > F-EMC > TF-DEC > DMC, if only the ease of electron abstraction is considered.

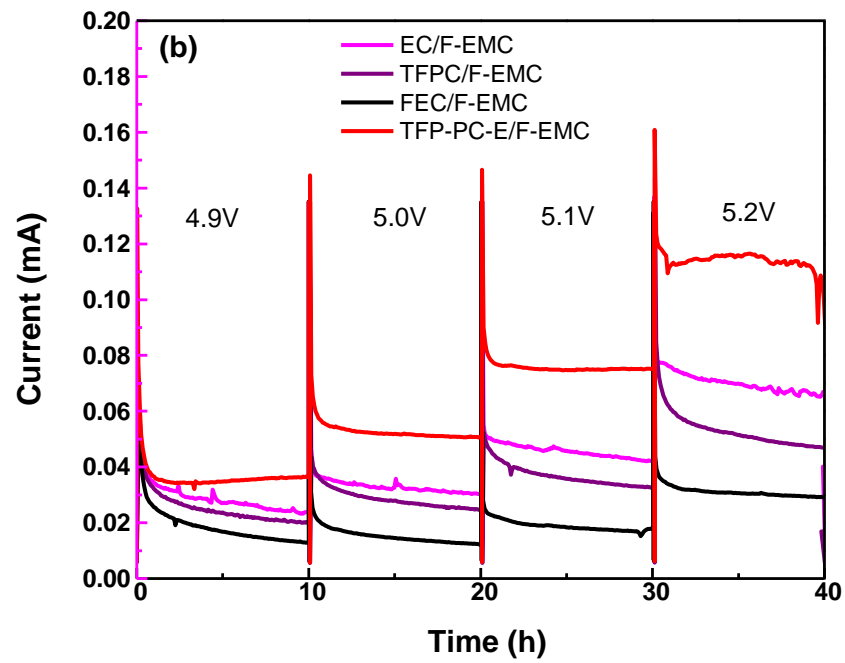
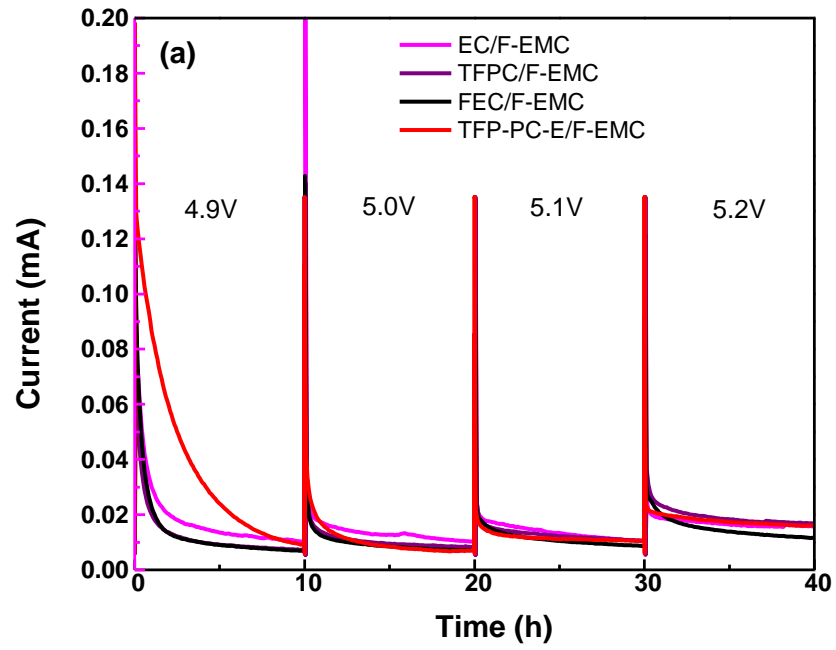
The oxidation potentials of solvent/salt anion complexes were also calculated. The geometries of several solvent/PF<sub>6</sub><sup>-</sup> anion complexes were optimized and then re-optimized as neutral doublets in the oxidized state. In most cases, hydrogen fluoride (HF) formed spontaneously upon oxidation of the neutral state. In two cases, HF did not form (DMC and HF-DEC), but the reaction products involved transferring a hydrogen to a fluorine and resulted in lower energy structures. A similar decomposition reaction upon oxidation resulting in HF was also noted by Borodin et al.<sup>18</sup>. In all cases, the interaction of the solvent with PF<sub>6</sub><sup>-</sup> lowers the oxidation

potential of the solvent, and due to the different interaction between the solvent and  $\text{PF}_6^-$ , the oxidation stability of the cyclic carbonates are in the order of  $\text{FEC} > \text{TFPC} \sim \text{EC} > \text{TFP-PC-E}$ , and the linear carbonates are in the order of  $\text{HF-DEC} > \text{F-EMC} > \text{DMC} \sim \text{TF-DEC}$ . The oxidation potentials of solvent/ $\text{TFSI}^-$  complexes were also calculated. In the case of the cyclic TFP-PC-E solvent, a hydrogen transfers to the nitrogen of TFSI spontaneously. In other cyclic solvent/ $\text{TFSI}^-$  complexes, the reaction energies for products with hydrogen transferred to the nitrogen of TFSI after oxidation were favorable, and the oxidation potential decreased. Oxidation potentials of cyclic solvent/ $\text{TFSI}^-$  complexes are lower than those of solvent/ $\text{PF}_6^-$  complexes because TFSI itself has a lower oxidation potential than  $\text{PF}_6^-$ . Borodin et al.<sup>18</sup> calculated the oxidation potentials as 5.78 V for TFSI and 8.58 V for  $\text{PF}_6^-$ .

With the theoretical predictions in hand, we next examined the oxidative stabilities of these solvents experimentally. To compare the voltage stability of different solvents in a simple manner, we used a binary solvent system with 1:1 ratio of a cyclic carbonate and a linear carbonate. To minimize the lithium salt solubility issue that may arise with certain highly fluorinated solvents, a relatively low salt concentration of 0.5 M  $\text{LiPF}_6$  was employed for all the electrolyte formulations.

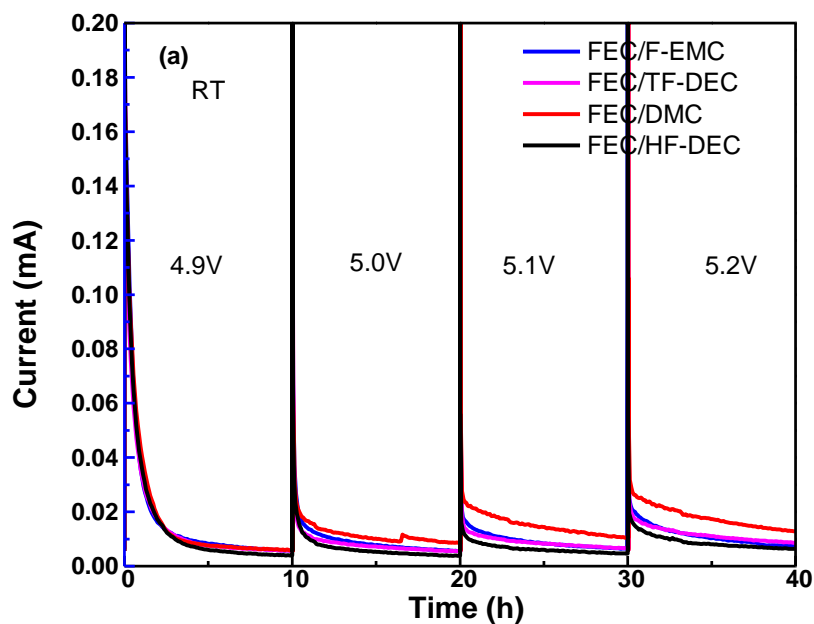
To begin, we selected the linear carbonate F-EMC as the fixed component and mixed it with different cyclic carbonates (EC, TFPC, FEC, and TFP-PC-E) to evaluate the voltage stability of the resulting mixtures. The solvent F-EMC was chosen since it has shown relatively good stability against the LNMO cathode<sup>9,19</sup>. The floating tests were carried out at room temperature

first, and the results are given in Figure 2.1a. Interestingly, all four cyclic carbonates showed similar levels of stability and overcharge tolerance at RT. The only different feature is that EC has higher leakage current at low potentials and TFP-PC-E has a less steep current drop at 4.9 V than the other three cyclic carbonates, possibly due to the polarization effect of the electrolyte on the LNMO cathode material. When the potential initially reached 4.9 V, the cathode might not be fully charged yet in the case of TFP-PC-E electrolyte due to high polarization, so the charging current dropped more slowly than that of the other electrolytes at the first constant voltage (CV) charging step. Such behavior can be eliminated by raising the temperature to improve the kinetics. When the temperature was raised to 55 °C, the voltage stability between the cyclic carbonates became clearly differentiated (Figure 2.1b), and the stability follows the order  $\text{FEC} > \text{TFPC} > \text{EC} > \text{TFP-PC-E}$ , the same order as predicted from the quantum chemistry calculations considering the anion effect of  $\text{PF}_6^-$  (Table 2.2). As can be seen from Figure 2.1b, FEC is insensitive to overcharge until 5.2 V vs.  $\text{Li}^+/\text{Li}$ , but the other three cyclic carbonates show different degrees of increment in the leakage current starting from 5.0 V vs.  $\text{Li}^+/\text{Li}$ , with TFP-PC-E exhibiting the most dramatic change. For TFP-PC-E, although there is an electron-withdrawing tetrafluoroethyl group at the far end of the molecule, a  $-\text{CH}_2-\text{O}-\text{CH}_2-$  link separates the F-alkyl from the carbonate ring; therefore, the electron-withdrawing effect is minimized. The  $-\text{CH}_2-\text{O}-\text{CH}_2-$  group actually acts as an electron-donating group, which lowers the oxidation potential of the carbonate ring. Moreover, the ether linkage  $-\text{CH}_2-\text{O}-\text{CH}_2-$  itself is vulnerable to oxidation as well.



**Figure 2.1.** Floating test of 0.5 M LiPF<sub>6</sub> salt and F-EMC solvent mixed with EC, TFPC, FEC, and TFP-PC-E at 1:1 ratio (a) RT and (b) 55 °C.

With FEC being the most anodically stable among the cyclic carbonates tested, we moved on to use it as the fixed component and tested it with DMC and the three fluorinated linear carbonates listed in Table 2.1. The results are shown in Figure 2.2. Unlike the cyclic carbonate, the linear carbonates were able to differentiate their oxidation stability quite well at RT when the potential was charged beyond 5.0 V vs. Li<sup>+</sup>/Li. The fluorinated linear carbonates clearly showed an advantage over DMC at higher potentials, with HF-DEC being the most stable and F-EMC, TF-DEC having similar level of stability, which agree with theoretical predication.



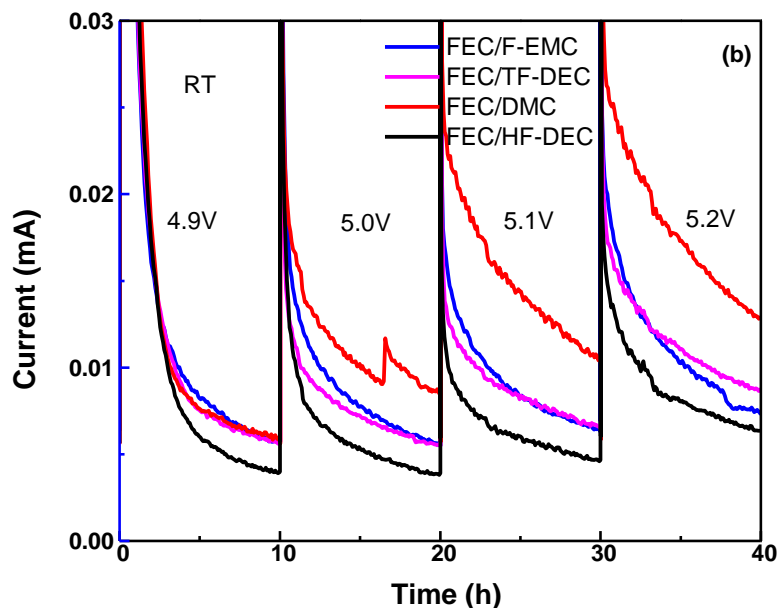


**Figure 2.2.** Floating test at RT of 0.5 M  $\text{LiPF}_6$  salt and FEC solvent mixed with DMC, F-EMC, HF-DEC, and TF-DEC at 1:1 ratio and with F-MiPC/F-EPE at 2:1:1 ratio: (a) same current range as in Figure 2.1 and (b) low current region (below 0.03 mA).

We also investigated the effect of cyclic carbonate/linear carbonate ratio on the stability of the electrolyte. Due to poorer salt solubility of  $\text{LiPF}_6$  in the fluorinated linear carbonates, we selected DMC as the linear carbonate with FEC as the cyclic carbonate for this study. We mixed FEC and DMC at ratios of 9:1 to 1:9 in 10% increments of DMC, with 0.5 M  $\text{LiPF}_6$  concentration. Unlike the previous tests, we employed glass fiber as the separator because the formulated electrolyte does not wet the PP/PE/PP separator when the FEC content is more than 50%. To make the comparison between different FEC concentrations more straightforward, we measured the current intensity at the end of each 10 hours of holding at different potentials and plotted these current intensities against the content of FEC in the electrolyte (Figure 2.3). The

resulting data in Figure 2.3 indicate that at lower potentials such as 4.9 V, the current intensities are not very sensitive to the FEC concentration. They only show a mild decline as the FEC concentration increases. This is an indication that both solvents are probably relatively stable at this potential. At higher potentials, the current intensities show much more dramatic decline over increasing FEC concentration. This finding indicates that DMC is more prone to oxidation than FEC, and its oxidation is greatly accelerated when the potential is greater than 5.1 V. Comparing the trend of current intensities at different FEC concentrations for all four potentials tested, the current intensities show that with more FEC, the electrolytes become more stable against oxidation, but the beneficial effect is not as dramatic after the concentration of cyclic carbonate is over 50%. This concludes that the cyclic carbonate FEC is more stable than the linear carbonate DMC, which again agrees with theoretical prediction. While considering the oxidation stability in formulating a new electrolyte, of course, practical concerns such as wettability of the separator and electrode also need to be considered.

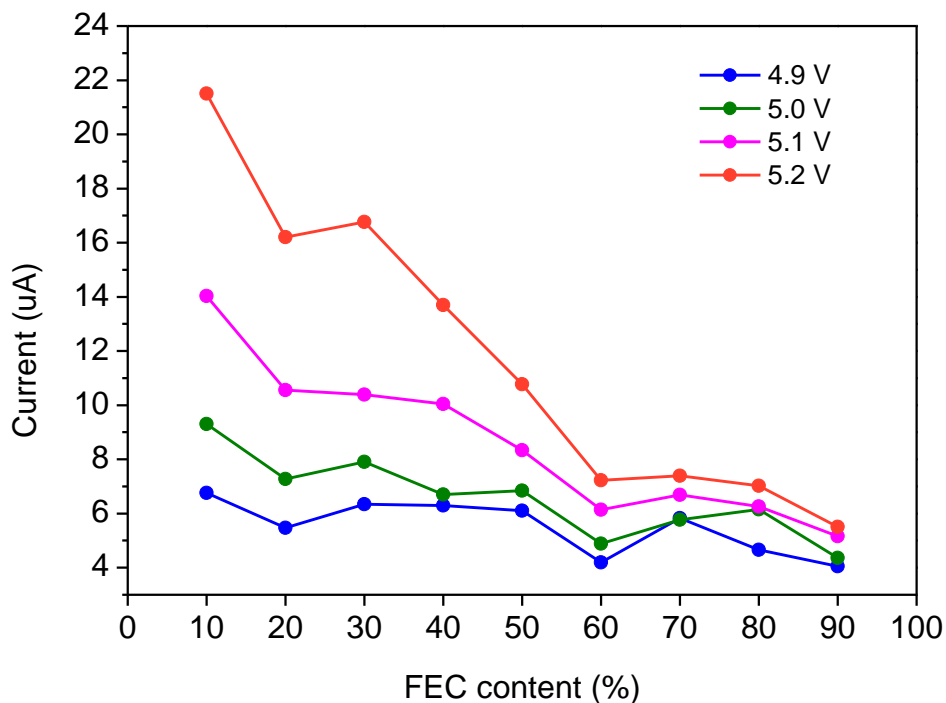


**Figure 2.3.** Current intensities of floating test using solvent of FEC mixed with DMC at 1:9 to 9:1 ratio and salt of 0.5 M LiPF<sub>6</sub>. The current intensities are taken at the end of 10-hour holding at potentials of 4.9 V, 5.0 V, 5.1 V, and 5.2 V.

We also studied the effect of salt concentration on the oxidation stability of the electrolyte. In this case, we chose FEC/DMC (1:1 ratio) as the fixed solvent base and varied the LiPF<sub>6</sub> concentration from 0.5 to 1.25 M in 0.25 M increments. The current intensities were determined in the same way as for the experiment shown in Figure 2.3, and the results are summarized in Figure 2.4. At lower potentials (4.9 and 5.0 V), the data follow the trend that the higher the salt concentration, the higher the stability of the electrolyte towards oxidation; at higher potentials (5.1 and 5.2 V) the results do not follow this pattern. It is more likely that salt concentration does not have a significant direct impact on the voltage stability of electrolyte at least in dilute electrolyte solutions, and the chosen solvent plays a dominant role. Extremely high salt

concentrations may dramatically enhance the oxidation stability of the electrolyte <sup>20</sup>, but it is beyond the scope of this study.

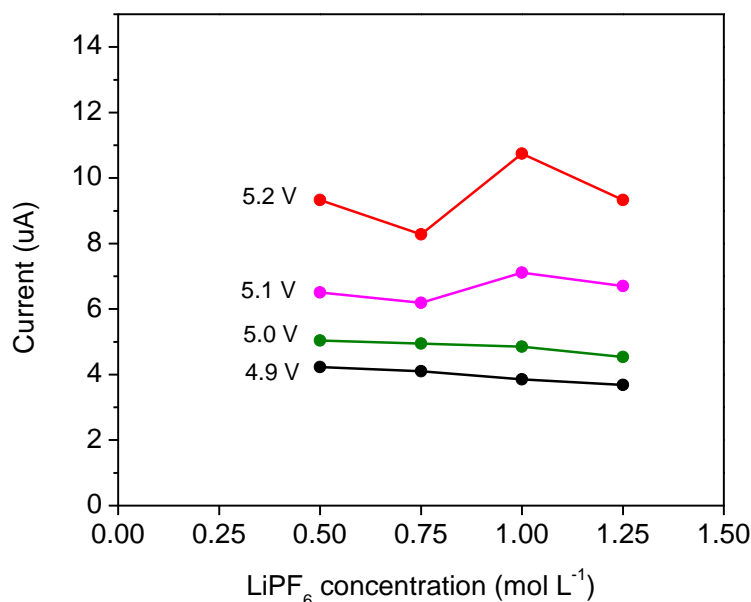


**Figure 2.4.** Current intensities of floating test using solvent of FEC mixed with DMC at 1:1 ratio and salt of LiPF<sub>6</sub> with concentrations from 0.5 M to 1.25 M. The current intensities are taken at the end of each 10-hour holding at each potential.

## 2.4. Conclusion

Electrochemical floating tests have been used as an evaluation tool for the voltage stability of electrolyte solvents. Of the cyclic carbonates screened, FEC is the most stable solvent, followed by TFPC, EC, and TFP-PC-E. The differences of voltage stability are much more pronounced at elevated temperature than at RT. For the linear carbonates, HF-DEC is the most stable, followed by F-EMC, TF-DEC and DMC. Mixtures of FEC and DMC in various ratios demonstrated that FEC is the more stable component in the binary formulations of FEC/DMC, although the beneficial effect is insignificant after the concentration of cyclic carbonate is increased over 50%,

and wetting issue begins to arise. Testing of various salt concentrations did not result in great variation of the electrolyte stability, implying that the effect of the salt on the electrolyte voltage stability is minimal in dilute electrolytes.

## References

1. Armand, M.; Tarascon, J. M., Building better batteries. *Nature* **2008**, *451* (7179), 652-657.
2. Croy, J. R.; Kim, D.; Balasubramanian, M.; Gallagher, K.; Kang, S. H.; Thackeray, M. M., Countering the Voltage Decay in High Capacity  $x\text{Li}_2\text{MnO}_3 \cdot (1-x)\text{LiMO}_2$  Electrodes (M=Mn, Ni, Co) for Li<sup>+</sup>-Ion Batteries. *J Electrochem Soc* **2012**, *159* (6), A781-A790.
3. Chemelewski, K. R.; Lee, E. S.; Li, W.; Manthiram, A., Factors Influencing the Electrochemical Properties of High-Voltage Spinel Cathodes: Relative Impact of Morphology and Cation Ordering. *Chem Mater* **2013**, *25* (14), 2890-2897.
4. Hao, X. G.; Bartlett, B. M., Improving the Electrochemical Stability of the High-Voltage Li-Ion Battery Cathode  $\text{LiNi}_0.5\text{Mn}_1.5\text{O}_4$  by Titanate-Based Surface Modification. *J Electrochem Soc* **2013**, *160* (5), A3162-A3170.
5. Oh, S. M.; Myung, S. T.; Sun, Y. K., Olivine  $\text{LiCoPO}_4$ -carbon composite showing high rechargeable capacity. *J Mater Chem* **2012**, *22* (30), 14932-14937.
6. Yang, L.; Ravdel, B.; Lucht, B. L., Electrolyte Reactions with the Surface of High Voltage  $\text{LiNi}_0.5\text{Mn}_1.5\text{O}_4$  Cathodes for Lithium-Ion Batteries. *Electrochem Solid St* **2010**, *13* (8), A95-A97.
7. Hu, L.; Zhang, Z.; Amine, K., Electrochemical investigation of carbonate-based electrolytes for high voltage lithium-ion cells. *J Power Sources* **2013**, *236*, 175-180.
8. Zhang, Z.; Hu, L.; Wu, H.; Weng, W.; Koh, M.; Redfern, P. C.; Curtiss, L. A.; Amine, K., Fluorinated electrolytes for 5 V lithium-ion battery chemistry. *Energ Environ Sci* **2013**, *6* (6), 1806-1810.
9. Hu, L.; Zhang, Z.; Amine, K., Fluorinated electrolytes for Li-ion battery: An FEC-based electrolyte for high voltage  $\text{LiNi}_0.5\text{Mn}_1.5\text{O}_4$ /graphite couple. *Electrochem Commun* **2013**, *35*, 76-79.
10. Shao, N.; Sun, X. G.; Dai, S.; Jiang, D. E., Electrochemical Windows of Sulfone-Based Electrolytes for High-Voltage Li-Ion Batteries. *J Phys Chem B* **2011**, *115* (42), 12120-12125.
11. Cui, X.; Zhang, H.; Li, S.; Zhao, Y.; Mao, L.; Zhao, W.; Li, Y.; Ye, X., Electrochemical performances of a novel high-voltage electrolyte based upon sulfolane and  $\gamma$ -butyrolactone. *J. Power Sources* **2013**, *240* (Copyright (C) 2014 American Chemical Society (ACS). All Rights Reserved.), 476-485.
12. Duncan, H.; Salem, N.; Abu-Lebdeh, Y., Electrolyte formulations based on dinitrile solvents for high voltage Li-ion batteries. *J. Electrochem. Soc.* **2013**, *160* (Copyright (C) 2014 American Chemical Society (ACS). All Rights Reserved.), A838-A848.
13. Xiang, J.; Wu, F.; Chen, R. J.; Li, L.; Yu, H. G., High voltage and safe electrolytes based on ionic liquid and sulfone for lithium-ion batteries. *J Power Sources* **2013**, *233*, 115-120.

14. Frisch, M. J.; Trucks, G. W.; Schlegel, H. B.; Scuseria, G. E.; Robb, M. A.; Cheeseman, J. R.; Scalmani, G.; Barone, V.; Mennucci, B.; Petersson, G. A.; Nakatsuji, H.; Caricato, M.; Li, X.; Hratchian, H. P.; Izmaylov, A. F.; Bloino, J.; Zheng, G.; Sonnenberg, J. L.; Hada, M.; Ehara, M.; Toyota, K.; Fukuda, R.; Hasegawa, J.; Ishida, M.; Nakajima, T.; Honda, Y.; Kitao, O.; Nakai, H.; Vreven, T.; Montgomery Jr., J. A.; Peralta, J. E.; Ogliaro, F.; Bearpark, M. J.; Heyd, J.; Brothers, E. N.; Kudin, K. N.; Staroverov, V. N.; Kobayashi, R.; Normand, J.; Raghavachari, K.; Rendell, A. P.; Burant, J. C.; Iyengar, S. S.; Tomasi, J.; Cossi, M.; Rega, N.; Millam, N. J.; Klene, M.; Knox, J. E.; Cross, J. B.; Bakken, V.; Adamo, C.; Jaramillo, J.; Gomperts, R.; Stratmann, R. E.; Yazyev, O.; Austin, A. J.; Cammi, R.; Pomelli, C.; Ochterski, J. W.; Martin, R. L.; Morokuma, K.; Zakrzewski, V. G.; Voth, G. A.; Salvador, P.; Dannenberg, J. J.; Dapprich, S.; Daniels, A. D.; Farkas, Ö.; Foresman, J. B.; Ortiz, J. V.; Cioslowski, J.; Fox, D. J. *Gaussian 09*, Gaussian, Inc.: Wallingford, CT, USA, **2009**.
15. Vollmer, J. M.; Curtiss, L. A.; Vissers, D. R.; Amine, K., Reduction mechanisms of ethylene, propylene, and vinylene carbonates - A quantum chemical study. *J Electrochem Soc* **2004**, *151* (1), A178-A183.
16. Aoyagi, N.; Furusho, Y.; Endo, T., Effective synthesis of cyclic carbonates from carbon dioxide and epoxides by phosphonium iodides as catalysts in alcoholic solvents. *Tetrahedron Lett* **2013**, *54* (51), 7031-7034.
17. Dang, V. A.; Olofson, R. A.; Wolf, P. R.; Piteau, M. D.; Senet, J. P. G., A Simple Conversion of 1-Chloroethyl Carbonates to Fluoroformates - Value in the Preparation of Tertiary Alkyl Fluoroformates. *J Org Chem* **1990**, *55* (6), 1847-1851.
18. Borodin, O.; Behl, W.; Jow, T. R., Oxidative Stability and Initial Decomposition Reactions of Carbonate, Sulfone, and Alkyl Phosphate-Based Electrolytes. *J Phys Chem C* **2013**, *117* (17), 8661-8682.
19. Hu, L.; Amine, K.; Zhang, Z., Fluorinated electrolytes for 5-V Li-ion chemistry: Dramatic enhancement of LiNi<sub>0.5</sub>Mn<sub>1.5</sub>O<sub>4</sub>/graphite cell performance by a lithium reservoir. *Electrochem Commun* **2014**, *44* (0), 34-37.
20. McOwen, D. W.; Seo, D. M.; Borodin, O.; Vatamanu, J.; Boyle, P. D.; Henderson, W. A., Concentrated electrolytes: decrypting electrolyte properties and reassessing Al corrosion mechanisms. *Energ Environ Sci* **2014**, *7* (1), 416-426.

### **Chapter 3. The Impact of Different Substituents in Fluorinated Cyclic Carbonates in the Performance of High Voltage Lithium-ion Battery Electrolyte**

#### **Abstract**

Ethylene carbonate (EC) has been used as the Solid-Electrolyte Interphase (SEI) former in the conventional electrolyte for decades. However, both EC and other linear carbonates in the commercial electrolyte suffer from the low oxidation potential, which may lead to severe capacity decay during cycling under high voltage operation. As a result, finding a viable electrolyte with high anodic stability and the ability to form robust SEI for the next-generation high voltage lithium-ion batteries is of primary importance. In this study, a series of electrolytes containing various fluorinated cyclic carbonates as the anode SEI former with trifluoroethyl methyl carbonate (F-EMC) and  $\text{LiPF}_6$  have been designed, synthesized and evaluated. The effect of fluorinated substitution groups on the cyclic carbonate on the electrolyte oxidation stability was examined by a 3-electrode cell with Pt as the working electrode. . Based on the cycling performance of  $\text{LiNi}_{0.5}\text{Co}_{0.2}\text{Mn}_{0.3}\text{O}_2$  (NCM523)/ graphite 4.6V full cells, the electrolyte with DFEC/FEMC (1.0M  $\text{LiPF}_6$ ) inhibits the oxidation side reaction on the cathode and forms a vigorous SEI on the anode. The high voltage NCM523/Graphite cell utilizing the novel electrolyte exhibits excellent cycling durability under both room and evaluated (55°C) temperature. SEM was employed to study the morphology and elemental change on the interfaces. XRD was used to quantify and compare the loss of active lithium and the change of crystal parameter of NCM523.

**Keywords:** Cyclic fluorinated electrolyte; fluorinated substituents; oxidation stability;

LiNi<sub>0.5</sub>Co<sub>0.2</sub>Mn<sub>0.3</sub>O<sub>2</sub> cathode; high voltage lithium-ion batteries

### 3.1 Introduction

The development of lithium-ion batteries with high energy and power density is essential for the massive commercialization of electric vehicles. Therefore, new cathode materials with good thermostability, elevated operating voltages (4.6 V vs. Li<sup>+</sup>/Li) <sup>1-2</sup> and improved specific capacity <sup>3</sup> have been developed. After the first lithium nickel manganese cobalt oxide, LiNi<sub>1/3</sub>Co<sub>1/3</sub>Mn<sub>1/3</sub>O<sub>2</sub> (NCM333), was synthesized by Ohzuku's group in 2000, <sup>4</sup> extensive research on the development and improvement of new Ni-rich layered LiNi<sub>x</sub>Co<sub>y</sub>Mn<sub>z</sub>O<sub>2</sub> materials has been conducted <sup>4-13</sup>. Among these cathode materials, LiNi<sub>0.5</sub>Co<sub>0.2</sub>Mn<sub>0.3</sub>O<sub>2</sub> (known as NCM523) has attracted much attention due to its excellent thermostability and electrochemical performance, as well as high specific capacity. <sup>7, 12, 14-16</sup> However, the high temperature and high voltage (> 4.6 V vs. Li<sup>+</sup>/Li) instability of the state-of-the-art electrolyte, which contains 1.2 M lithium hexafluorophosphate (LiPF<sub>6</sub>) dissolved in a mixture of ethylene carbonate (EC) and dimethyl carbonate (DMC)/ethyl methyl carbonate (EMC), hinders the extensive application of these new cathode materials. <sup>17,18</sup> Several explanations for performance deterioration in conventional electrolyte have been suggested, including: (i) the low anodic stability of EC may lead to its continuous oxidation on the cathode surface, causing gassing and impedance issues. (ii) The regular carbonates, EC/EMC/DMC, show poor thermostability and limit the high temperature performance of the battery.

Conventionally, EC is considered to be an essential electrolyte component for Li-ion batteries to form a kinetic barrier passivating the graphite surface.<sup>19</sup> As a result, it is essential to design a new EC free electrolyte with promising anodic stability and thermostability. Researchers have been actively exploring new SEI former with elevated voltage stability<sup>20,21-22</sup>. Xia *et al* recently showed that the removal of EC from carbonated based electrolytes enable a good high voltage stability<sup>19, 23</sup>. Zhang *et al.*<sup>20, 24</sup> proposed a fluorinated electrolyte consisting of a mixture of fluorinated carbonates with a fluorinated ether for 5 V operation of LiNi<sub>0.5</sub>Mn<sub>1.5</sub>O<sub>4</sub> spinel cathode coupled with lithium titanate anode.

Among those studies, the superior anodic stability of fluorinated carbonates makes them highly promising candidates for high voltage electrolytes. The fluorinated substitution group typically makes molecule more resistant to anodic decomposition by increasing their oxidation potential due to its electron withdrawing effect. Moreover, most of the cyclic fluorinated carbonate can form a good kinetic barrier on the graphite anode to enable the long term cycling<sup>25</sup>. However, the role of this substitution in the fluorinated cyclic carbonates has not yet been systematically studied in detail.

In this work, fluorinated cyclic carbonates with different substituents including fluoroethylene carbonate (FEC), difluoroethylene carbonate (DFEC), trifluoropropylene carbonate (TFPC), 4-((2,2,3,3-tetrafluoropropoxy)methyl)-1,3-dioxolan-2-one (HFEEC) and 4-(2,2,3,3,4,4,5,5,5-nonafluoropentyl)-1,3-dioxolan-2-one (NFPEC) were designed, synthesized and evaluated. The performance of graphite/LiNi<sub>0.5</sub>Co<sub>0.2</sub>Mn<sub>0.3</sub>O<sub>2</sub> (NCM523) full cell using electrolyte containing

various fluorinated cyclic carbonates with FEMC and LiPF<sub>6</sub> salt was evaluated. All of the fluorinated cyclic carbonates were used in an attempt to form superior solid electrolyte interphases (SEI). Moreover, the superior properties of fluorinated cyclic carbonate based electrolyte over EC based electrolyte under high operation voltage on both room temperature and high temperature, 55°C were also presented.

### 3.2 Experimental

All measurements were carried out at 30 °C in an inert atmosphere and 55 °C evaluated temperature. Electrochemical cycling stability was evaluated using 2032 coin cells. The cathode was composed of 90 wt% LiNi<sub>0.5</sub>Co<sub>0.2</sub>Mn<sub>0.3</sub>O<sub>2</sub>, 5 wt% C45 carbon black, and 5 wt% Solvay 5130 polyvinylidene fluoride (PVDF) binder coated on aluminum foil. The active material loading was 9.15 mg/cm<sup>2</sup>. The graphite anode consisted of 89.8 wt% ConocoPhillips CGPA12, 4 wt% Super P-Li, 6 wt% Kureha 9300 PVDF binder, and 0.2 wt% oxalic acid that were coated on copper foil. The active material loading was 5.3 mg/cm<sup>2</sup>. Celgard 2325 was used as the separator. The effective diameters of the cathode, anode and separator were 14, 15, and 16 mm, respectively. Gen2 electrolyte containing 1.2 M LiPF<sub>6</sub> in 3:7 wt/wt mixture of ethylene carbonate (EC) and ethyl methyl carbonate (EMC) was used as the “baseline” electrolyte.

*3.2.1 Fluorinated cyclic carbonates.* Fluorinated cyclic carbonates such as tetrafluoropropyl-propylene carbonate-ether (TFP-PC-E) were synthesized along with corresponding fluorinated epoxides and carbon dioxide (CO<sub>2</sub> gas) according to a procedure in the literature <sup>26</sup>. In a typical procedure for TFP-PC-E, glycidyl 2,2,3,3-tetrafluoropropyl ether (Sigma-Aldrich, 7.52 g, 40 mmol, 1 equiv) and methyltriphenylphosphonium iodide (Sigma-Aldrich, 0.812 g, 2 mmol, 5

mol%) were dissolved in 8 mL of 1-methoxy-2-propanol and stirred at room temperature under a CO<sub>2</sub> atmosphere (1 atm). The reaction mixture was stirred at ambient condition for 4 days, until the conversion reached 96%, as detected by gas chromatography-mass spectrometry. The reaction solvent was then removed by a rotary evaporator. The crude product was dried over 4 Å molecular sieves, decanted, and purified by fractional distillation under reduced pressure. Pure product (99.8% by gas chromatography) was obtained as fractions (90-100 °C/0.2 mm Hg) with an isolated yield of 37% and 10 ppm water content as measured by Karl-Fischer titration. Fractions containing trace amounts (<0.5%) of starting materials were combined for further purification.

*3.2.2 Trifluoroethyl methyl carbonate (F-EMC).* The asymmetric fluorinated linear carbonates were synthesized from the corresponding fluorinated alcohols with methyl chloroformate following a procedure in the literature<sup>27</sup>. 2,2,2-trifluoroethanol (Sigma-Aldrich, 50.02 g, 0.5 mol, 1 equiv), triethylamine (Sigma-Aldrich, 55.65 g, 0.55 mol, 1.1 equiv), and 4-dimethylaminopyridine (Sigma-Aldrich, 0.61 g, 5 mmol, 1% mol) were mixed together in a round-bottom flask and cooled to 0 °C. Methyl chloroformate (Sigma-Aldrich, 47.25 g, 0.5 mol, 1 equiv) was added into the mixture dropwise via a syringe pump over the course of 6 h. The mixture was then allowed to warm up to ambient temperature and stirred for 24 h. The reaction was then quenched with 1N HCl solution, and the product was washed further with HCl and then brine solution. After being dried with 4 Å molecular sieves, the crude product was fractional distilled twice to obtain pure product (99.7% by gas chromatography) with an isolated yield of 50% and 15 ppm water content as measured by Karl-Fischer titration.

*3.2.3 Electrochemical testing* Galvanostatic charge/discharge cycling was conducted between 4.6 and 3.0 V cutoff voltages at C/3 rate following the two initial (“formation”) cycles carried out at C/10 rate. Cell voltage profiles and capacity were recorded using a MACCOR Electrochemical Analyzer (MIMSciEnt). The impedance spectra were obtained using a Solartron analyzer operated between 0.01 Hz and 1 MHz with the amplitude of 10 mV. Linear sweep voltammetry was performed using a Bio-Logic VMP3 station in a three-electrode configuration with Pt electrode (8 mm in diameter) as a working electrode and lithium metal as counter and reference electrodes; the scan rate was 10 mV/s.

*3.2.4 Post analysis* The cycled cells were disassembled in an argon-filled glovebox. The electrodes were thoroughly rinsed with anhydrous dimethyl carbonate and dried in a vacuum oven. The morphologies of the harvested electrodes were examined with scanning electron microscopy (SEM) using a Hitachi S-4700-II microscope in the Electron Microscopy Center of Argonne National Laboratory. Synchrotron X-ray Diffraction (SXRD) was performed to quantify the structure and compositions of electrode materials at beamline 11 ID D at Advanced Photon Source (APS) at ANL using X-ray wavelength of 0.7998 Å. Samples were attached to Kapton® tapes and measured in transmission mode. A PerkinElmer® amorphous silicon flat panel detector was used to collect two-dimensional XRD data.

### 3.3 Results and discussion

#### 3.3.1 Oxidative Stability

To determine the oxidation stability of different fluorinated cyclic carbonates shown in Figure 3.1, linear sweep voltammetry measurements were performed under room temperature and the results are displayed in Figure 3.2. To begin, linear carbonate F-EMC and  $\text{LiPF}_6$  were selected as the co-solvent and lithium salt respectively, because of their high anodic stability. The oxidation potential of the electrolytes containing different fluorinated cyclic carbonates (FEC, DFEC, TFPC, HFEEC and NFPEC) with FEMC and  $\text{LiPF}_6$  was evaluated by linear sweep voltammetry. For the baseline EC/EMC electrolyte, the anodic current increases drastically at 6.5 V, indicating the onset of solvent decomposition. Besides HFEEC, most of fluorinated cyclic carbonate based electrolytes showed higher voltage stability than the baseline electrolyte and the anodic stability follows the order  $\text{NFPEC} > \text{DFEC} > \text{FEC} > \text{TFPC} > \text{EC} > \text{HFEEC}$ , the same order as predicted from the quantum chemistry calculations considering the anion effect of  $\text{PF}_6^-$  we proposed before<sup>28</sup>. For HFEEC, although there is an electron-withdrawing tetrafluoroethyl group at the far end of the molecule, a  $-\text{CH}_2-\text{O}-\text{CH}_2-$  link separates the F-alkyl group from the carbonate ring; therefore, the electron-withdrawing effect is minimized. Moreover, the ether linkage  $-\text{CH}_2-\text{O}-\text{CH}_2-$  itself is vulnerable to oxidation as well.

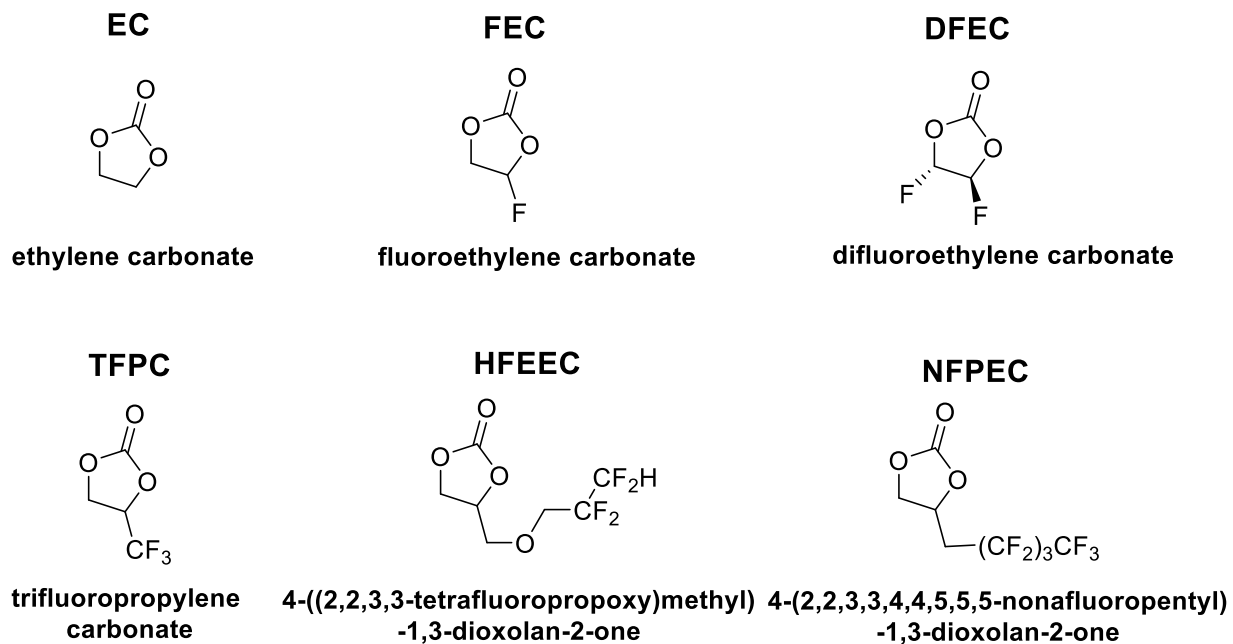


**Figure3.1.** Chemical structures for different cyclic carbonates.

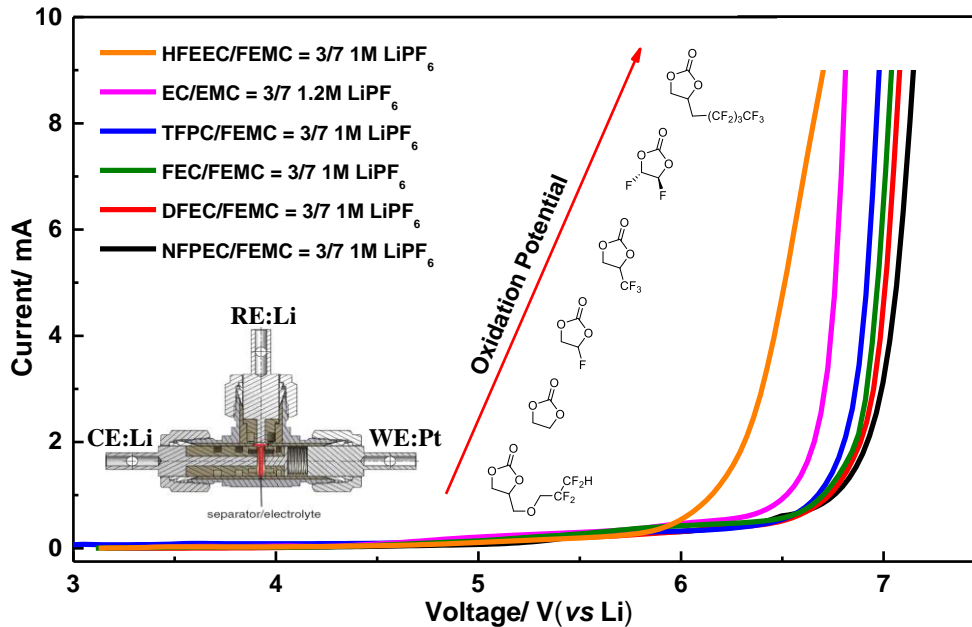


**Figure 3.2.** Linear oxidation sweep voltammogram of baseline electrolyte and fluorinated electrolytes containing different cyclic carbonates.

### 3.3.2 Conductivity

Conductivity is one of the most important properties of electrolyte because it affects the rate performance of the cell<sup>29-30</sup>. Together with the liquid range, conductivity also affects the evaluated temperature performance. Compared with SOA electrolyte, fluorinated electrolytes generally have lower conductivity depending on the degree of fluorination<sup>2, 17</sup>. Even with this negative effect, the conductivity of most fluorinated electrolyte is still within the same order of magnitude of the conductivity of SOA electrolyte. Figure 3.3 shows the ionic conductivity of the cyclic fluorinated carbonate based formulations as a function of temperature. The conductivity increased simultaneously with increasing temperature in the whole investigated temperature range. The fluorinated electrolytes containing FEC shows the highest ionic conductivity and the electrolyte comprising HFEEC or NFPEC shows relatively low ionic conductivity due to the

long fluorinated substituents and high viscosity. Meanwhile, DFEC or TFPC based electrolyte exhibits intermediate conductivity.

The temperature dependence of the conductivity also shows a typical non-Arrhenius behavior of liquid electrolytes and is well described by the VTF (Vogel–Tamman–Fulcher) function<sup>31-32</sup>. The applicability of the VFT function to the conductivity data also illustrates the close relationship between the conductivity and the viscosity of electrolytes.

$$\ln\sigma = \ln\sigma_0 + \frac{-B}{T - T_0}$$

In the VTF equation,  $\sigma_0$  is the pre-exponential factor,  $T_0$  represent the glass transition temperature, and T is the absolute temperature. B is related to the activation energy of ion transport associated with the configurational entropy of the electrolyte. The fitted VTF equation results are shown in table 3.1. The electrolyte containing HFEEC shows the highest activation energy of ion transport while the DFEC based electrolyte is the lowest.

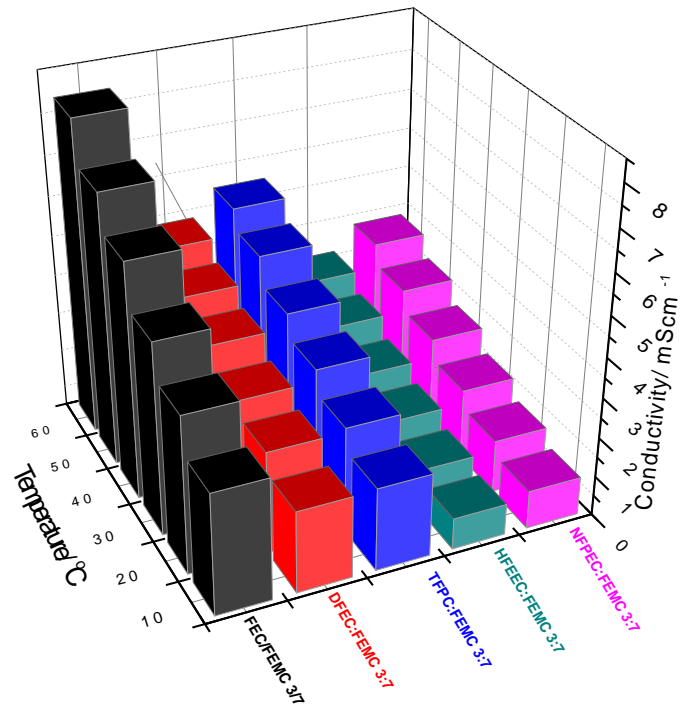


**Figure3.3** Conductivity measurement of different fluorinated electrolytes (1.0 M LiPF<sub>6</sub>).

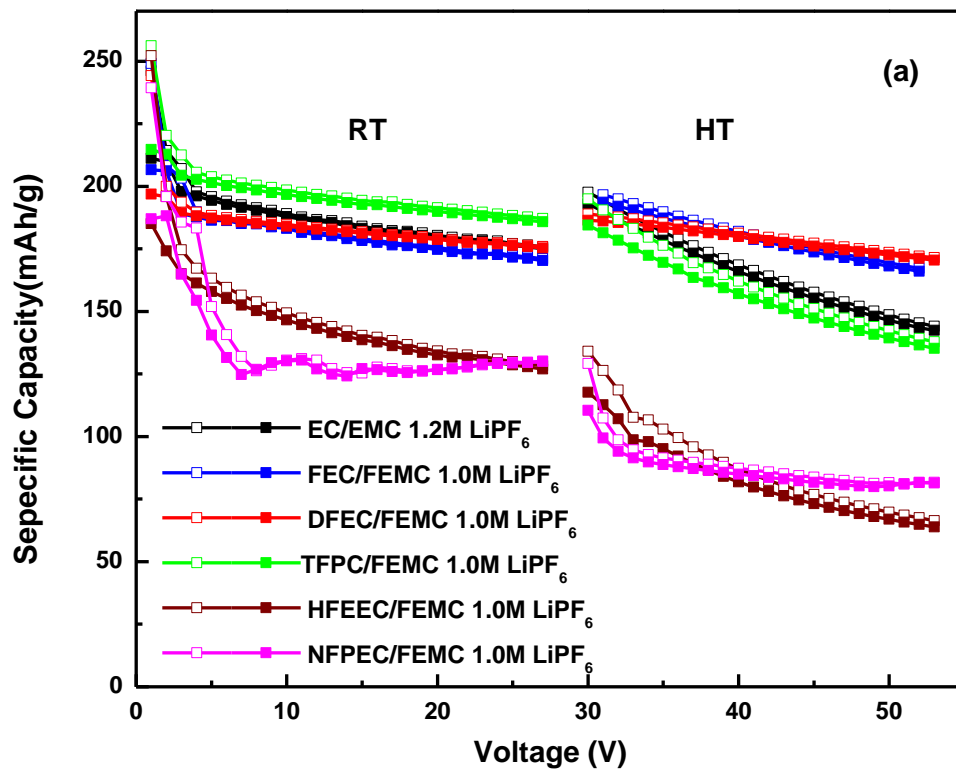
**Table 3.1: Fitted VFT Empirical equation results**

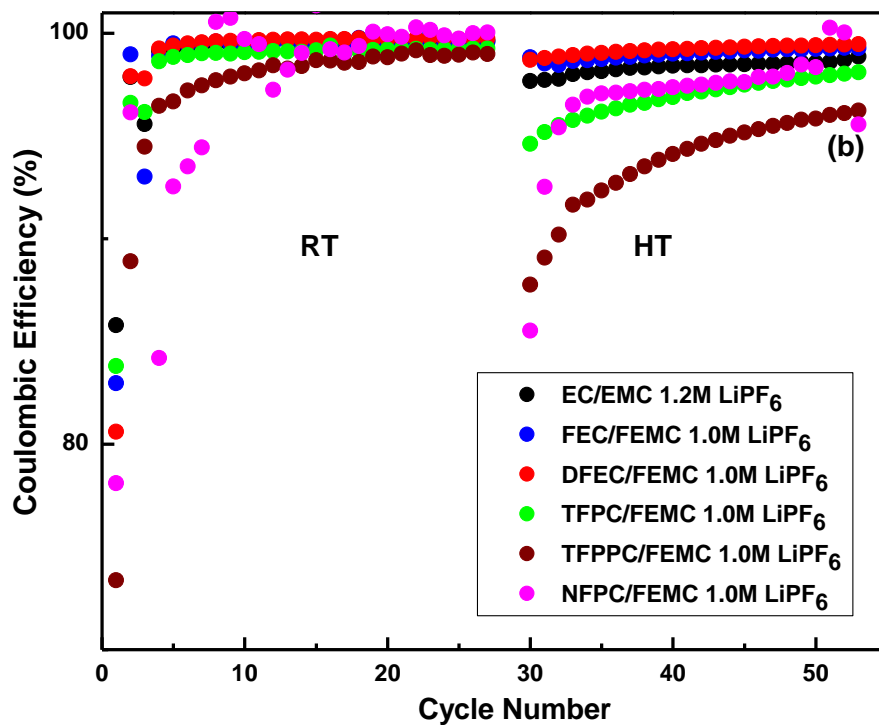
Electrolyte (1M LiPF <sub>6</sub> )	B (K)	$\sigma_0$ (mS/cm)	T <sub>0</sub> (K)
FEC:FEMC 3:7	317	59.7	177
DFEC:FEMC 3:7	226	19.5	183
TFPC:FEMC 3:7	251	27.8	186
HFEC:FEMC 3:7	517	54.4	161
NFPEC:FEMC 3:7	388	42.8	181

### 3.3.3 NCM523/graphite cell performance

LiNi<sub>0.5</sub>Co<sub>0.2</sub>Mn<sub>0.3</sub>O<sub>2</sub>/graphite cells were subjected to charge-discharge cycling at a rate of C/3 with the cutoff voltage between 4.6 V and 3.0 V. The first 25 cycles were tested under room temperature. To test the thermostability of different electrolytes, from the 26th to 50th cycle, the cell were put into a 55 °C oven. Figure 3.4a and b presents the cycling performance of these cells. 3.2 concludes the cell cycling performance detail in different electrolyte. For the baseline cell under room temperature, the initial charge and discharge capacities are 246 and 211 mAh/g, respectively (that corresponds to 85.7% Coulombic efficiency). The capacity retention is 84.5% after 25 room temperature cycles, and the Coulombic efficiency (CE) is maintained at 99.4% over 25 cycles. All of the cells cycled in the fluorinated electrolyte showed a lower 1<sup>st</sup> cycle CE compared with the baseline electrolyte, which follows the order HFEEC > NFPC > DFEC > FEC > TFPC. It is well known that SEI formation on graphite electrode leads to loss of Li<sup>+</sup> inventory causing the decrease in initial capacity. For the fluorinated cyclic carbonate based electrolytes, more active Li<sup>+</sup> ion might be consumed to form the SEI layer on the graphite surface during the first cycle because of the reductive reaction of the C-F bond. Furthermore, the formation of LiF on the electrode surface may increase the anode impedance at the same time. Under room temperature, TFPC, FEC and DFEC based electrolytes show similar capacity retention. Moreover, due to superior anodic stability, FEC and DFEC based electrolytes show higher CE than the baseline electrolyte. For the cell cycled with HFEEC based electrolyte, a low 1<sup>st</sup> cycle CE and high resistance surface lead to the dramatic capacity fade even at room temperature. For the cell cycled with NFPEC based electrolyte, due to the low anodic stability of NFPEC, it displays poor capacity retention and low CE.

It is well known that oxidative decomposition of organic solvents on the cathode surface causes the active lithium loss in the closed circuit<sup>33</sup>. This process depletes the lithium salt and changes the bulk properties of the electrolyte and will be accelerated under high temperature. As a result, both the Coulombic efficiency and capacity retention under high temperature cycling is always worse than those under room temperature cycling. However, the high temperature performance of LIBs is extremely important for the hybrid vehicles application. Unlike the room temperature performance, when the temperature was raised to 55 °C, the difference between fluorinated electrolytes containing TFPC, FEC or DFEC based electrolytes and the baseline electrolyte became clearly differentiated. The cell containing DFEC as the SEI former exhibits the highest Coulombic efficiency and the best capacity retention. Presumably, the electrolyte decomposition is suppressed due to the high oxidation potential of DFEC, and DFEC can form a good passivation SEI on the graphite anode, rendering the best electrochemical performance of the cell using DFEC based electrolyte.





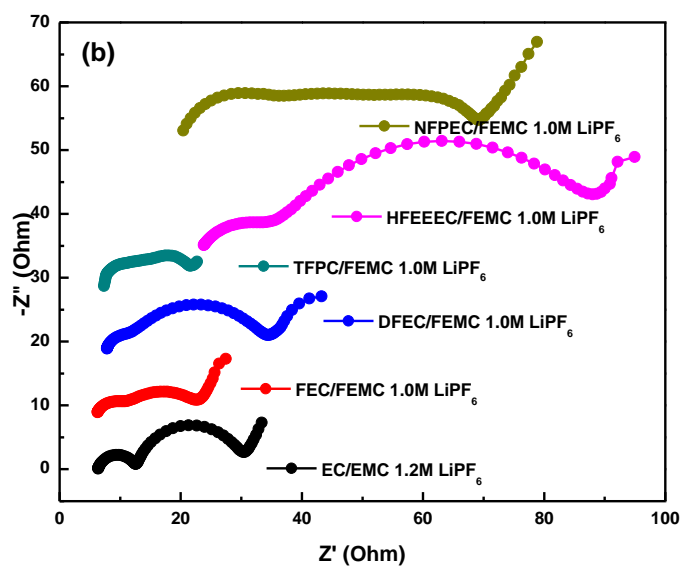
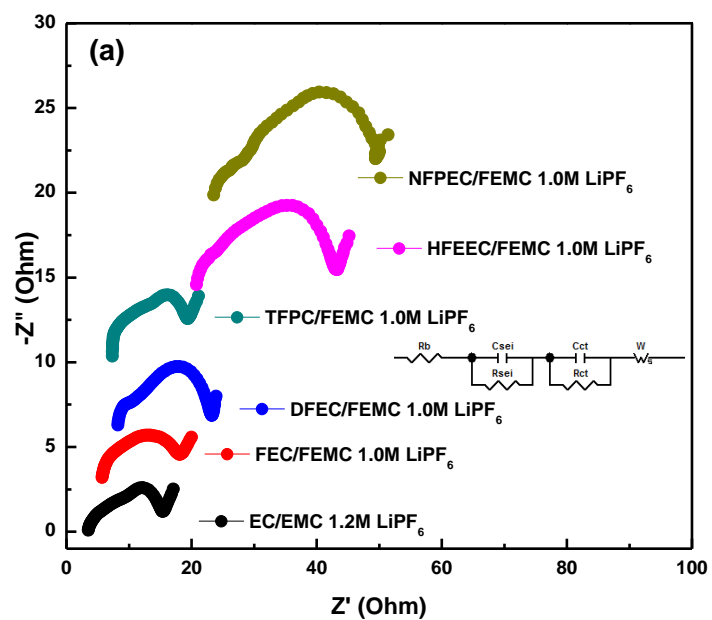
**Figure 3.4.** Electrochemical performance of  $\text{LiNi}_{0.5}\text{Co}_{0.2}\text{Mn}_{0.3}\text{O}_2/\text{graphite}$  cells containing different electrolytes under room/evaluate temperature. Panel (a) capacity retention and (b)Coulombic efficiency for these cells as a function of the cycle number.

Table 3.2. Data associated with Figure 3.4 (NCM523/Graphite, 3.0–4.6 V, 30°C+55°C) showing 1st cycle's coulombic efficiency (1st CE), 1st cycle's discharge capacity (1st DC), Capacity retention after 25 room temperature cycles (CR-RT) and Capacity retention after 25 55°C cycles (CR-HT) of the various electrolytes.

Electrolyte	1st CE	1st DC (mAh/g)	CR-RT	CR-HT
<b>EC/EMC 1.2M LiPF<sub>6</sub></b>	<b>85.72 %</b>	<b>211.1</b>	<b>89%</b>	<b>73.9%</b>
<b>FEC/FEMC 1.0M LiPF<sub>6</sub></b>	<b>82.96 %</b>	<b>206.6</b>	<b>89.9%</b>	<b>84.6%</b>
<b>DFEC/FEMC 1.0M LiPF<sub>6</sub></b>	<b>80.61 %</b>	<b>196.9</b>	<b>92.6%</b>	<b>91.3%</b>
<b>TFPC/FEMC 1.0M LiPF<sub>6</sub></b>	<b>83.81 %</b>	<b>214.6</b>	<b>90.6%</b>	<b>73.3%</b>
<b>HFEEC/FEMC 1.0M LiPF<sub>6</sub></b>	<b>73.38 %</b>	<b>185.0</b>	<b>76.9%</b>	<b>53.8%</b>
<b>NFPEC/FEMC 1.0M LiPF<sub>6</sub></b>	<b>78.09 %</b>	<b>194.9</b>	<b>77.7%</b>	<b>64.7%</b>

### 3.3.4 Electrochemical impedance spectroscopy (EIS)

Impedance spectroscopy was used to better understand the electrochemical performance of the electrode surfaces. The impedance spectra obtained after the room temperature formation, cycling and the subsequent high temperature cycling are shown in Figure 3.5a, b and c respectively, these impedance spectra consist of two partially overlapped semi-circles and a straight sloping line at low frequency end. The EIS can be fitted by the equivalent circuit shown in the inset of Figure 3.5a<sup>34-35</sup>. The  $R_{\text{bulk}}$  is the bulk resistance of the whole battery that represents the electric conductivity of the electrolyte, separator and electrodes. The semicircle at high frequencies is related with  $R_{\text{sei}}$  and  $C_{\text{sei}}$ , which are resistance and capacitance of the solid electrolyte interface on the electrodes.  $R_{\text{ct}}$  and  $C_{\text{ct}}$  are faradic charge-transfer resistance and its relative double-layer capacitance, which correspond to the semicircle at medium frequencies.  $W$  is the Warburg impedance which is related to a combination of the diffusional effects of lithium ion on the interface between the active material particles and electrolyte and is generally indicated by a straight sloping line at low frequency end. Total resistance ( $R_{\text{cell}}$ ) of the Li-ion cell, as shown in Figure 3.5a inset, is mainly contributed by the  $R_{\text{b}}$ ,  $R_{\text{sf}}$ , and  $R_{\text{ct}}$ , but not a simply summation of these three individual values. In this work, the  $R_{\text{cell}}$  value was directly fitted from the EIS. All of those resistances were estimated by fitting of the impedance spectra and given in Figure 3.5d. (Add more explanation)



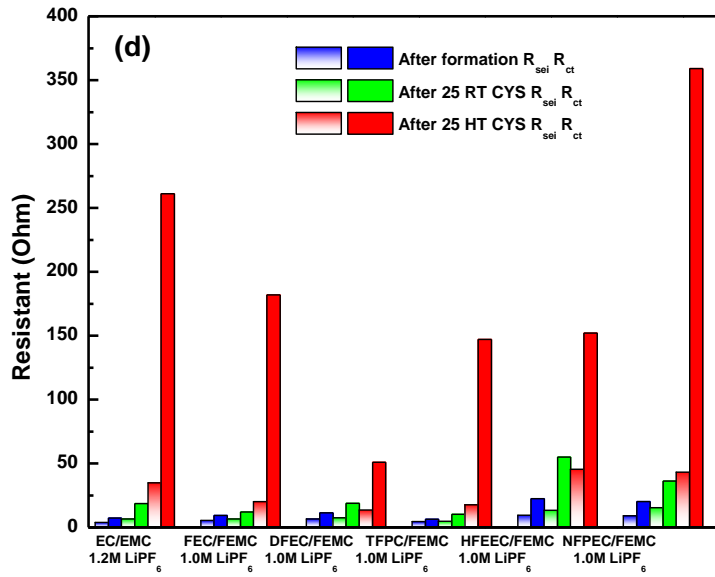
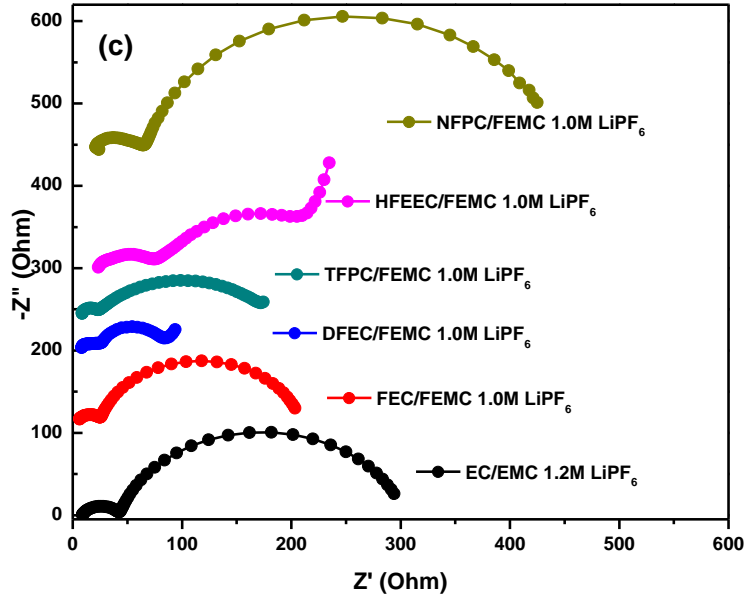


**Figure3.5.** Electrochemical impedance spectra for  $\text{LiNi}_{0.5}\text{Co}_{0.2}\text{Mn}_{0.3}\text{O}_2$ /graphite cells after the (a) two initial formation cycles (b) 25 room temperature cycles and (c) after 25 high temperature cycles in different electrolyte (d) summarized fitted data

### 3.5 Extended cycling performance and EIS Results

To further investigate the stability of the DFEC/FEMC electrolyte system, full cells were also cycled for longevity, 100 cycles, under both room temperature and 55 °C. Figure 3.6a compares the performance of NCM523/Graphite full cells assembled with conventional EC/EMC (1.2 M LiPF<sub>6</sub>) and DFEC/FEMC (1.0 M LiPF<sub>6</sub>) electrolytes. Both cells presented in Fig. 6a were operated and controlled under the same parameters, C/10 formation and C/3 cycling between 3.0-4.6V, for fair comparison. The cell cycled in the baseline electrolyte delivered 207 mAh/g discharge capacity and 84.9% 1<sup>st</sup> cycle CE. The cell cycled in DFEC/FEMC electrolyte showed similar initial charge capacity; however, a lower 79.8 % 1<sup>st</sup> cycle CE was obtained. Again, the difference in 1<sup>st</sup> cycle CE is attributed to the reaction of C-F bond and consumption of active Li<sup>+</sup> of the DFEC specie. However, this limitation is countered by unparalleled cycling stability. After 50 room temperature cycles, the cell cycled in GEN2 degraded and showed 79.6% capacity retention with the CE stabilized on 99.4%. In contrast, the cell cycled in DFEC/FEMC (1.0 M LiPF<sub>6</sub>) electrolyte showed remarkable stability, represented by the improved capacity retention of 90.2% and the high CEs around 99.7% for the first 50 room temperature cycles. Difference between the two electrolytes becomes noticeable under high temperature cycling followed by the room temperature cycling. Under 55°C cycling, the cell with baseline electrolyte suffered from severe irreversible lithium loss and the discharge capacity dropped from 186mAh/g to 115mAh/g with the CE around 98.5%. On the other hand, the cell with DFEC/FEMC (1.0 M LiPF<sub>6</sub>) electrolyte demonstrates better capacity retention, from 184mAh/g to 155mAh/g and higher average CE, 99.2%.

The impedance spectra obtained after the 50 room temperature cycles and the subsequent high temperature cycling are shown in Figure 3.6b. These impedance spectra also consist of two semi-

cycles and one straight line. These resistances were estimated by fitting of the impedance spectra using the equivalent circuits shown in the inset and are given in Table 3.3. After the 50 room temperature cycles, the cells with baseline electrolyte showed lower interfacial resistance and higher charge transfer resistance compared with the cell cycled in DFEC/FEMC electrolyte. After the subsequent 50 high temperature cycles, DFEC/FEMC cells displayed significantly lower surface and charge transfer resistances, suggesting that SEI derived from DFEC/FEMC electrolyte efficiently suppressed electrolyte decomposition (that normally results in the formation of thick, insulating deposits with large resistance). In contrast, the cells containing baseline electrolyte exhibited higher charge transfer resistance after the initial cycling, and this resistance became even greater upon the subsequent cycling, suggesting that the SEI derived from the baseline electrolyte was relatively less lithium ion conducting.

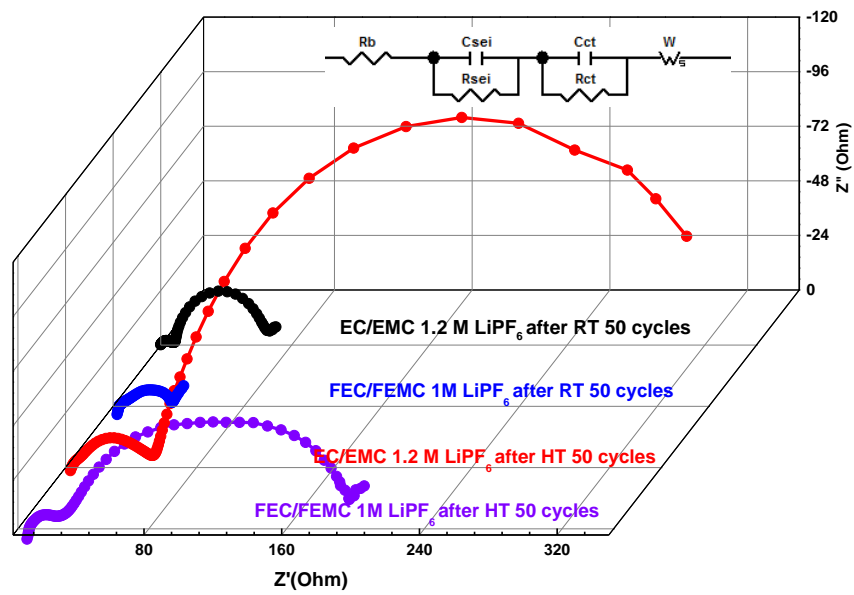
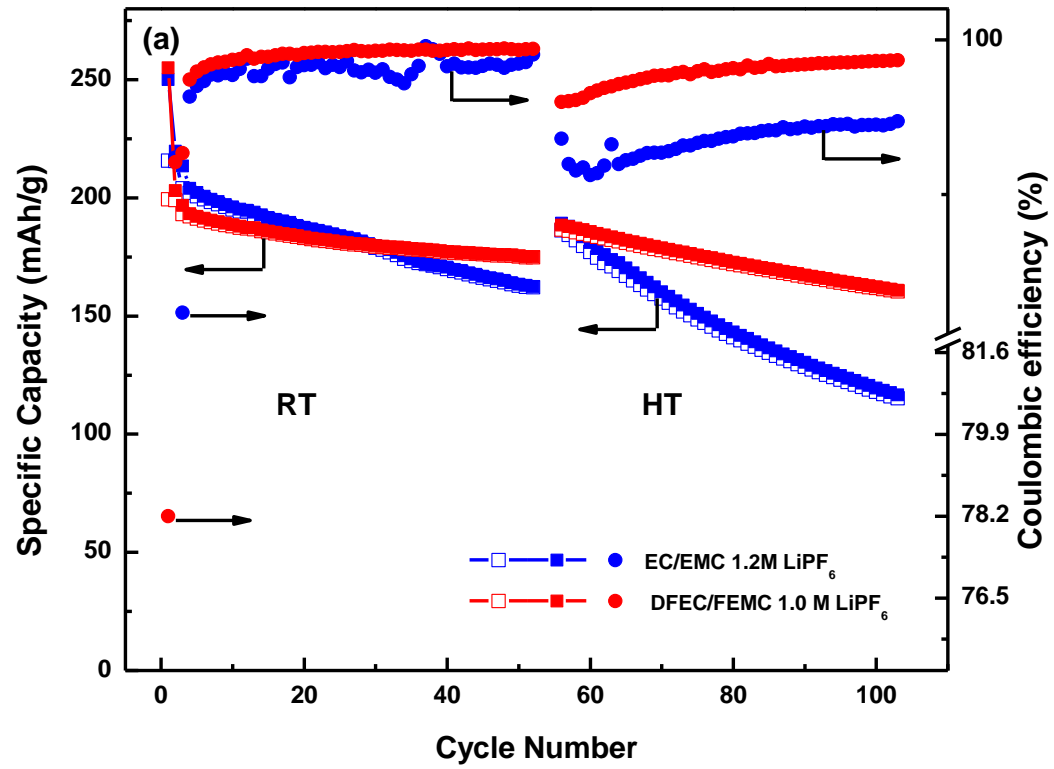


**Figure3.6.** Electrochemical performance of  $\text{LiNi}_{0.5}\text{Co}_{0.2}\text{Mn}_{0.3}\text{O}_2/\text{graphite}$  cells containing different electrolytes under room/evaluate temperature. Panel (a) capacity retention and Coulombic efficiency for these cells as a function of the cycle number. (b) Impedance spectra for  $\text{LiNi}_{0.5}\text{Co}_{0.2}\text{Mn}_{0.3}\text{O}_2/\text{graphite}$  cells after the 50 room temperature cycles and 50 high temperature cycles in different electrolyte.

**Table 3.3.** Estimates for interfacial and charge transfer resistances for the cell cycled in different electrolytes

Electrolyte	After room temperature cycling (Ohm)			After 55°C high temperature cycling (Ohm)		
	$R_{\text{bulk}}$	$R_{\text{sei}}$	$R_{\text{ct}}$	$R_{\text{bulk}}$	$R_{\text{sei}}$	$R_{\text{ct}}$
EC/EMC	4.83	9.3	54.8	8.15	57.63	363.68
DFEC/FEMC	7.3	15.6	29.5	10.48	21.858	183.61

### 3.6 Post mortem analyses of harvested electrodes

**3.6.1 SEM results** Figure3.7 shows the SEM images of the pristine anode and cathode, as well as the electrodes after cycling. In the pristine cathode (Figure3.7a), the secondary particle surface is clean and unobstructed. In the baseline electrolyte, the surface of the cycled cathode was covered with thick deposits (Figure3.7b), suggesting extensive electrolyte decomposition. The electrodes cycled in DFEC/FEMC electrolyte (Figure3.7c) exhibit compact layers; there is no indication of thick deposits due to electrolyte decomposition. On the anode side, clean layered graphite can be identified in the pristine electrode, as shown in Figure3.7d. The surface of the cycled graphite particle in the baseline electrolyte is fully covered with thick electrolyte decomposition byproducts as displayed in Figure3.7e. This observation suggests that effective SEI film cannot be formed. As a result, electrolyte decomposition proceeds dramatically and active lithium was consumed continuously<sup>33</sup>. Differently, the naked surface can be observed on

graphite particle in the cycled anode in fluorinated electrolyte, as shown in Figure 3.7f. Figure 3.8 shows the EDAX spectroscopy of the anodes cycled in different electrolyte. For the anode cycled in the baseline electrolyte, there is identifiable manganese peak on the anode surface. The manganese came from the transition metal dissolution of the cathode under high cut off voltage charging process<sup>36</sup> and reduced on the anode by forming  $\text{MnF}_2$ , Mn metal or  $\text{MnO}$ <sup>37-38</sup>. Moreover, the manganese plating will accelerate the electrolyte decomposing on the anode<sup>39</sup>, as a result, a thicker electrolyte decomposition layer was obtained from the electrode cycled in the baseline electrolyte. On the other hand, for the anode cycled in the fluorinated electrolyte, no manganese element was detected. Apparently, the preferential oxidation stability of fluorinated carbonates and the use of DFEC as the SEI former contribute to the formation of the protective SEI film on both anode and cathode.

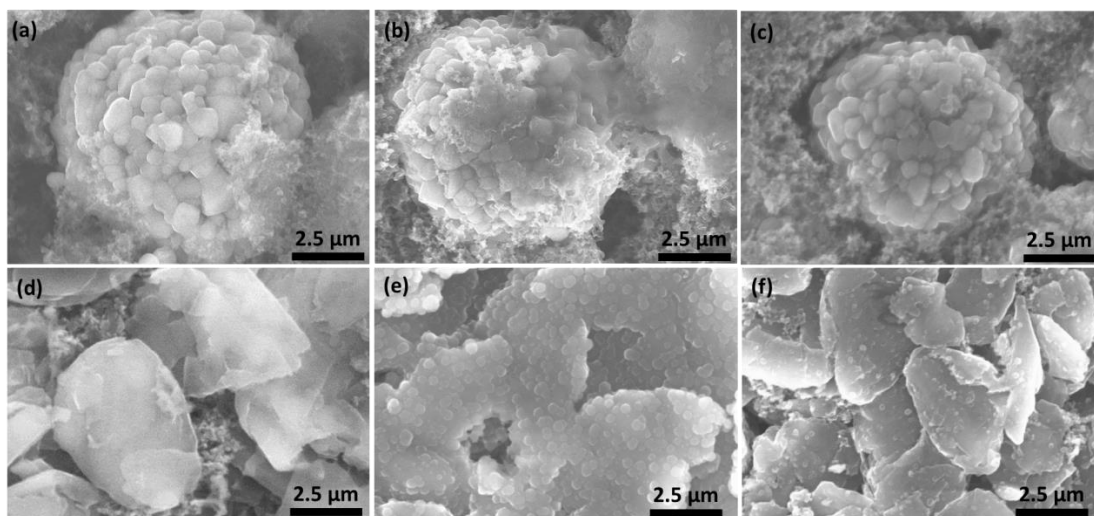


**Figure3.7.** SEM images of (a) NCM523 particles prior to the test, (b) the same materials from the cycled cell containing Gen2 electrolyte, (c) DFEC/FEMC 1.0M LiPF<sub>6</sub> electrolyte (d) (a) Graphite particles prior to the test, (e) the same materials from a cycled cell containing Gen2 electrolyte, (f) DFEC/FEMC 1.0M LiPF<sub>6</sub> electrolyte.

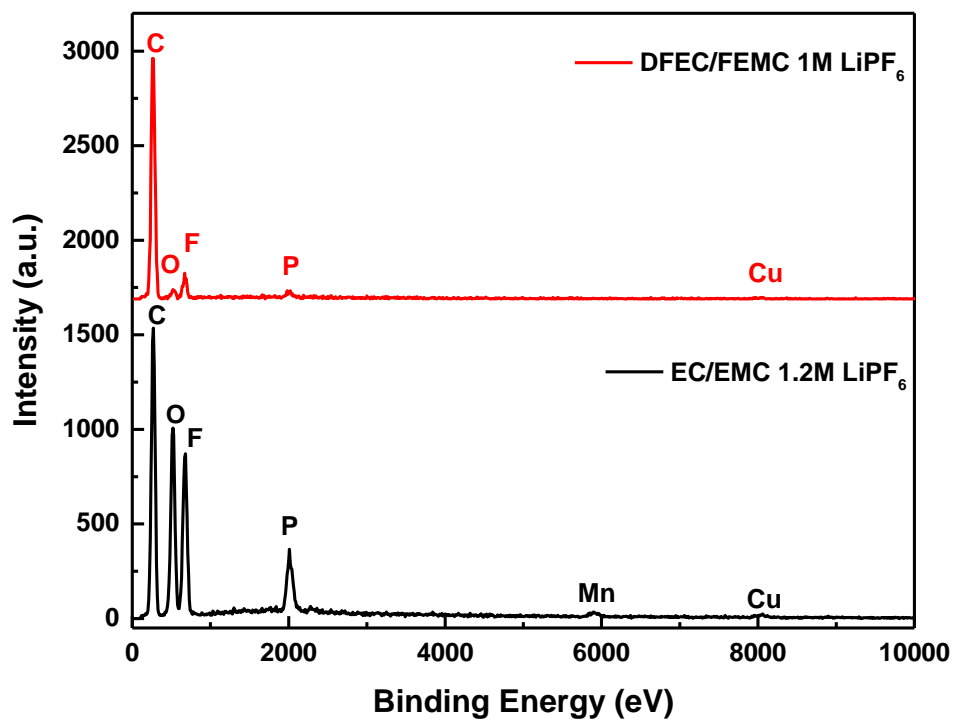


**Figure 3.8.** EDAX of the cycled anode in different electrolytes

### 3.6.2 Ex situ XRD analysis of cycled and fresh NCM523 electrodes

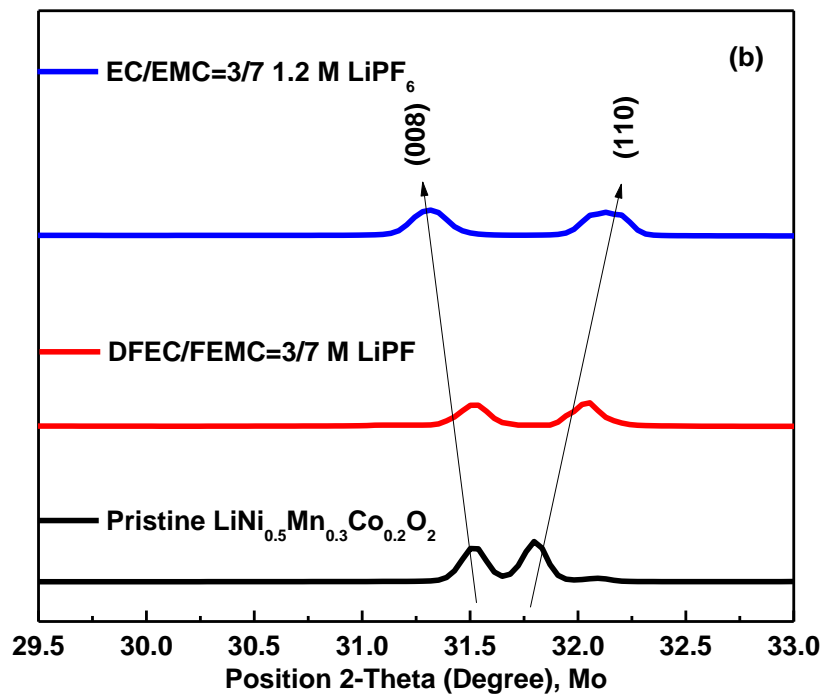
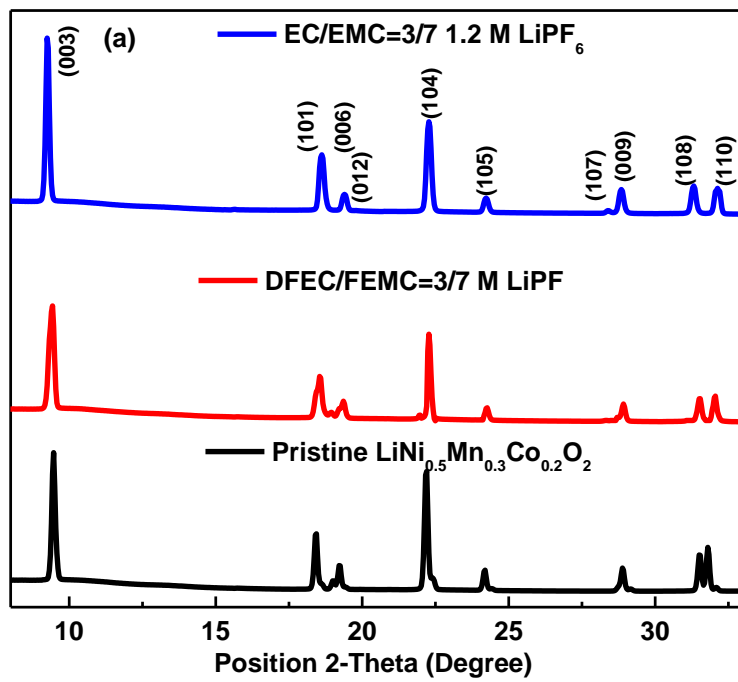
Figure 3.9a shows the XRD patterns of a pristine NCM523 electrode and the electrodes harvested in the discharge state after cycling in different electrolytes with 50 room temperature and 50 high temperature cycles. No additional bulk phase besides NCM523 was detected, indicating the absence of any severe structural damage to the NCM523 materials after cycling (note that possible surface structural changes would not be detectable in this analysis). The XRD results can be indexed and refined in the hexagonal  $R\bar{3}m$  space group.

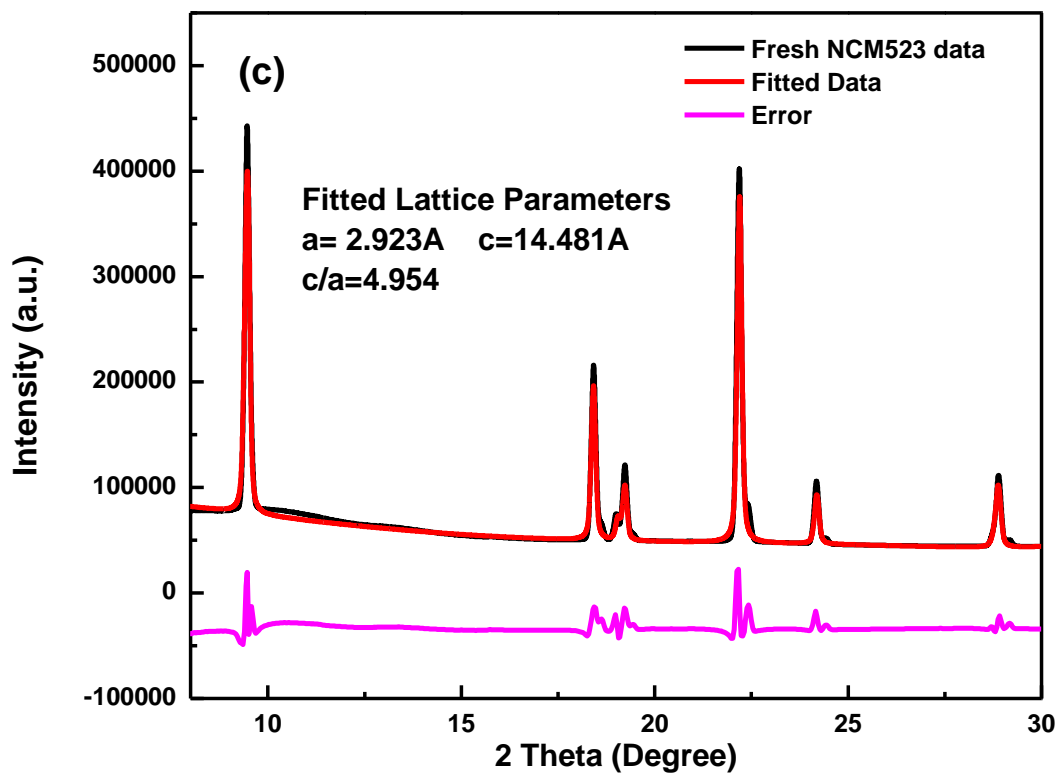
Comparing with the pristine electrode, the reflections of the harvested electrodes deviate from their original position, as clearly seen in the splitting of the (108) and (110) peaks in Figure 3.9b. These shifts can be correlated with the lattice shrinkage along a and b direction and the expansion along c direction of the unit cell<sup>40-42</sup>. The XRD refinement data are shown in Figure 3.9c, d and e. The fitting results of c/a ratio from the pristine electrode, harvest electrode cycled in DFEC/FEMC (1.0M LiPF<sub>6</sub>) and harvest electrode cycled in the baseline electrolyte are 4.954, 4.977 and 5.08 respectively.

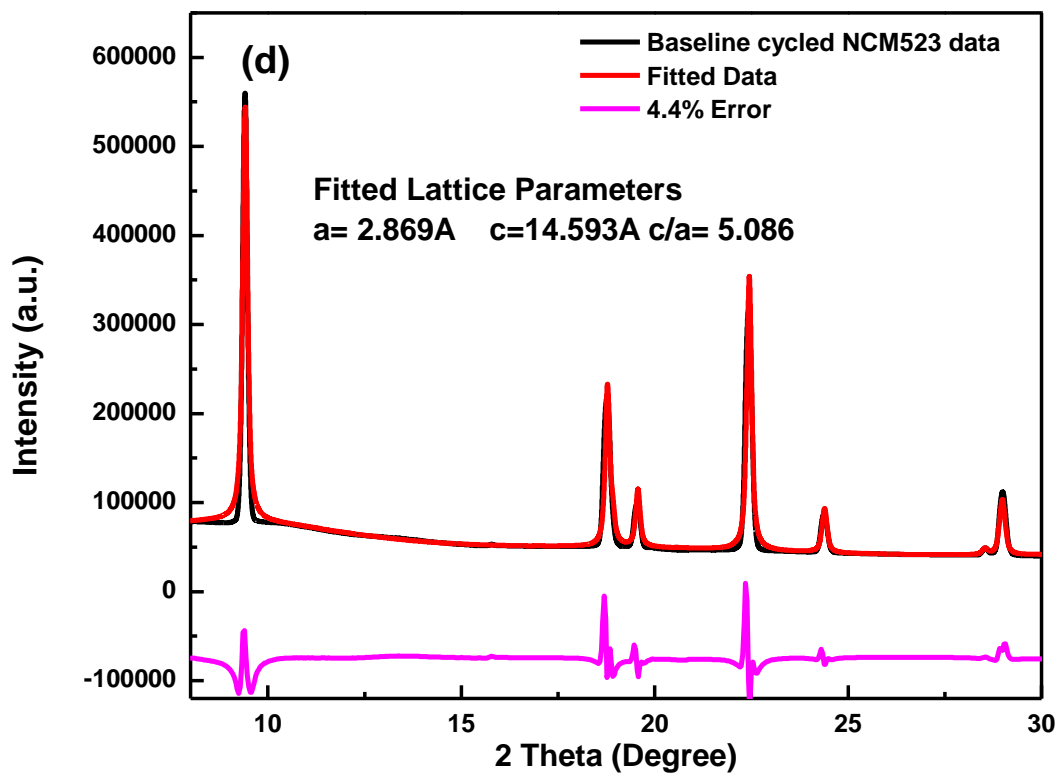
For the cell cycled in the fluorinated electrolyte, the small c/a ratio change is because of the irreversible lithium loss in the 1<sup>st</sup> cycle. During cycling, the cathode surface is effectively protected because of the preferable anodic stability of the electrolyte<sup>43</sup> and the robust negative electrode SEI formed by the reductive decomposition of DFEC.<sup>22, 44</sup> Consequently, it almost has no crystal parameter changes during cycling and both the capacity retention and specific capacity are more promising than those of the baseline electrolyte.

On the other hand, for the cell cycled in the baseline electrolyte, the change of the c parameter can be further attributed to the loss of active lithium during cycling<sup>45-46</sup>. For the LiMeO<sub>2</sub>

material, where Me refers to transition metal, the oxygen anions have a close-packed arrangement in ABCABC framework with transition metal cations located in the 6 coordinated octahedral crystal site. The slabs and Li layer are stacked alternatively<sup>47</sup>. The absence of lithium ions leads to the two negatively charged oxides layers losing the bonding connection with each other. As a result, the c parameter was increased. In the cell cycled in the baseline electrolyte, the active lithium is consumed continuously due to the unstable SEI on anode and low anodic stability on cathode. As a result, the amount of lithium ions that can intercalate back into the cathode decreased. To reach a valance balance, the decrease of lithium content in the cathode electrode leads to the increase of the overall transition metal valance state. The bond length of Ni<sup>2+</sup> is 0.69 Å and Co<sup>3+</sup> is 0.61 Å; meanwhile, the bond lengths are 0.56 Å and 0.53 Å for Ni<sup>3+</sup> and Co<sup>4+</sup> respectively<sup>48</sup>. The increase of the transition metal valance state also leads to the shrinkage of a and b parameters as indicated in the refined results.







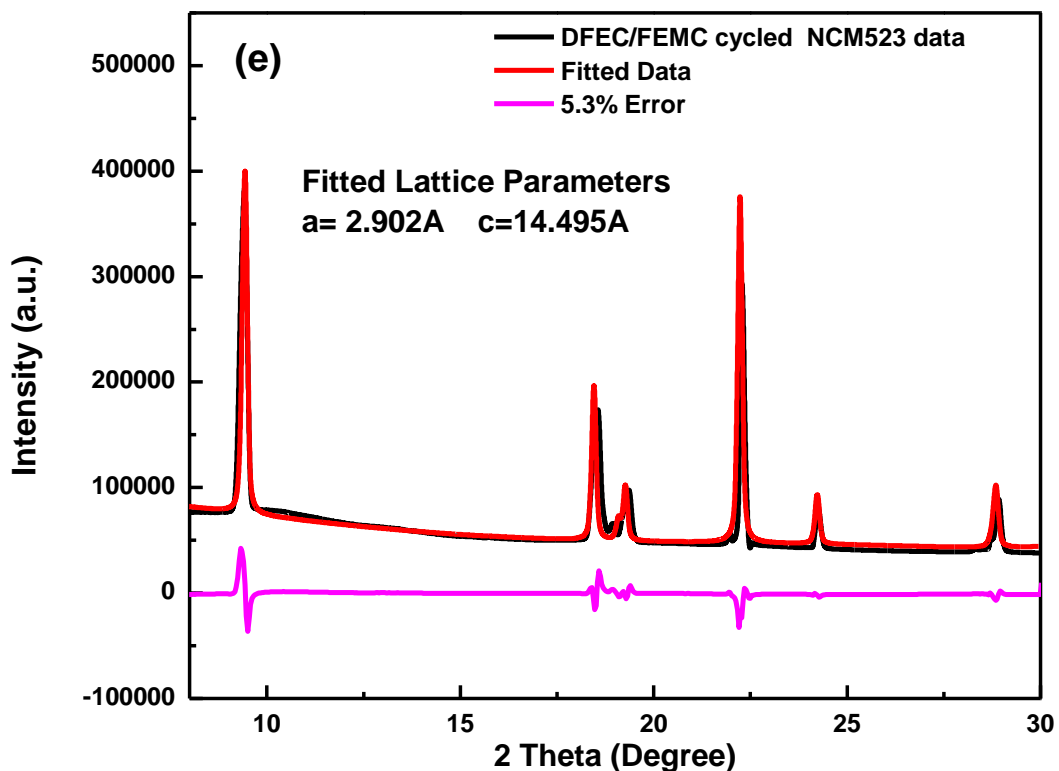


**Figure 3.8.** XRD patterns of the fresh NCM523 electrode and electrodes harvested in the discharged state after the cycling experiment: (a) complete diffractogram; (b) expanded view of the (1 0 8), (1 1 0) reflections. The fitted lattice parameters are: fresh NCM523 electrode:  $a = 2.923 \text{ \AA}$ ,  $c = 14.481 \text{ \AA}$ ; after baseline electrolyte cycling:  $a = 2.869 \text{ \AA}$ ,  $c = 14.593 \text{ \AA}$ ; after DFEC/FEMC 1M LiPF<sub>6</sub> cycling:  $a = 2.912 \text{ \AA}$ ,  $c = 14.495 \text{ \AA}$

### 3.7 Conclusion

In summary, a series of electrolytes containing fluorinated cyclic carbonates as the anode SEI former with trifluoroethyl methyl carbonate (F-EMC) and LiPF<sub>6</sub> have been designed, synthesized and evaluated. Linear sweep voltammetry has been used as an evaluation tool for the voltage

stability of the fluorinated cyclic carbonates. Among the cyclic carbonates screened, DFEC is the most stable solvent and the HFEEC is the least due to the vulnerability of its ether bond towards oxidation. The conductivity test result showed that long chain fluorinated substituents may lead to a low dielectric constant and high viscosity. The graphite/ NCM523 full cell using DFEC and FEC based fluorinated electrolytes displayed improved capacity retention and increased Coulombic efficiency compared to the cell using conventional electrolyte under both room and high temperature. The differences of electrochemical performance are much more pronounced at elevated temperature than room temperature. In order to better understand the performance enhancement for cells employing DFEC/FEMC (1M LiPF<sub>6</sub>) electrolyte, a series of interfacial analysis techniques were performed on the cycled electrodes with extended room and evaluated temperature (55 °C) cycling. The SEM images of the cell using fluorinated electrolyte show much cleaner surface and less decomposition on both graphite anode and NCM523 cathode compared to the cell using conventional electrolyte and the result is consistent with the lower interfacial impedance of the fluorinated electrolyte cell measured by EIS. The EDAX result indicates transition metal dissolution occurs in the cell using conventional electrolyte and is inhibited with the use of fluorinated electrolyte. Most importantly, bulk electrode analysis *via* SXRD was carried out to reveal the differences in the structural changes for the cathode electrodes of the cells using fluorinated electrolyte and conventional electrolyte. The SXRD findings indicate the use of fluorinated electrolyte assists the preservation of the crystal structure of NCM523 cathode by inhibiting the loss of active lithium during cycling. All of the results converge to the conclusion that the use of DFEC based electrolyte can form a good anode SEI, relieve the electrolyte decomposition, inhibit transition metal dissolution and facilitate the charge changes of the NCM523 cathode.

## References:

1. Hu, M.; Pang, X.; Zhou, Z., Recent progress in high-voltage lithium ion batteries. *Journal of Power Sources* **2013**, *237*, 229-242.
2. Xu, K., Nonaqueous liquid electrolytes for lithium-based rechargeable batteries. *Chemical reviews* **2004**, *104* (10), 4303-4418.
3. Santhanam, R.; Rambabu, B., Research progress in high voltage spinel  $\text{LiNi}_{0.5}\text{Mn}_{1.5}\text{O}_4$  material. *Journal of Power Sources* **2010**, *195* (17), 5442-5451.
4. Ohzuku, T.; Makimura, Y., Layered Lithium Insertion Material of  $\text{LiCo}_{1/3}\text{Ni}_{1/3}\text{Mn}_{1/3}\text{O}_2$  for Lithium-Ion Batteries. *Chem. Lett.* **2001**, *7*, 642-643.
5. Xu, K., Nonaqueous liquid electrolytes for lithium-based rechargeable batteries. *Chem. Rev.* **2004**, *104*, 4303-4418.
6. Zhang, S.; Ding, M. S.; Xu, K.; Allen, J.; Jow, T. R., Understanding solid electrolyte interface film formation on graphite electrodes. *Electrochem. Solid State Lett.* **2001**, *4*, A206-A208.
7. Xu, B.; Qian, D.; Wang, Z.; Meng, Y. S., Recent progress in cathode materials research for advanced lithium ion batteries. *Mater. Sci. Eng. Reports* **2012**, *73*, 51-65.
8. Lin, F.; Markus, I. M.; Nordlund, D.; Weng, T.-C.; Asta, M. D.; Xin, H. L.; Doeff, M. M., Surface reconstruction and chemical evolution of stoichiometric layered cathode materials for lithium-ion batteries. *Nat. Commun.* **2014**, *5*, 3529 (9 pages).
9. Mohanty, D.; Kalnaus, S.; Meisner, R. A.; Rhodes, K. J.; Li, J.; Payzant, E. A.; Wood III, D. L.; Daniel, C., Structural transformation of a lithium-rich  $\text{Li}_{1.2}\text{Co}_{0.1}\text{Mn}_{0.55}\text{Ni}_{0.15}\text{O}_2$  cathode during high voltage cycling resolved by in situ X-ray diffraction. *J. Power Sources* **2013**, *229*, 239-248.
10. Abe, K.; Yoshitake, H.; Kitakura, T.; Hattori, T.; Wang, H.; Yoshio, M., Additives-containing functional electrolytes for suppressing electrolyte decomposition in lithium-ion batteries. *Electrochim. Acta* **2004**, *49*, 4613-4622.
11. Sa, Q.; Gratz, E.; He, M.; Lu, W.; Apelian, D.; Wang, Y., Synthesis of high performance  $\text{LiNi}_{1/3}\text{Mn}_{1/3}\text{Co}_{1/3}\text{O}_2$  from lithium ion battery recovery stream. *J. Power Sources* **2015**, *282*, 140-145.
12. Chikkannavar, S. B.; Bernardi, D. M.; Liu, L., A review of blended cathode materials for use in Li-ion batteries. *J. Power Sources* **2014**, *248*, 91-100.
13. Huang, Z.-D.; Liu, X.-M.; Oh, S.-W.; Zhang, B.; Ma, P.-C.; Kim, J.-K., Microscopically porous, interconnected single crystal  $\text{LiNi}_{1/3}\text{Co}_{1/3}\text{Mn}_{1/3}\text{O}_2$  cathode material for Lithium ion batteries. *J. Mater. Chem.* **2011**, *21*, 10777-10784.
14. Le, A. V.; Wang, M.; Shi, Y.; Noelle, D.; Qiao, Y.; Lu, W., Effects of additional multiwall carbon nanotubes on impact behaviors of  $\text{LiNi}_{0.5}\text{Mn}_{0.3}\text{Co}_{0.2}\text{O}_2$  battery electrodes. *J. Appl. Phys.* **2015**, *118*, 085312 (5 pages).
15. Jung, S.-K.; Gwon, H.; Hong, J.; Park, K.-Y.; Seo, D.-H.; Kim, H.; Hyun, J.; Yang, W.; Kang, K., Understanding the degradation mechanisms of  $\text{LiNi}_{0.5}\text{Co}_{0.2}\text{Mn}_{0.3}\text{O}_2$  cathode material in lithium ion batteries. *Adv. Energy Mater.* **2014**, *4*, 1-7.
16. Sun, X.; Zhang, X.; Huang, B.; Zhang, H.; Zhang, D.; Ma, Y., ( $\text{LiNi}_{0.5}\text{Co}_{0.2}\text{Mn}_{0.3}\text{O}_2$  + AC)/graphite hybrid energy storage device with high specific energy and high rate capability. *J. Power Sources* **2013**, *243*, 361-368.

17. Xu, K., Electrolytes and interphases in Li-ion batteries and beyond. *Chemical reviews* **2014**, *114* (23), 11503-11618.
18. Xia, J.; Petibon, R.; Xiong, D.; Ma, L.; Dahn, J., Enabling linear alkyl carbonate electrolytes for high voltage Li-ion cells. *Journal of Power Sources* **2016**, *328*, 124-135.
19. Verma, P.; Maire, P.; Novák, P., A review of the features and analyses of the solid electrolyte interphase in Li-ion batteries. *Electrochimica Acta* **2010**, *55* (22), 6332-6341.
20. Zhang, Z.; Hu, L.; Wu, H.; Weng, W.; Koh, M.; Redfern, P. C.; Curtiss, L. A.; Amine, K., Fluorinated electrolytes for 5 V lithium-ion battery chemistry. *Energy & Environmental Science* **2013**, *6* (6), 1806-1810.
21. Xu, M.; Zhou, L.; Dong, Y.; Chen, Y.; DEMEAUX, J.; MacIntosh, A. D.; Garsuch, A.; Lucht, B. L., Development of Novel Lithium Borate Additives for Designed Surface Modification of High Voltage LiNi<sub>0.5</sub>Mn<sub>1.5</sub>O<sub>4</sub> Cathodes. *Energy & Environmental Science* **2016**.
22. Xu, M.; Zhou, L.; Hao, L.; Xing, L.; Li, W.; Lucht, B. L., Investigation and application of lithium difluoro (oxalate) borate (LiDFOB) as additive to improve the thermal stability of electrolyte for lithium-ion batteries. *Journal of Power Sources* **2011**, *196* (16), 6794-6801.
23. Meyer, W. H., Polymer electrolytes for lithium-ion batteries. *Advanced materials* **1998**, *10* (6), 439-448.
24. Zhang, Z.; Hu, L.; Wu, H.; Weng, W.; Koh, M.; Redfern, P. C.; Curtiss, L. A.; Amine, K., Fluorinated electrolytes for 5 V lithium-ion battery chemistry. *Energy Environ. Sci.* **2013**, *6*, 1806-1810.
25. Hu, L.; Xue, Z.; Amine, K.; Zhang, Z., Fluorinated electrolytes for 5-V Li-ion chemistry: synthesis and evaluation of an additive for high-voltage LiNi<sub>0.5</sub>Mn<sub>1.5</sub>O<sub>4</sub>/graphite cell. *Journal of The Electrochemical Society* **2014**, *161* (12), A1777-A1781.
26. Aoyagi, N.; Furusho, Y.; Endo, T., Effective synthesis of cyclic carbonates from carbon dioxide and epoxides by phosphonium iodides as catalysts in alcoholic solvents. *Tetrahedron Lett* **2013**, *54* (51), 7031-7034.
27. Dang, V. A.; Olofson, R. A.; Wolf, P. R.; Piteau, M. D.; Senet, J. P. G., A Simple Conversion of 1-Chloroethyl Carbonates to Fluoroformates - Value in the Preparation of Tertiary Alkyl Fluoroformates. *J Org Chem* **1990**, *55* (6), 1847-1851.
28. He, M.; Hu, L.; Xue, Z.; Su, C. C.; Redfern, P.; Curtiss, L. A.; Polzin, B.; von Cresce, A.; Xu, K.; Zhang, Z., Fluorinated Electrolytes for 5-V Li-Ion Chemistry: Probing Voltage Stability of Electrolytes with Electrochemical Floating Test. *Journal of The Electrochemical Society* **2015**, *162* (9), A1725-A1729.
29. Tarascon, J.-M.; Armand, M., Issues and challenges facing rechargeable lithium batteries. *Nature* **2001**, *414* (6861), 359-367.
30. Zhang, S. S., A review on the separators of liquid electrolyte Li-ion batteries. *Journal of Power Sources* **2007**, *164* (1), 351-364.
31. Vila, J.; Gines, P.; Pico, J.; Franjo, C.; Jimenez, E.; Varela, L.; Cabeza, O., Temperature dependence of the electrical conductivity in EMIM-based ionic liquids: evidence of Vogel–Tamman–Fulcher behavior. *Fluid Phase Equilibria* **2006**, *242* (2), 141-146.
32. Angell, C.; Smith, D., Test of the entropy basis of the Vogel-Tammann-Fulcher equation. Dielectric relaxation of polyalcohols near T<sub>g</sub>. *The Journal of Physical Chemistry* **1982**, *86* (19), 3845-3852.
33. Aurbach, D.; Markovsky, B.; Salitra, G.; Markevich, E.; Talyossef, Y.; Koltypin, M.; Nazar, L.; Ellis, B.; Kovacheva, D., Review on electrode–electrolyte solution interactions,

- related to cathode materials for Li-ion batteries. *Journal of Power Sources* **2007**, *165* (2), 491-499.
34. Xu, K.; Zhang, S.; Jow, R., Electrochemical impedance study of graphite/electrolyte interface formed in LiBOB/PC electrolyte. *Journal of power sources* **2005**, *143* (1), 197-202.
35. Zhang, S.; Ding, M. S.; Xu, K.; Allen, J.; Jow, T. R., Understanding solid electrolyte interface film formation on graphite electrodes. *Electrochemical and Solid-State Letters* **2001**, *4* (12), A206-A208.
36. He, M.; Su, C.-C.; Peebles, C.; Feng, Z.; Connell, J. G.; Liao, C.; Wang, Y.; Shkrob, I. A.; Zhang, Z., Mechanistic Insight in the Function of Phosphite Additives for Protection of LiNi<sub>0.5</sub>Co<sub>0.2</sub>Mn<sub>0.3</sub>O<sub>2</sub> Cathode in High Voltage Li-Ion Cells. *ACS Applied Materials & Interfaces* **2016**, *8* (18), 11450-11458.
37. Nguyen, D.-T.; Kang, J.; Nam, K.-M.; Paik, Y.; Song, S.-W., Understanding interfacial chemistry and stability for performance improvement and fade of high-energy Li-ion battery of LiNi<sub>0.5</sub>Co<sub>0.2</sub>Mn<sub>0.3</sub>O<sub>2</sub>/silicon-graphite. *Journal of Power Sources* **2016**, *303*, 150-158.
38. Zhan, C.; Lu, J.; Kropf, A. J.; Wu, T.; Jansen, A. N.; Sun, Y.-K.; Qiu, X.; Amine, K., Mn (II) deposition on anodes and its effects on capacity fade in spinel lithium manganate-carbon systems. *Nature communications* **2013**, *4*.
39. Qiao, R.; Wray, L. A.; Kim, J.-H.; Pieczonka, N. P.; Harris, S. J.; Yang, W., Direct Experimental Probe of the Ni (II)/Ni (III)/Ni (IV) Redox Evolution in LiNi<sub>0.5</sub>Mn<sub>1.5</sub>O<sub>4</sub> Electrodes. *The Journal of Physical Chemistry C* **2015**, *119* (49), 27228-27233.
40. Zheng, H.; Sun, Q.; Liu, G.; Song, X.; Battaglia, V. S., Correlation between dissolution behavior and electrochemical cycling performance for LiNi<sub>1/3</sub>Co<sub>1/3</sub>Mn<sub>1/3</sub>O<sub>2</sub>-based cells. *Journal of Power Sources* **2012**, *207*, 134-140.
41. Jung, S. K.; Gwon, H.; Hong, J.; Park, K. Y.; Seo, D. H.; Kim, H.; Hyun, J.; Yang, W.; Kang, K., Understanding the degradation mechanisms of LiNi<sub>0.5</sub>Co<sub>0.2</sub>Mn<sub>0.3</sub>O<sub>2</sub> cathode material in lithium ion batteries. *Advanced Energy Materials* **2014**, *4* (1).
42. Huang, Z.-D.; Liu, X.-M.; Oh, S.-W.; Zhang, B.; Ma, P.-C.; Kim, J.-K., Microscopically porous, interconnected single crystal LiNi<sub>1/3</sub>Co<sub>1/3</sub>Mn<sub>1/3</sub>O<sub>2</sub> cathode material for Lithium ion batteries. *Journal of Materials Chemistry* **2011**, *21* (29), 10777-10784.
43. Pham, H. Q.; Nam, K.-M.; Hwang, E.-H.; Kwon, Y.-G.; Jung, H. M.; Song, S.-W., Performance Enhancement of 4.8 V Li<sub>1.2</sub>Mn<sub>0.525</sub>Ni<sub>0.175</sub>Co<sub>0.1</sub>O<sub>2</sub> Battery Cathode Using Fluorinated Linear Carbonate as a High-Voltage Additive. *Journal of The Electrochemical Society* **2014**, *161* (14), A2002-A2011.
44. Zhu, Y.; Li, Y.; Bettge, M.; Abraham, D. P., Positive electrode passivation by LiDFOB electrolyte additive in high-capacity lithium-ion cells. *Journal of The Electrochemical Society* **2012**, *159* (12), A2109-A2117.
45. Petersburg, C. F.; Li, Z.; Chernova, N. A.; Whittingham, M. S.; Alamgir, F. M., Oxygen and transition metal involvement in the charge compensation mechanism of LiNi<sub>1/3</sub>Mn<sub>1/3</sub>Co<sub>1/3</sub>O<sub>2</sub> cathodes. *Journal of Materials Chemistry* **2012**, *22* (37), 19993-20000.
46. Castro, L.; Dedryvere, R.; Ledeuil, J.-B.; Bréger, J.; Tessier, C.; Gonbeau, D., Aging mechanisms of LiFePO<sub>4</sub>/graphite cells studied by XPS: redox reaction and electrode/electrolyte interfaces. *Journal of The Electrochemical Society* **2012**, *159* (4), A357-A363.
47. Ohzuku, T.; Makimura, Y., Layered Lithium Insertion Material of LiCo<sub>1/3</sub>Ni<sub>1/3</sub>Mn<sub>1/3</sub>O<sub>2</sub> for Lithium-Ion Batteries. *Chemistry Letters* **2001**, (7), 642-643.

48. Shizuka, K.; Kobayashi, T.; Okahara, K.; Okamoto, K.; Kanzaki, S.; Kanno, R., Characterization of  $\text{Li}_{1+y}\text{Ni}_x\text{Co}_{1-2x}\text{Mn}_x\text{O}_2$  positive active materials for lithium ion batteries. *Journal of Power Sources* **2005**, *146* (1), 589-593.

## **Chapter 4. Mechanistic Study of Fluorinated Electrolytes for High Voltage LiNi<sub>0.5</sub>Co<sub>0.2</sub>Mn<sub>0.3</sub>O<sub>2</sub> Cathode of Lithium ion Batteries**

### **Abstract**

Lithium ion batteries have dominated the portable electronics market and will potentially dominate large applications including hybrid and electric vehicles, as well as grid storage because of their high energy and power densities. It is well known that conventional electrolyte shows a poor anodic stability above 4.5V versus Li/Li<sup>+</sup>. However, high voltage electrolyte is technologically important for many applications such as hybrid and electrical vehicles, aerospace and power grids. As a result, high voltage electrolyte is essentially needed for the development of next generation lithium ion batteries. One possible solution is to develop the fluorinated electrolyte, which can kinetically suppress the oxidative decomposition of electrolyte due to their high oxidation potential. In this work, a novel fluorinated electrolyte was introduced in a graphite-LiNi<sub>0.5</sub>Co<sub>0.2</sub>Mn<sub>0.3</sub>O<sub>2</sub> 4.6V system. The electrolyte contains 1.0 M LiPF<sub>6</sub> dissolving in a mixture of FEC and HFDEC solvent, and 1wt % LiDFOB was used as the additive. Comparing with the conventional EC and EMC based electrolyte, the fluorinated electrolyte shows an excellent cycle life under 4.6V cut off voltage. SEM and XPS were employed to study the interface between the electrolyte and bulk electrode. The most definitive characterization in this work is to use the HR-XRD and XANS to investigate and compare the cycled bulk cathode electrode in different electrolyte. To the best of our knowledge, the structural changes of the cycled cathode materials in different electrolytes have never been reported before. Therefore, we believe this research is really an exciting scientific breakthrough for studying the interaction

between the electrolyte and electrode. And it could be potentially used as a direction to design and study the next generation lithium ion batteries electrolyte in the future.

**Keywords:** Fluorinated electrolyte; oxidation stability; electrochemical floating test;  $\text{LiNi}_{0.5}\text{Co}_{0.2}\text{Mn}_{0.3}\text{O}_2$  cathode; Synchrotron X ray technic

## 4.1 Introduction

Conventional lithium ion batteries (LIBs) with working voltage up to 3.7 V have been widely used in portable electronics.<sup>1</sup> They also show potentials for grid storage and transportation applications such as hybrid and full electric vehicles. To dominate large-scale electronic market it is necessary to increase the energy and power density of current LIBs, which can be achieved

by increasing the working voltage as energy density is proportional to the voltage,  $DE = \int_0^{DQ} V \cdot qdq$ ,

where  $E$  is the energy,  $V$  is the voltage and  $q$  is the charge. Therefore, the next generation batteries are expected to contain high voltage cathode materials (up to 4.8V),<sup>2-3</sup> and one promising cathode materials is  $\text{LiNi}_{1/3}\text{Co}_{1/3}\text{Mn}_{1/3}\text{O}_2$  (NCM) based layered oxides that were initially synthesized by Ohzuku's group in 2001.<sup>4</sup> In particular,  $\text{LiNi}_{0.5}\text{Co}_{0.2}\text{Mn}_{0.3}\text{O}_2$  (NCM523) shows good electrochemical performance and high specific capacity under high voltage,<sup>5-6</sup> thus catching much attention recently for scientific and industrial research. However, the electrolyte development in such high voltage battery has been the bottleneck. Among the three major components (cathode, anode and electrolyte) of a LIB, electrolyte plays an important role in facilitating the  $\text{Li}^+$  transportation and maintaining the voltage difference between the two electrodes. Conventional electrolytes (*e.g.*, 1.2 M  $\text{LiPF}_6$  in EC/EMC with volume ratio 3/7) show poor anodic stabilities above 4.5 V versus  $\text{Li}/\text{Li}^+$ .<sup>7</sup> At high cut-off voltages, the cathode material that contains active transition metal species (*i.e.*,  $\text{Ni}^{4+}$  and  $\text{Mn}^{4+}$ ) oxidizes conventional electrolytes and cause rapidly degradation of the cell electrochemical performance.<sup>8-10</sup> As a result, high voltage electrolytes are essential for the development of next generation high voltage lithium ion batteries.

In recent years, fluorinated electrolytes<sup>11</sup> have shown interesting properties as promising candidates to replace conventional electrolytes, as they not only form kinetically stable solid-electrolyte interphase (SEI), but also are resistant to oxidative decomposition due to their high oxidation potential.<sup>12-15</sup> A majority of scientific studies have been focused on finding a good combination of suitable fluorinated electrolytes and additives for NCM cathodes, and to understand effects for different electrolytes on battery performances. For example, Lee *et al.* showed that the addition of 5 wt % methyl(2,2,2-trifluoroethyl) carbonate (henceforth, FEMC) as an electrolyte, with 1.0M LiPF<sub>6</sub> in EC/EMC (3/7 volume ratio) and additive could improve the cycling performance as the FEMC can form a passivation layer and can prevent the transition metal from dissolution on the cathode material surface.<sup>16</sup> Using a combination of fluorinated cyclic, linear carbonates and a fluorinated ether, Zhang *et al.* improved the electrolyte stability when operating at 5 V using LiNi<sub>0.5</sub>Mn<sub>1.5</sub>O<sub>4</sub> spinel as the cathode and lithium titanate as the anode in a full cell setup.<sup>11</sup> They proposed that the introduction of fluorinated group into an organocarbonate results in the drop of energy levels for both the highest occupied molecular orbital and the lowest unoccupied molecular orbital, thus simultaneously leading to better oxidation stability and higher reduction potential as compared to electrolytes without fluorinated group. In addition, Zhu *et al.* have shown that the cycling performance of graphite- Li rich NCM cell can be improved by incorporating 2 wt % LiDFOB as an electrolyte additive,<sup>17</sup> as the addition of LiDFOB could form a thin but robust SEI at the anode electrode to maintain cell capacity, and form a thick passivation layer on the cathode to further prevent the transition metal dissolution.

However, most of these works focused mainly on the understanding of the interface between the electrolyte and electrode,<sup>1, 7, 18-21</sup> such as using X-ray photoelectron spectroscopy (XPS) and

Fourier transform infrared spectroscopy (FTIR) to identify the functional groups on the surface,<sup>22-23</sup> and using scanning electron microscopy (SEM) and transmission electron microscopy (TEM) to study the morphology of the surface<sup>24</sup>. Although interfaces are important parts of LIBs, the Li<sup>+</sup> intercalation and battery performance are strongly correlated to bulk electrode changes. Recent studies have revealed that the irreversible capacity loss not only are related to the electrolyte decomposition on the surface or the loss of active Li ion, but also can be attributed to the change of bulk electrode structure.<sup>1</sup> It is, therefore, vital to understand the changes of bulk electrodes when using different electrolytes, which can help identify the key functions of electrolytes to design novel electrolyte for high voltage battery applications. Herein, we investigate the commercialized electrolyte (1.2 M LiPF<sub>6</sub> in EC/EMC) and fluorinated electrolyte (1.0 M LiPF<sub>6</sub> in FEC/HFDEC with 1 wt % LiDFOB) for a 4.6 V LiNi<sub>0.5</sub>Co<sub>0.2</sub>Mn<sub>0.3</sub>O<sub>2</sub>-graphite system, and compare the electrochemical performance of both fluorinated and non-fluorinated electrolyte. Besides conventional SEM, XPS and nuclear magnetic resonance (NMR) characterizations, synchrotron X-ray diffraction (SXRD) was employed to study the crystallographic phase changes of the cathode materials. To better understand the oxidation states of transition metals at different battery charging/discharging states, X-ray absorption spectroscopy (XAS) were performed on NCM cathodes used for different electrolytes. To our best knowledge, it is the first systematical investigation of electrochemical performance and bulk cathode material changes under different electrolytes to reveal the detailed mechanism. Our findings provide insights for the design of advanced electrolyte used in the next generation lithium ion batteries.

## **4.2 Material and methods**

Electrochemical cycling ability of the cell was evaluated using 2032 coin cells. The cathode was made of 90wt% NCM 523, 5wt% C45, and 5wt% Solvey 5130 polyvinylidene fluoride (PVDF) binder coated on aluminum foil. The active material loading averaged  $9.15 \text{ mg cm}^{-2}$ . The graphite anode was made of 89.8 wt% Conoco Phillips CGPA12, 4 wt% Super P-Li, 6 wt% Kureha 9300 PVDF binder, and 0.2 wt% oxalic acid coated on copper foil. The active material loading averaged  $5.3 \text{ mg cm}^{-2}$ . polypropylene/polyethylene/polypropylene (PP/PE/PP), Celgard 2325, was used as the separator. The effective diameters of cathode, anode and separator were 14mm, 15mm and 16mm, respectively. 1.2 M  $\text{LiPF}_6$  in ethylene carbonate (EC): ethyl methyl carbonate (EMC) (3:7 volume ratio) and GEN2 electrolyte were used as the baseline electrolyte. The fluorinate electrolyte was made of 1.2M  $\text{LiPF}_6$  in fluoroethylene carbonate (FEC): di-trifluoroethyl carbonate (HFDEC) (5:5 volume ratio) with 1 wt % LiDFOB as the additive.

Galvanostatic charge-discharge cycling tests were conducted on Maccor Electrochemical Analyzer (MIMSciEnt) with voltages in-between 3.0V and 4.6V at 0.3C after 2 formation cycles at 0.1C using a full cell setup, namely  $\text{LiNi}_{0.5}\text{Co}_{0.2}\text{Mn}_{0.3}\text{O}_2$  as the cathode and graphite as the anode. Impedance measurements were tested at 30 °C that was maintained by an oven. The spectra were collected using an Solartron impedance analyzer in the frequency range from 1M Hz to 0.01 Hz, with an amplitude of 10 mV.

For *ex situ* analysis on electrode materials at different charge-discharge states, the cycled cells were disassembled in the glove box, and the electrodes were washed with anhydrous DMC to remove residual EC and salt, followed by drying overnight at the glove box. The morphologies of the electrodes after cycling were investigated by SEM using a Hitachi S-4700-II microscope

in the Electron Microscopy Center, Argonne National Laboratory. XPS measurements were carried out at with an Omicron ESCA probe using Al K $\alpha$  as the monochromated X-ray source. A low-energy electron flood gun was used to compensate the surface charging effects. Carbon 1s (284.8 eV) was used as reference to calibrate the XP spectra.

Synchrotron X-ray Diffraction (SXRD) was performed to quantify the structure and compositions of electrode materials at beamline 17-BM at Advanced Photon Source (APS) at ANL using X-ray wavelength of 0.72768 Å. Samples were attached to Kapton® tapes and measured in transmission mode. A PerkinElmer® amorphous silicon flat panel detector was used to collect two-dimensional XRD data. Integration of the 2D data to conventional plots of intensity versus 2-theta, which was converted to a 2-theta values at X-ray wavelength of 1.5406 Å (Cu K $\alpha$ 1 source) for the convenience of comparison with reference database.

*Ex situ* X-ray absorption near edge spectroscopy (XANES) and extend X-ray absorption fine structure (EXAFS) experiments were carried out at beamline 9BM-C of APS at ANL. The following electrode materials were used: pristine NCM523 (called pristine in the rest discussion), NCM523 cathodes discharged in GEN2 electrolyte at 3V (G2\_3V) and charged at 4.6 V (G2\_4.6V) after 100 cycles, and NCM523 cathodes discharged in fluorinated electrolyte at 3V (F\_3V) and charged at 4.6 V (F\_4.6V) after 100 cycles. Samples were placed in a chamber with helium flow as the protection. All data were collected in transmission mode. A Lytle detector was used to collect all transition metal X (X=Ni, Mn, and Co) while the Si(111) monochromator scanned the incident X-ray photon energy through X K-edge absorption edge. The monochromator was detuned to 80% of the maximum intensity at X K edges to minimize the

presence of higher harmonics. The X-ray beam was calibrated using the corresponding transition metal foil K edges, namely Ni, Mn and Co foils. Data reduction and data analysis were performed with the Athena software packages. Standard procedures were used to extract the EXAFS data from the measured absorption spectra. The pre-edge was linearly fitted and subtracted. The post-edge background was determined by using a cubic-spline-fit procedure and then subtracted. Normalization was performed by dividing the data by the height of the absorption edge at 50 eV.

### **4.3. Results and discussion**

#### *4.3.1. Electrochemical performances*

Figure 4.1 summarizes the chemical structure and acronym of the fluorinated carbonate solvents, non-fluorinated carbonate solvents, lithium salt and electrolyte additive used in this study. Fluorinated cyclic carbonate fluoroethylene carbonate (FEC), linear fluorinated carbonate bis(2,2,2-trifluoroethyl) carbonate (HFDEC) and lithium difluoro(oxalato) borate (LiDFOB) were synthesized in our lab and purified by fractional vacuum distillation and recrystallization prior use. 1.0 M LiPF<sub>6</sub> FEC/HFDEC (5/5 in volume) with 1.0% LiDFOB was formulated in the Argon-filled glove-box.

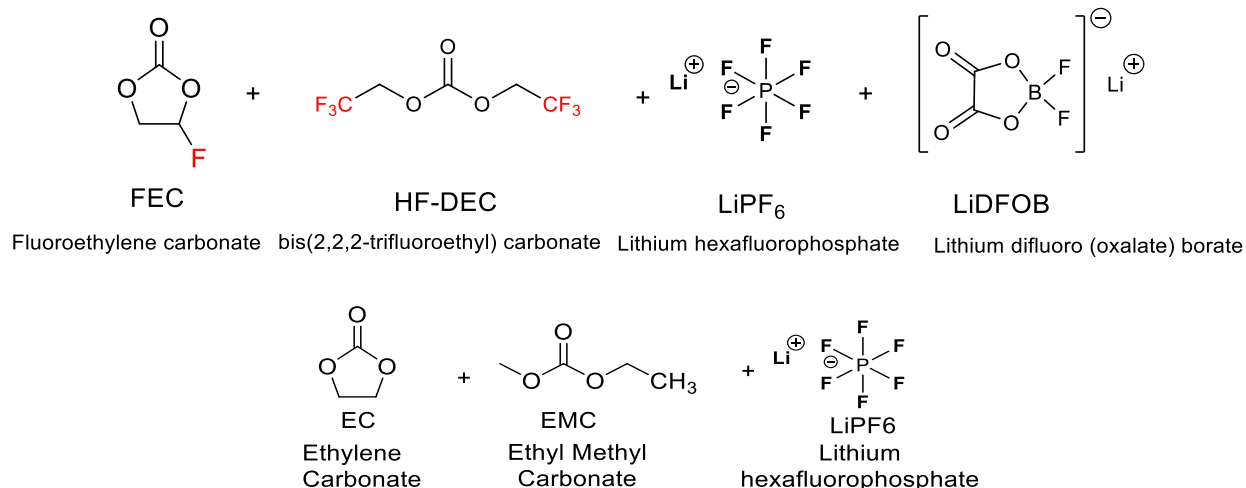
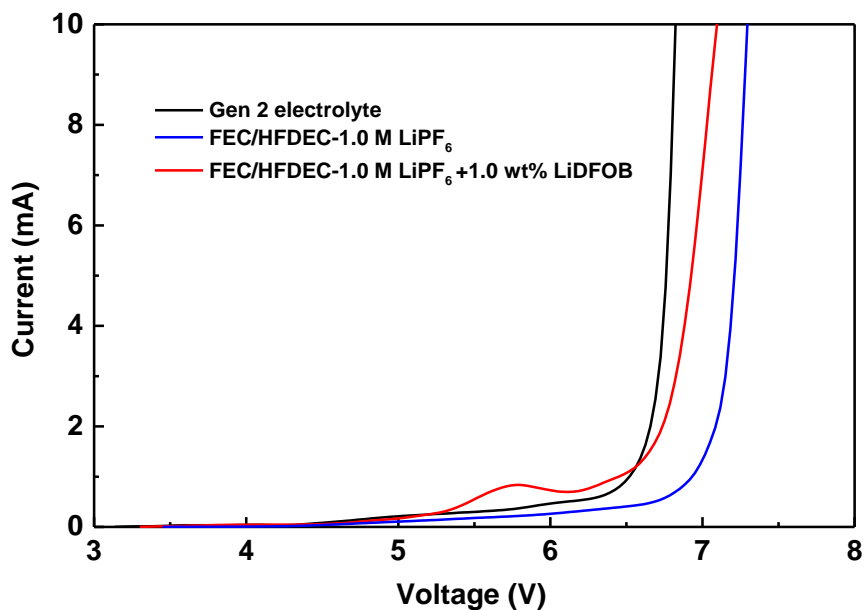


Fig.4.1. Chemical structures and names of carbonates and salt used in the electrochemical test.

### Linear Sweep Voltammetry (LSV) of the Electrolytes.

Substitution groups of fluorine (-F) on FEC molecule and fluorinated alkyl (-CH<sub>2</sub>CF<sub>3</sub>) on HFDEC molecule exert strong electron-withdrawing effect on the carbonate core and lower the HOMO energy level of the solvents based on the quantum chemistry simulation. Oxidation stability is the important criteria in designing high voltage electrolyte<sup>25-26</sup>. Linear sweep voltammetry (LSV) using an inert working electrode of platinum was first performed on the formulated fluorinated electrolyte and the GEN 2 electrolyte with a scan rate of 10 mV/s. Figure 4.2 presents the LSV voltammograms covering the voltage window from 3-7 V vs Li<sup>+</sup>/Li. The drastic increase of the oxidation current was observed for the GEN 2 electrolyte at 6.85 V indicating the main oxidative decomposition of the carbonate solvents. For the fluorinated electrolyte, the same oxidation current was observed at a delayed voltage of 7.05 V. Based on the density function theory (DFT) calculation,<sup>13</sup> the theoretical oxidation potential of EC and EMC are 6.95 V and 6.91 V, respectively. Comparatively, the oxidation potential of FEC and HFDEC were calculated to be 7.24 V and 7.25 V, respectively, a 0.2-0.3 V higher than that of the Gen 2 electrolyte. The thermodynamic stability of the fluorinated electrolyte is expected to stabilize the

cathode/electrolyte interface thus suppress the parasitic reactions causing ultimate transition metal ion dissolution.

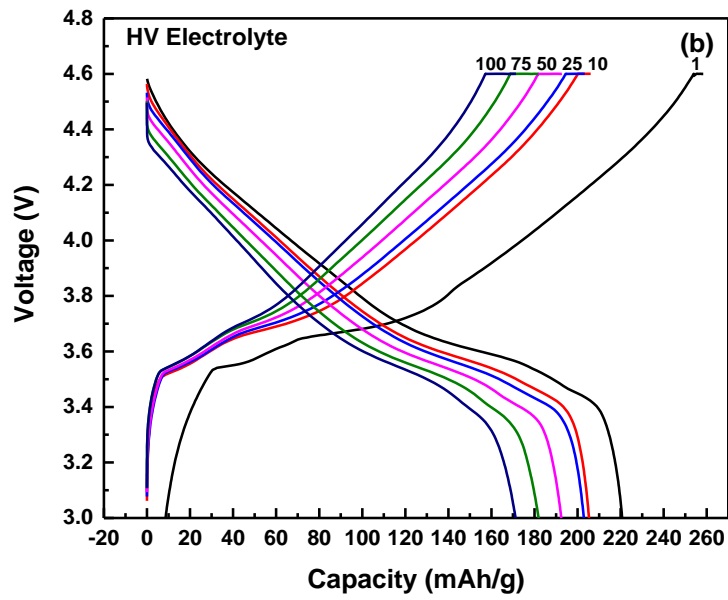
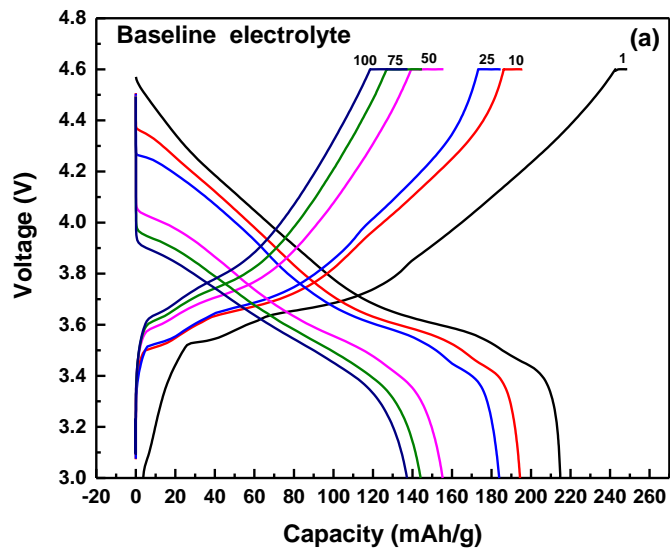


**Figure 4.2.** Linear sweep voltammograms of fluorinated electrolytes with a scan rate of 10 mV/s. Inset shows an expansion of the electrolyte oxidation peaks from 3-5 V vs. Li<sup>+</sup>/Li. Three-electrode cell with Pt (disc with a diameter of 2 mm) as working electrode and Li as reference and counter electrodes.

#### **Stable cycling of a NCM523/graphite cell charged to 4.6 V**

In addition to the enhanced oxidation stability on an inert working electrode, the 1.0 M LiPF<sub>6</sub> FEC/HFDEC fluorinated electrolyte showed excellent performance in a NCM523/graphite full cell cycled at a rate of C/3 with voltage window from 3.0 to 4.6 V.

Figure 4.3a and 3b show the charge and discharge voltage profiles for the 1<sup>st</sup>, 10<sup>th</sup>, 25<sup>th</sup>, 50<sup>th</sup>, 75<sup>th</sup> and 100<sup>th</sup> cycle for Gen 2 electrolyte and fluorinated electrolyte. It is manifest that the voltage polarization for both charging and discharging process increases significantly for Gen 2 cell<sup>27</sup>, while much less polarization was observed for fluorinated electrolyte cell suggesting higher resistance was built up at the electrode interface caused by the deposit of organic decomposition species of Gen 2 electrolyte<sup>10</sup>. Figure 4.3c shows the capacity retention for the first 100 cycles. The 1<sup>st</sup> charge and discharge capacities for GEN 2 cell are 248 mAh g<sup>-1</sup> and 214 mAh g<sup>-1</sup> (86.4% Coulombic efficiency) and the capacity retention is 67% for 100 cycles. In contrast, despite lower first cycle efficiency (85.4%), the fluorinated electrolyte cell shows a capacity retention of 82% for 100 cycles, a significant improvement over Gen 2 cell even in such a limited cycle number. In a lithium-limited full cell, the capacity fading could be caused by the oxidative decomposition of electrolyte on charged cathode and/or the reductive decomposition on the lithiated anode. For the FEC-based fluorinated electrolyte, it proved to be compatible with graphitic anode due to the sufficient passivation by the reductive decomposition of FEC solvent.<sup>14</sup>In addition, an SEI formation additive LiDFOB was added to further assist the SEI formation from FEC, which accounts for the more loss of active lithium and thus lower 1<sup>st</sup> cycle Coulombic efficiency.<sup>28-30 31-34</sup>



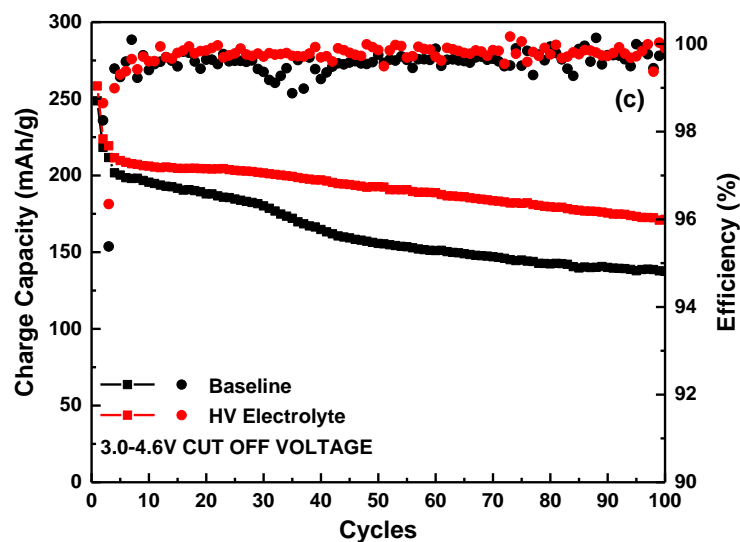


**Figure 4.3.** Voltage profiles for  $\text{LiNi}_{0.5}\text{Co}_{0.2}\text{Mn}_{0.3}\text{O}_2/\text{graphite}$  full cells in (a) Gen 2 electrolyte, (b) fluorinated electrolyte, and (c) capacity retention and Coulombic efficiency (cycling condition: C/10 for 2 cycles formation and then C/3 for 100 for cycling with 3.0-4.6 V cutoff voltage).

### Electrochemical Impedance Spectroscopy

Impedance spectroscopy was used to probe the nature of the cathode surface. The impedance spectra obtained after the formation cycles and the subsequent cycling are shown in Figures 4.4, respectively. These impedance spectra consist of two semi-circles, the high frequency semicircle relates to Li-ion migration through the passivation surface layer (RSL), and the mid frequency semicircle relates to the charge transfer (Rct). The low frequency part that appears as a ‘Warburg’ type element reflects the solid state diffusion of lithium into the bulk electrode.<sup>35</sup>

After the two initial (formation) cycles, the cells with Gen2 and fluorinated electrolyte showed similar interfacial and charge transfer resistances. After the subsequent 100 cycles, fluorinated electrolyte cells displayed significantly lower cathode charge transfer resistances than the baseline cells, suggesting that fluorinated electrolyte efficiently suppressed electrolyte breakdown. In contrast, baseline electrolyte cells exhibited higher cathode charge transfer resistance, suggesting that baseline electrolyte -derived surface layers did not maintain a surface during cycling.

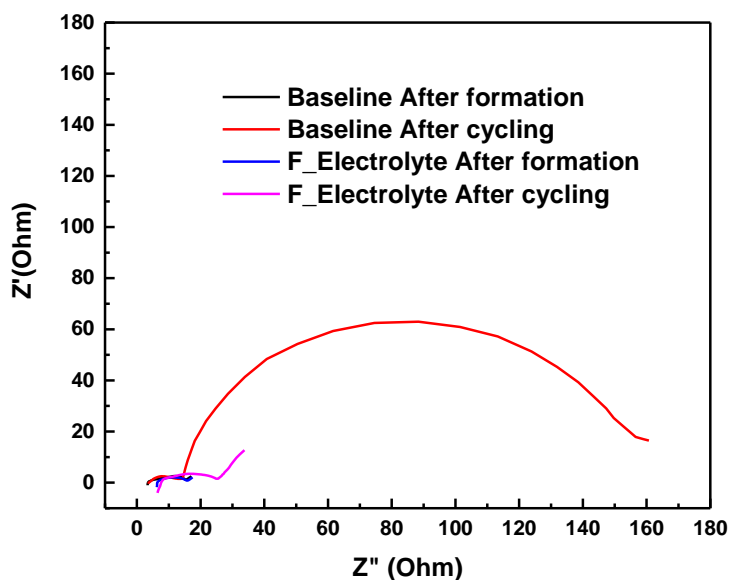


**Figure 4.4.** Electrochemical impedance spectra for  $\text{LiNi}_{0.5}\text{Co}_{0.2}\text{Mn}_{0.3}\text{O}_2/\text{graphite}$  cells after the two initial cycles and after 100 cycles in different electrolyte.

#### 4.3.2. Post analyses of harvested electrodes and electrolytes

##### Scanning Electron Microscope Analysis of Cycled Cathodes.

Figure 4.5 showed the SEM images of the cycled NCM523 cathodes and cycled graphite anodes in two electrolytes and the pristine cathode (Figure 4.5a) and anode (Figure 4.5d). For the GEN 2 electrolyte cell, the morphologies of both cathode (Figure 4.5b) and anode (Figure 4.5e) were completely changed compared with the pristine electrodes and heavy decomposition of decomposition products were observed on both electrodes. However, little change in morphology was observed for the cycled cathode (Figure 4.5c) and cycled anode (Figure 4.5f) with fluorinated electrolyte. It is surprising that the cycled graphite anode in the fluorinated electrolyte almost resembles the pristine one (Figure 4.5a) confirming the effective passivation layer formed by fluorinated electrolyte. Since Gen 2 electrolyte forms excellent SEI on the graphite anode, the

heavy deposition on the graphite surface is totally unexpected and new degradation mechanism must exist.

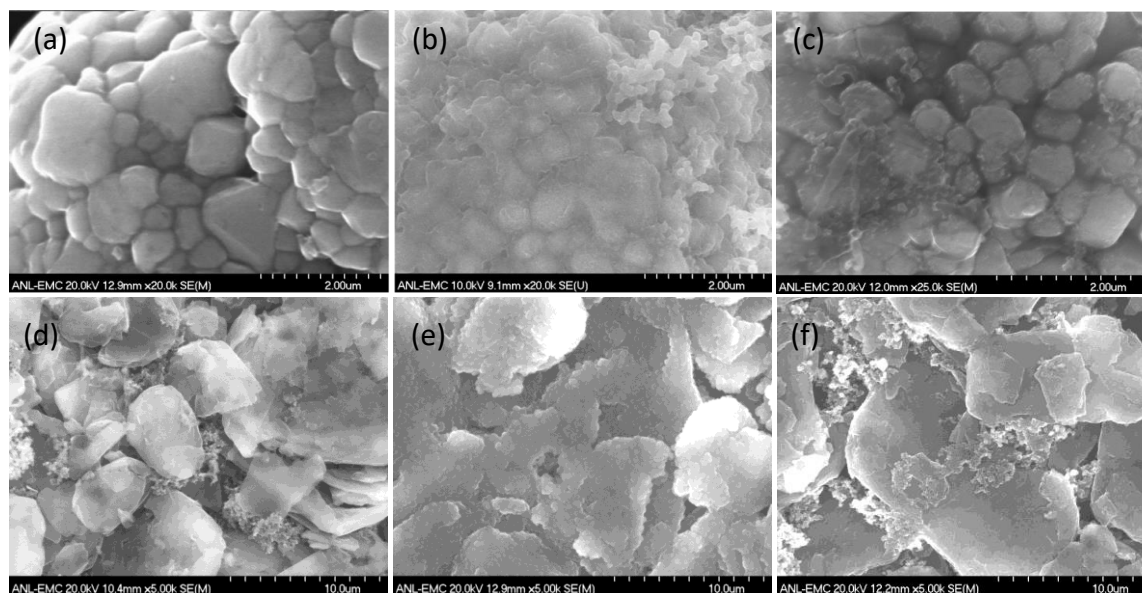


**Figure 5.** SEM images electrode at different stages. (a) Pristine NCM523 cathode, (b) cycled cathode with Gen 2 electrolyte, (c) cycled cathode with fluorinated electrolyte, (d) pristine anode, (e) cycled anode with Gen 2 electrolyte, and (f) cycled anode with fluorinated electrolyte. Magnification for cathode is higher than for anode in order to show the surface morphology change

Figure 4.6 shows the EDX spectroscopy of the cycled graphite anodes. Two distinguished Mn peaks were observed in the EDX spectrum of the Gen 2 anode and the same species was also detected by the XPS  $Mn_{2P}$  spectroscopy. The deposition of Mn species on the cycled anode originated from the dissolution of the cathode active material, migration through the electrolyte and deposition on the anode by forming the metal fluoride ( $MnF_2$ ), metal oxide ( $MnO$ ) or metal (Mn).<sup>36, 38</sup> Moreover, the Mn plating catalyzes the electrolyte decomposition on the anode<sup>39</sup>, resulting a thick electrolyte decomposition layer covering the surface of the anode. No Mn peaks were observed on the EDS spectrum (Figure 4.6, red curve) of the fluorinated electrolyte cycled anode.

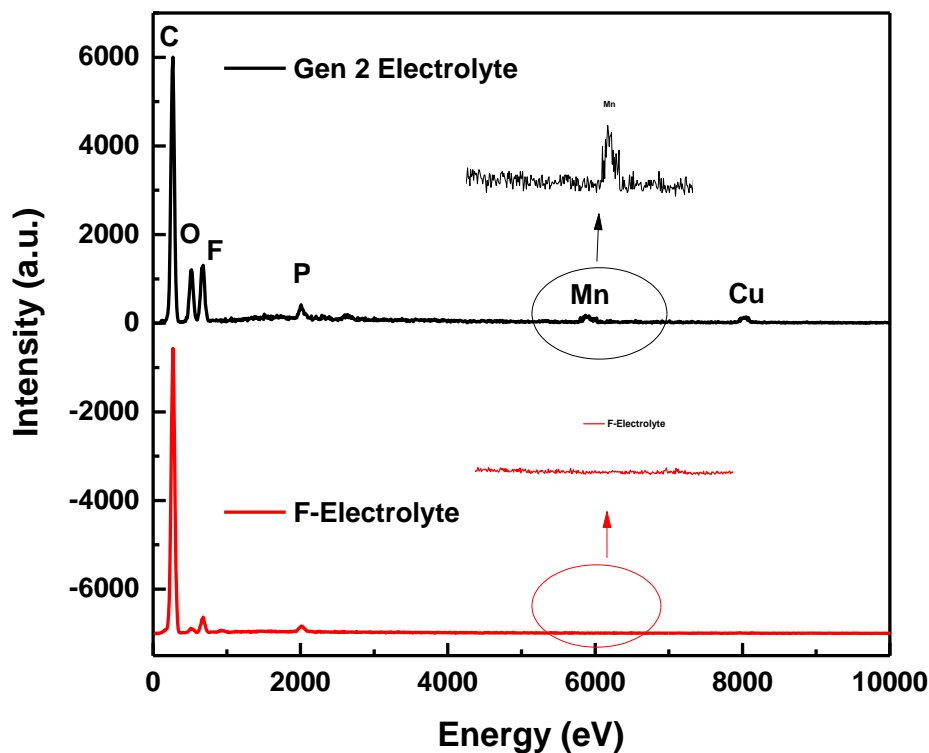
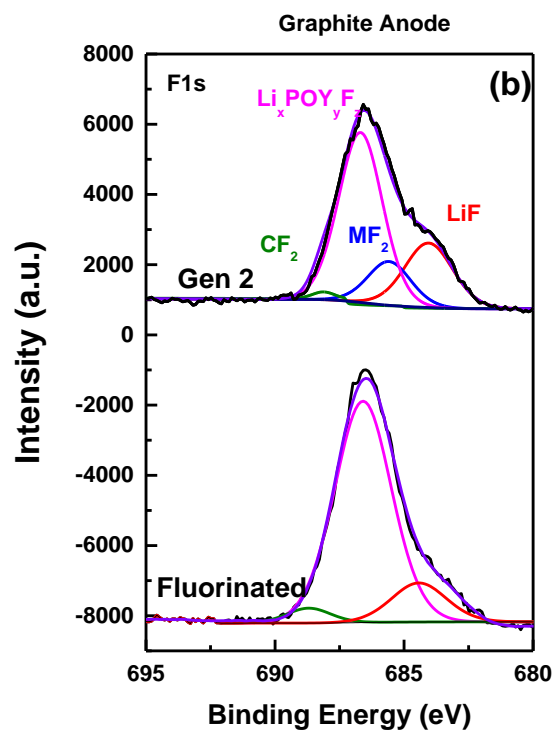
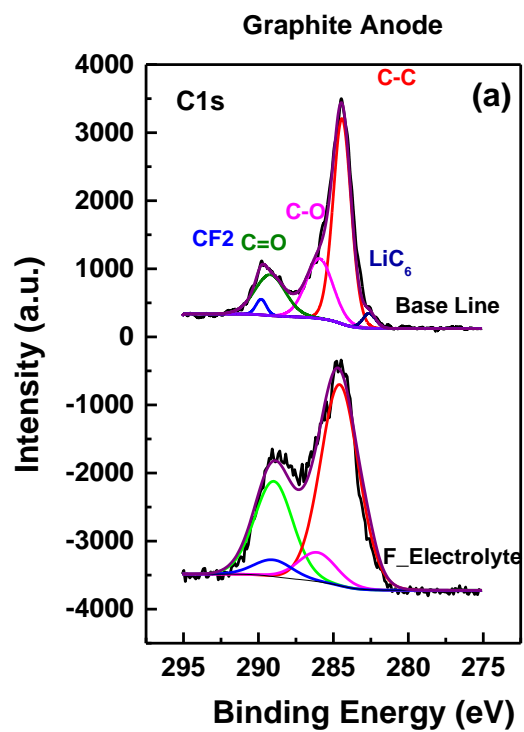


**Figure 4.6.** EDX spectra of the harvest graphite anode cycled with Gen 2 electrolyte (top black curve) and with fluorinated electrolyte (bottom red curve). Various

**X-ray Photoelectron Spectroscopy of Cycled Anodes and Cathodes.** XPS was used to identify surface components. Figure 4.7 presents the harvest anode XPS data in different electrolytes at fully discharge state (3.0 V). In C 1s spectra (Figure 4.7a), the peak located at 284.8 eV is assigned to C-C bond in carbon black,<sup>36-37</sup> and the peaks at 286.5 and ~288 eV are associated with C-O and C=O bond, respectively.<sup>36-37</sup> These groups can be attributed to

ROCO<sub>2</sub>Li, ROLi and LiCO<sub>3</sub>, which are originated from the well-known electrolyte decomposition on the electrode surface under high voltage.<sup>38</sup> Furthermore the peak on 282.6 eV represents the Li intercalated graphite, LiC<sub>6</sub>, and the peak at 291.5eV corresponds to a -CF<sub>2</sub> bond which can be attributed to the PVDF binder.<sup>39</sup> Related peaks are observed in the O1s spectrum at 534 and 532.5 eV consistent with the presence of C–O and C=O containing species. New peaks are also observed in the F1s spectrum at 688, 687, and 685 eV characteristic of LiPF<sub>6</sub>, Li<sub>x</sub>PF<sub>y</sub>O<sub>z</sub>, and LiF, respectively. The related peaks for LiPF<sub>6</sub> and Li<sub>x</sub>PF<sub>y</sub>O<sub>z</sub> are observed in the P 2p spectrum at 138 and 135 eV.<sup>39</sup> Comparing with the cell cycled in fluorinated electrolyte, the cell with baseline electrolyte shows high C=O and C-O peak, meanwhile a weak CF<sub>2</sub> signal. It indicated the anode surface of the baseline cell was covered by the thick electrolyte decomposition, so that the signal of binder is limited<sup>40</sup>. And the identified LiC<sub>6</sub> signal of the baseline cell indicate that even under the fully discharge state, there still have significant amount of Li inside the graphite that cannot be transferred into the cathode due to a high overpotential.

Moreover, the Mn in different chemical state, MnF<sub>2</sub> and MnO were observed in the Mn2p, F1s and O1s spectra respectively on the baseline cell as shown in Figure 4.7b, c and d. During discharge, the dissolved Mn<sup>2+</sup> ions migrate to the anode side and catalyze the electrolyte side reactions. On the other hand, the fluorinated electrolyte cell showed negligible Mn signal and a borate species were also found due to the addition of LiDFOB.



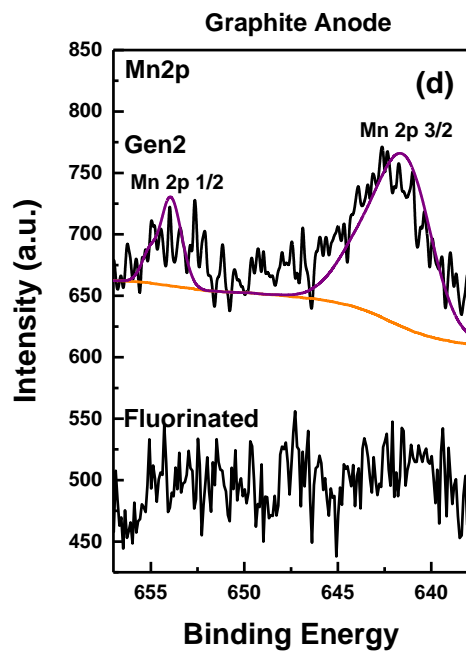
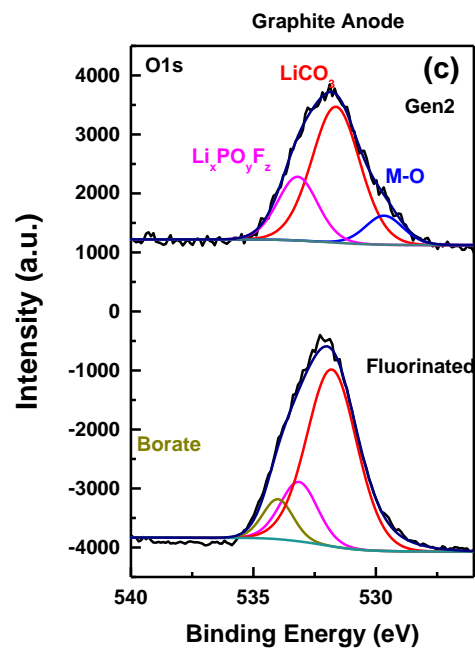


Figure.4.7. XPS spectra of the cycled Graphite electrodes in different electrolytes. (a) C1s, (b) F1s, (c) O1s (d) Mn2p

## X-ray absorption spectroscopy

To understand the element-specific chemical and structure changes, Ni, Co, and Mn K-edge X-ray absorption near edge structure (XANES) as well as Fourier transformed extended X-ray absorption fine structure (EXAFS) spectra of 100 cycles harvest NCM523 cathode in pristine, charged (4.6 V) and discharge (3.0 V) states are compared in Figure 4.8. The strong arising edge features are ascribed to the purely dipole-allowed  $1s \rightarrow 4p$  transition, which can reflect the chemical state changes, while the weak pre-edge absorption peaks, shown in the insets in Figure 4.8, are the formally electric dipole-forbidden transition of a  $1s$  electron to an unoccupied  $3d$  orbital, which gains peak intensity from pure electric quadrupole coupling and/or  $3d$ - $4p$  orbital mixing arising from the noncentrosymmetric environment of the slightly distorted octahedral  $3a$  site in the rhombohedral  $R3m$  space group. Clearly significant differences are seen for each element at charged and discharged states, suggesting each element changes accordingly under both GEN2 and fluorinated electrolytes. However, changes under fluorinated electrolyte are more dramatic compared to GEN2.

Figure 4.8a shows that the Ni chemical state in the pristine sample is approximately  $\sim +2$  as the averaged edge position of the pristine sample and NiO are the same. At the discharged state, Ni XANES edge under both GEN2 and F electrolytes are overlapped, but shift to higher energy compared to the pristine one. Interestingly, at the charged state, Ni XANES edge under fluorinated electrolyte shifts to higher energy compared to that under GEN2. This means that Ni goes to higher chemical state ( $\text{Ni}^{3+}/\text{Ni}^{4+}$ ) under fluorinated electrolyte due to less electrolyte oxidation side reactions. On the other words, during the charge process, the oxidation of the

baseline electrolyte consumed the active Li ion, it leads to the Ni cannot be charge to the higher chemical valence to balance the chemical state.<sup>41</sup> This is also seen from pre-edge peaks in the Figure 4.8a inset, as their intensities arise and positions shift to high energy for fluorinated electrolyte. These changes in Ni XANES have been reported for ex situ studies of  $\text{Li}_{1-x}\text{Co}_{1/3}\text{Ni}_{1/3}\text{Mn}_{1/3}\text{O}_2$ <sup>42</sup>. Shifts of XANES spectra to higher energy correspond to lower lithium concentration. In our case these suggest that F-electrolyte can better avoid the loss of active Li ion in NCM523 cathode than GEN2 electrolyte during charge process. As pre-peak intensity is associated with local structure due to local symmetry, the Ni bond distance and coordination numbers are expected to change, which is evidenced from EXAFS spectra in Figure 4.8b. The spectra of discharged and pristine are nearly the same, indicating that the local structures of NCM523 are not altered too much, even as Ni chemical state in discharged is no longer +2. For the charged state, the dramatic changes of the first coordination peaks indicate that the charge compensation mainly occurs at the Ni sites and results in significant alternations in the average Ni-O bond length. The large changes seen for the first Ni-O shell are similar to those observed for the  $\text{Li}_{1-x}\text{Co}_{1/3}\text{Ni}_{1/3}\text{Mn}_{1/3}\text{O}_2$  systems.<sup>42</sup> This change is suggested to be the oxidation of  $\text{Ni}^{2+}$  to  $\text{Ni}^{4+}$ . Again more changes are observed for fluorinated electrolyte, supporting fluorinated electrolyte has better electrochemical performance than GEN2. Results of EXAFS at charged and discharged states are consistent with the observations in SXRD.

Similar changes are observed for Mn. In the pristine state, Mn edge is slightly on the right side of  $\text{MnO}_2$ , as shown in Figure 4.8c, suggesting the chemical state of Mn in NCM523 is  $\sim (4+\Omega)$ , where  $\Omega$  refers to a small number close to 0. In the discharged state, although XANES for Mn under fluorinated and GEN2 electrolyte is very close to pristine one. The charged XANES

spectra exhibit some changes in the shape of the edge due to changes in the Mn local environment, but do not show a rigid shift to higher energy values. The energy position and the shape of these edges are very similar to those of the  $\text{Li}_{1.2}\text{Cr}_{0.4}\text{Mn}_{0.4}\text{O}_2$  and  $\text{LiNi}_{0.5}\text{Mn}_{0.5}\text{O}_2$  electrode materials<sup>42</sup>, and similar trends of XANES spectra as a function of lithium concentration in  $\text{Li}_{1-x}\text{Ni}_{0.5}\text{Mn}_{0.5}\text{O}_2$ , which suggests manganese remains as their original chemical state,  $\text{Mn}^{(4+\delta)+}$  throughout the charge-discharge processes. This is also supported by previous studies on Mn L<sub>II,III</sub>-edge XAS.<sup>42</sup> In addition, the pre-edge region (Figure 4.8c inset) of Mn is much resolved. This pre-edge is assigned to  $1s \rightarrow 3d$ , particularly  $1s$  to  $e_g$  and  $t_{2g}$  of  $3d$  transitions.<sup>43</sup> The peak separation between the resolved two peaks at the pre-edge region can represent the crystal-splitting field,  $\Delta$ , the energy gap between  $e_g$  and  $t_{2g}$ . During delithiation from discharged state to charged state, both peaks grow in height without shifting in energy. The peak separation between the two peaks steadily shrinks with increasing delithiation. As delithiation will cause the contraction of Mn-O distance that should promote a larger crystal field splitting, the crystal field splitting is actually decreasing, likely due to symmetry effects. From the EXAFS of the Mn K-edge in Figure 4.8d, the Mn-O bond length remains mostly unchanged during charge/discharge in different electrolytes, however, the Mn-M bond length ( $2 \text{ \AA} < R < 3 \text{ \AA}$ ) during charge were decreased, as the peak position in this region becomes smaller. As the inactive Mn cations do not change the bond distance between Mn and O during charge, the reduction of the Mn-M bond length can be ascribed to the reduction of the a-axis during charge processes.<sup>41</sup> Although both Mn XANES and EXAFS results indicate that the Mn do not involve too much in the reaction, the fluorinated electrolyte is better to recover the structural change of Mn during charge-discharged process, thus reducing Mn cation lost.

The interpretation of Co K-edge spectra is more complicated, as pointed out by previous studies on NCM system.<sup>41</sup> Here we focus on the comparison the effects from the two electrolytes. Figure 4.8e shows that XANES spectra for Co under GEN2 and fluorinated electrolytes at the discharged state are overlapped, very close to pristine one and reference  $\text{Co}_2\text{O}_3$ , suggesting Co cations mostly stay at  $\text{Co}^{3+}$ . Although Co K-edge XANES spectra do not show a rigid edge shift during charge, some changes can be found from the edge shape. This could be ascribed to the local structure changes as seen from Mn case above. Previous theoretical studies<sup>44</sup> showed that  $\text{Co}^{3+}/\text{Co}^{4+}$  redox couple would occur at fairly high potentials in the 4.88-5.20 V range for NCM systems. As our charged state is only up to 4.6 V, we attributed the changes in Co XANES spectra to the change of bond length and covalency<sup>42</sup> as also seen from the EXAFS changes in Figure 4.8f. Note that under fluorinated electrolyte Co XANES spectra shape change more compared to that under GEN2 electrolyte, suggesting fluorinated electrolyte is better in promoting Co participation in electrochemical reactions without sacrificing any cathode materials, as the discharged XANES spectra overlap. As previous studies<sup>42</sup> suggest Co in NCM systems are critical for the charge compensation during Li-ion deintercalation, more changes in Co XAS spectra under fluorinated electrolyte suggest the better electrochemical performance compared to GEN2 electrolyte. The comparison studies from XAS on all three elements all infers the advantage of using fluorinated electrolyte to promote and protect NCM cathode during charge-discharge processes.

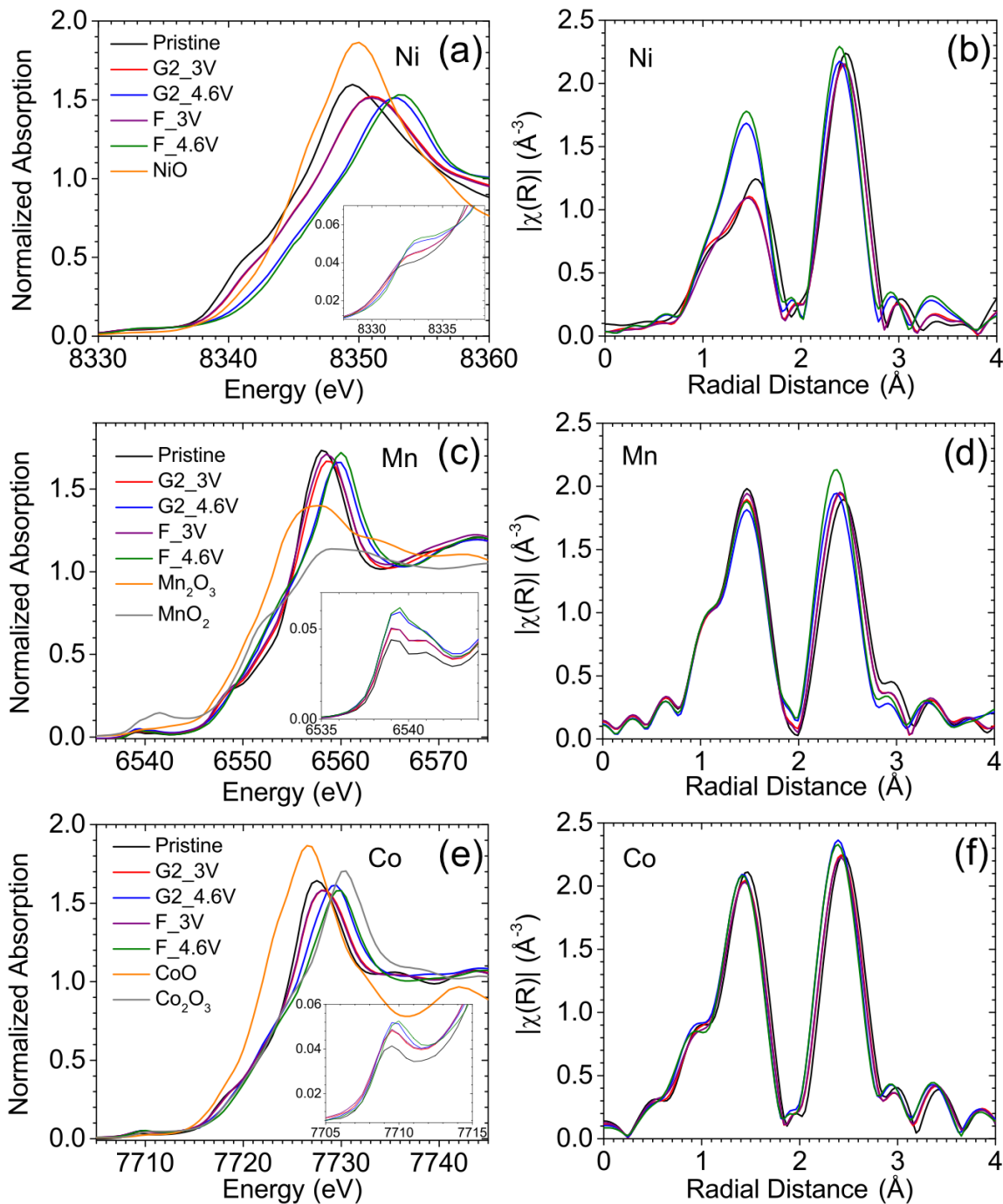


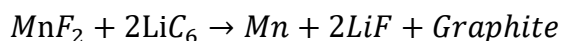
**Figure 4.8.** Normalized K-edge X-ray near edge structure (XANES) spectra at (a) Ni K-edge, (c) Mn K-edge, (e) Co K-edge for NCM523 in pristine, charged (4.6 V) and discharged (3 V) states using GEN2 (G2) and fluorinated (F) electrolyte after 100 cycles, and comparisons with reference samples such as NiO,  $\text{Mn}_2\text{O}_3$ ,  $\text{MnO}_2$ , CoO and  $\text{Co}_2\text{O}_3$  powders. The insets in XANES plots are the pre-peaks of corresponding elements at different electrochemical states. Fourier transforms of (b) Ni, (d) Mn, and (f) Co K-edge extended X-ray absorption fine structure (EXAFS) spectra for NCM523 in pristine, charged and discharged states. Note that the radial distances in EXAFS spectra have not been phase corrected.

## Synchrotron X-ray Diffraction (SXRD) Results

Figure 4.9 shows the Ex situ X-ray diffraction pattern of pristine and cycled NCM523 electrode. The original data were converted to a Cu target data (1.54 Å) and all of the cycled electrode were tested under a fully discharge state. All of three XRD patterns are consistent with a single phase with the  $\bar{R}3m$  NaFeO<sub>2</sub> structure; all the reflections can be indexed by assuming the hexagonal axes setting of the rhombohedral  $\bar{R}3m$  space group. And no new phases were detected. The 006/012 and the 108/110 pairs of reflections are well resolved, which is typical of a well-developed layered structure. The refinement data are shown on table 1. Comparing with the pristine NCM523 cathode material, the electrode cycled in fluorinated electrolyte shows few crystallographic changes. Meanwhile, the electrode cycled in the baseline electrolyte shows 3 percent volume shrinkage, which comes from the contraction of a, b axis and the enlargement of c axis.

For the cell cycled in the baseline electrolyte, the change of c parameter can be attributed to the loss of active lithium during cycling<sup>41</sup>. For the LiMeO<sub>2</sub> material, where Me refers to transition metal, the oxygen anions have a close-packed arrangement in ABCABC framework with transition metal cations located in the 6 coordinated octahedral crystal site. The slabs and Li layer are stacked alternatively<sup>4</sup>. The absence of lithium ions leads to the two negative charged oxides layers losing the bonding connection with each other. As a result, the c parameter was increased. . Ideally, the electrolyte reduction should be only happened on the first couple formation cycles to form LiF or LiP<sub>x</sub>F<sub>y</sub>O<sub>z</sub> on the anode electrode<sup>45</sup> to reach a thermodynamically stable on the anode side and does not continue during the steady cycling of the cell<sup>46</sup>. However,

in the high voltage NCM based system, the cathode suffer from the transition metal dissolution issue. During charging process, the  $Mn^{2+}$  were dissolute from the cathode and formed the  $MnF_2$ .<sup>8</sup> When discharging, the dissolved  $Mn^{2+}$  ion are reduced on the surface of graphite negative electrodes by partly depleting active  $Li^+$  to form LiF by the following reaction:



Due to the low solubility of LiF, it will deposit on the surface of the anode. As a result, a higher LiF peak was identified on XPS F 1s spectroscopy meanwhile the Mn element were detected by the EDAX on the baseline electrolyte cycled anode. Because of the loss of active lithium, the amounts of lithium ion that can feed back to the cathode were decreased. It not only leads to the change of cathode crystal parameter, but also the irreversible capacity losing during cycling.

To reach a valance balance, the decrease of lithium content in the cathode electrode also leads to the increasing of transition metal valance state. The bond length of  $Ni^{2+}$  is 0.69 Å and  $Co^{3+}$  is 0.61 Å, meanwhile, 0.56 Å for  $Ni^{3+}$  and 0.53 Å for  $Co^{4+}$ .<sup>47</sup> The increasing of the transition metal valance state will lead to the shrinkage of the transition meatal plane in the crystal structure. In other words, both a and b parameter were decreased as shown in the refinement data table 4.1.

On the other hand, for the cell cycled in the fluorinated electrolyte, the cathode surface is effectively passivated by a stable SEI composed of fluorinated electrolyte decomposition products, which inhibit the transition metal dissolution<sup>48</sup> and a robust negative electrode SEI were formed by evolving the LiDFOB.<sup>17, 49</sup> As a result we can see a much more cleanly cycled anode surface by the SEM, EDAX and XPS data. Moreover, it almost has no crystal parameter change on the cathode part. Therefore, both the capacity retention and specific capacity of the

cell cycled in the fluorinated electrolyte is much more promising than those of the baseline electrolyte.

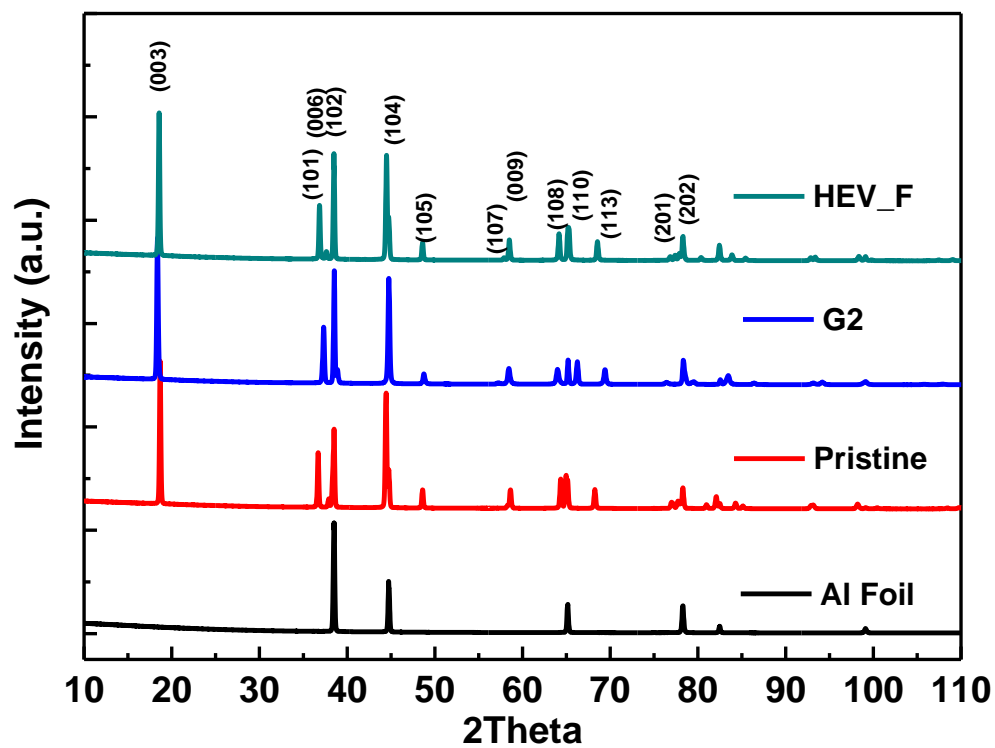


Figure 4.9. SXR D results of the pristine and harvest electrode in different electrolyte

**Table 4.1. Refined XRD Lattice Parameters  $a, c$  And Cell Volume For NCM523 Cathodes Cycled With Gen 2 Electrolyte (Gen 2) And Fluorinated Electrolyte (F-Electrolyte).**

<i>NCM523 Cathode</i>	<i>Lattice parameters</i>			<i>V (Å<sup>3</sup>)</i>
	<i>a=b (Å)</i>	<i>c (Å)</i>	<i>c/a</i>	
<b>Pristine</b>	2.866	14.8944	5.196	122.34
<b>Gen 2</b>	2.798	15.1494	5.083	118.60
<b>F-Electrolyte</b>	2.871	14.8964	5.182	122.03

#### 4.4 Conclusion

In this paper, we report a fluorinated electrolyte based on 1.0 M LiPF<sub>6</sub> FEC/HFDEC with 1.0 wt% LiDFOB for the high voltage lithium ion battery. It met all the basic requirements as a non-aqueous electrolyte including graphite anode passivation, high conductivity and excellent wettability with cell components. On top of these properties, this fluorinated electrolyte is oxidatively stable against high voltage charging and showed significantly improved cell performance when charged to 4.6 V in NCM523/graphite couple. Linear sweep voltammetry, repeated charge-discharge cycling and a series of post-test analysis including NMR, SEM/EDS, XPS, XRD and XAS confirm its voltage advantage over the Gen 2 electrolyte. Charge transfer impedance of the cell cycled with fluorinated is much smaller than that cycled with Gen 2 electrolyte and significant deposition were detected on the both NCM523 cathode and graphite anode. Interestingly, the transition metal dissolution is not detected by EDS and XPS on the fluorinated electrolyte cycled graphite anode, suggesting the enhanced voltage stability on the cathode side and the robust SEI formation on the graphite anode. This has been evidenced from the XAS experiment confirming the Ni and also Co could be charged to higher oxidation state

(Ni<sup>3+</sup>/Ni<sup>4+</sup>) with fluorinated electrolyte due to its enhanced oxidation stability. Furthermore, fluorinated electrolyte was proved to assist the preservation of the crystal structure of NCM523 cathode by SXRD results. The lattice structure of NCM523 is almost intact while significant shrinkage in its unit cell for Gen 2 electrolyte cycled cathode. All results converge to the conclusion that FEC/HFDEC based fluorinated electrolyte is intrinsic ally stable towards oxidation and is suitable high voltage electrolyte for high voltage high energy density lithium ion cell. This example research demonstrated that new electrolyte design could provide an approach to solve the technical barriers encountered by the high voltage high energy density lithium-ion batteries.

## Reference

1. Xu, K., Electrolytes and Interphases in Li-Ion Batteries and Beyond. *Chemical reviews* **2014**, *114*, 11503-11618.
2. Ohzuku, T.; Ueda, A.; Nagayama, M.; Iwakoshi, Y.; Komori, H., Comparative Study of Lico<sub>2</sub>, Lini Co O<sub>2</sub> and Lini<sub>2</sub> for 4 Volt Secondary Lithium Cells. *Electrochimica Acta* **1993**, *38*, 1159-1167.
3. Ates, M. N.; Jia, Q.; Shah, A.; Busnaina, A.; Mukerjee, S.; Abraham, K., Mitigation of Layered to Spinel Conversion of a Li-Rich Layered Metal Oxide Cathode Material for Li-Ion Batteries. *Journal of The Electrochemical Society* **2014**, *161*, A290-A301.
4. Ohzuku, T.; Makimura, Y., Layered Lithium Insertion Material of Lico<sub>1/3</sub>ni<sub>1/3</sub>mn<sub>1/3</sub>o<sub>2</sub> for Lithium-Ion Batteries. *Chemistry Letters* **2001**, 642-643.
5. Kong, J.-Z.; Ren, C.; Tai, G.-A.; Zhang, X.; Li, A.-D.; Wu, D.; Li, H.; Zhou, F., Ultrathin ZnO Coating for Improved Electrochemical Performance of Lini<sub>0.5</sub> Co<sub>0.2</sub> Mn<sub>0.3</sub> O<sub>2</sub> Cathode Material. *Journal of Power Sources* **2014**, *266*, 433-439.
6. Liu, S.; Xiong, L.; He, C., Long Cycle Life Lithium Ion Battery with Lithium Nickel Cobalt Manganese Oxide (Ncm) Cathode. *Journal of Power Sources* **2014**, *261*, 285-291.
7. Xu, K., Nonaqueous Liquid Electrolytes for Lithium-Based Rechargeable Batteries. *Chemical reviews* **2004**, *104*, 4303-4418.
8. Pieczonka, N. P.; Liu, Z.; Lu, P.; Olson, K. L.; Moote, J.; Powell, B. R.; Kim, J.-H., Understanding Transition-Metal Dissolution Behavior in Lini<sub>0.5</sub>mn<sub>1.5</sub>o<sub>4</sub> High-Voltage Spinel for Lithium Ion Batteries. *The Journal of Physical Chemistry C* **2013**, *117*, 15947-15957.
9. Nelson, K.; Abarbanel, D.; Xia, J.; Lu, Z.; Dahn, J., Effects of Upper Cutoff Potential on Lapo<sub>4</sub>-Coated and Uncoated Li [Ni<sub>0.42</sub>mn<sub>0.42</sub>co<sub>0.16</sub>] O<sub>2</sub>/Graphite Pouch Cells. *Journal of The Electrochemical Society* **2016**, *163*, A272-A280.
10. Xu, M.; Zhou, L.; Dong, Y.; Chen, Y.; DEMEAUX, J.; MacIntosh, A. D.; Garsuch, A.; Lucht, B. L., Development of Novel Lithium Borate Additives for Designed Surface Modification of High Voltage Lini<sub>0.5</sub>mn<sub>1.5</sub>o<sub>4</sub> Cathodes. *Energy & Environmental Science* **2016**.
11. Zhang, Z.; Hu, L.; Wu, H.; Weng, W.; Koh, M.; Redfern, P. C.; Curtiss, L. A.; Amine, K., Fluorinated Electrolytes for 5 V Lithium-Ion Battery Chemistry. *Energy & Environmental Science* **2013**, *6*, 1806-1810.
12. Benmayza, A.; Lu, W.; Ramani, V.; Prakash, J., Electrochemical and Thermal Studies of Lini<sub>0.8</sub> Co<sub>0.15</sub> Al<sub>0.015</sub> O<sub>2</sub> under Fluorinated Electrolytes. *Electrochimica Acta* **2014**, *123*, 7-13.
13. He, M.; Hu, L.; Xue, Z.; Su, C. C.; Redfern, P.; Curtiss, L. A.; Polzin, B.; von Cresce, A.; Xu, K.; Zhang, Z., Fluorinated Electrolytes for 5-V Li-Ion Chemistry: Probing Voltage Stability of Electrolytes with Electrochemical Floating Test. *Journal of The Electrochemical Society* **2015**, *162*, A1725-A1729.
14. Hu, L.; Zhang, Z.; Amine, K., Fluorinated Electrolytes for Li-Ion Battery: An Fec-Based Electrolyte for High Voltage Lini<sub>0.5</sub> Mn<sub>1.5</sub> O<sub>4</sub>/Graphite Couple. *Electrochemistry Communications* **2013**, *35*, 76-79.
15. Hu, L.; Xue, Z.; Amine, K.; Zhang, Z., Fluorinated Electrolytes for 5-V Li-Ion Chemistry: Synthesis and Evaluation of an Additive for High-Voltage Lini<sub>0.5</sub>mn<sub>1.5</sub>o<sub>4</sub>/Graphite Cell. *Journal of The Electrochemical Society* **2014**, *161*, A1777-A1781.

16. Lee, Y.-M.; Nam, K.-M.; Hwang, E.-H.; Kwon, Y.-G.; Kang, D.-H.; Kim, S.-S.; Song, S.-W., Interfacial Origin of Performance Improvement and Fade for 4.6 V Lini<sub>0.5</sub>Co<sub>0.2</sub>Mn<sub>0.3</sub>O<sub>2</sub> Battery Cathodes. *The Journal of Physical Chemistry C* **2014**, *118*, 10631-10639.
17. Zhu, Y.; Li, Y.; Bettge, M.; Abraham, D. P., Positive Electrode Passivation by Lidfob Electrolyte Additive in High-Capacity Lithium-Ion Cells. *Journal of The Electrochemical Society* **2012**, *159*, A2109-A2117.
18. Xu, K.; Zhang, S.; Jow, T. R.; Xu, W.; Angell, C. A., Libob as Salt for Lithium-Ion Batteries: A Possible Solution for High Temperature Operation. *Electrochemical and Solid-State Letters* **2002**, *5*, A26-A29.
19. Zhang, S.; Ding, M. S.; Xu, K.; Allen, J.; Jow, T. R., Understanding Solid Electrolyte Interface Film Formation on Graphite Electrodes. *Electrochemical and Solid-State Letters* **2001**, *4*, A206-A208.
20. Xu, K.; Ding, M. S.; Zhang, S.; Allen, J. L.; Jow, T. R., An Attempt to Formulate Nonflammable Lithium Ion Electrolytes with Alkyl Phosphates and Phosphazenes. *Journal of The Electrochemical Society* **2002**, *149*, A622-A626.
21. Xu, K.; Zhang, S.; Jow, T. R., Formation of the Graphite/Electrolyte Interface by Lithium Bis (Oxalato) Borate. *Electrochemical and Solid-State Letters* **2003**, *6*, A117-A120.
22. Madec, L. n.; Xia, J.; Petibon, R. m.; Nelson, K. J.; Sun, J.-P.; Hill, I. G.; Dahn, J. R., Effect of Sulfate Electrolyte Additives on Lini<sub>1/3</sub>Mn<sub>1/3</sub>Co<sub>1/3</sub>O<sub>2</sub>/Graphite Pouch Cell Lifetime: Correlation between Xps Surface Studies and Electrochemical Test Results. *The Journal of Physical Chemistry C* **2014**, *118*, 29608-29622.
23. Madec, L.; Ma, L.; Nelson, K. J.; Petibon, R.; Sun, J.-P.; Hill, I. G.; Dahn, J. R., The Effects of a Ternary Electrolyte Additive System on the Electrode/Electrolyte Interfaces in High Voltage Li-Ion Cells. *Journal of The Electrochemical Society* **2016**, *163*, A1001-A1009.
24. Wu, H.-C.; Su, C.-Y.; Shieh, D.-T.; Yang, M.-H.; Wu, N.-L., Enhanced High-Temperature Cycle Life of Lifepo<sub>4</sub>-Based Li-Ion Batteries by Vinylene Carbonate as Electrolyte Additive. *Electrochemical and Solid-State Letters* **2006**, *9*, A537-A541.
25. Zhang, S.; Jow, T., Aluminum Corrosion in Electrolyte of Li-Ion Battery. *Journal of Power Sources* **2002**, *109*, 458-464.
26. Lee, H.; Choi, S.; Choi, S.; Kim, H.-J.; Choi, Y.; Yoon, S.; Cho, J.-J., Sei Layer-Forming Additives for Lini<sub>0.5</sub>Mn<sub>1.5</sub>O<sub>4</sub>/Graphite 5v Li-Ion Batteries. *Electrochemistry Communications* **2007**, *9*, 801-806.
27. Lu, L.; Han, X.; Li, J.; Hua, J.; Ouyang, M., A Review on the Key Issues for Lithium-Ion Battery Management in Electric Vehicles. *Journal of power sources* **2013**, *226*, 272-288.
28. Aurbach, D.; Markovsky, B.; Salitra, G.; Markevich, E.; Talyossef, Y.; Koltypin, M.; Nazar, L.; Ellis, B.; Kovacheva, D., Review on Electrode–Electrolyte Solution Interactions, Related to Cathode Materials for Li-Ion Batteries. *Journal of Power Sources* **2007**, *165*, 491-499.
29. Shim, J.; Kosteki, R.; Richardson, T.; Song, X.; Striebel, K. A., Electrochemical Analysis for Cycle Performance and Capacity Fading of a Lithium-Ion Battery Cycled at Elevated Temperature. *Journal of Power Sources* **2002**, *112*, 222-230.
30. Aurbach, D.; Markovsky, B.; Rodkin, A.; Levi, E.; Cohen, Y.; Kim, H.-J.; Schmidt, M., On the Capacity Fading of Licoo<sub>2</sub> Intercalation Electrodes: The Effect of Cycling, Storage, Temperature, and Surface Film Forming Additives. *Electrochimica Acta* **2002**, *47*, 4291-4306.
31. Goodenough, J. B.; Park, K.-S., The Li-Ion Rechargeable Battery: A Perspective. *Journal of the American Chemical Society* **2013**, *135*, 1167-1176.

32. Etacheri, V.; Marom, R.; Elazari, R.; Salitra, G.; Aurbach, D., Challenges in the Development of Advanced Li-Ion Batteries: A Review. *Energy & Environmental Science* **2011**, *4*, 3243-3262.
33. Cho, T.-H.; Tanaka, M.; Onishi, H.; Kondo, Y.; Nakamura, T.; Yamazaki, H.; Tanase, S.; Sakai, T., Battery Performances and Thermal Stability of Polyacrylonitrile Nano-Fiber-Based Nonwoven Separators for Li-Ion Battery. *Journal of Power Sources* **2008**, *181*, 155-160.
34. Chikkannanavar, S. B.; Bernardi, D. M.; Liu, L., A Review of Blended Cathode Materials for Use in Li-Ion Batteries. *Journal of Power Sources* **2014**, *248*, 91-100.
35. Xu, B.; Qian, D.; Wang, Z.; Meng, Y. S., Recent Progress in Cathode Materials Research for Advanced Lithium Ion Batteries. *Mater. Sci. Eng. Reports* **2012**, *73*, 51-65.
36. Wang, Z.; Xing, L.; Li, J.; Xu, M.; Li, W., Triethylborate as an Electrolyte Additive for High Voltage Layered Lithium Nickel Cobalt Manganese Oxide Cathode of Lithium Ion Battery. *Journal of Power Sources* **2016**, *307*, 587-592.
37. Chen, J.; Zhang, H.; Wang, M.; Liu, J.; Li, C.; Zhang, P., Improving the Electrochemical Performance of High Voltage Spinel Cathode at Elevated Temperature by a Novel Electrolyte Additive. *Journal of Power Sources* **2016**, *303*, 41-48.
38. Andreu, N.; Flahaut, D.; Dedryvère, R.; Minvielle, M.; Martinez, H.; Gonbeau, D., Xps Investigation of Surface Reactivity of Electrode Materials: Effect of the Transition Metal. *ACS applied materials & interfaces* **2015**, *7*, 6629-6636.
39. Castro, L.; Dedryvère, R.; Ledeuil, J.-B.; Bréger, J.; Tessier, C.; Gonbeau, D., Aging Mechanisms of Lifepo4//Graphite Cells Studied by Xps: Redox Reaction and Electrode/Electrolyte Interfaces. *Journal of The Electrochemical Society* **2012**, *159*, A357-A363.
40. Nie, M.; Abraham, D. P.; Chen, Y.; Bose, A.; Lucht, B. L., Silicon Solid Electrolyte Interphase (Sei) of Lithium Ion Battery Characterized by Microscopy and Spectroscopy. *The Journal of Physical Chemistry C* **2013**, *117*, 13403-13412.
41. Petersburg, C. F.; Li, Z.; Chernova, N. A.; Whittingham, M. S.; Alamgir, F. M., Oxygen and Transition Metal Involvement in the Charge Compensation Mechanism of Lini 1/3 Mn 1/3 Co 1/3 O 2 Cathodes. *Journal of Materials Chemistry* **2012**, *22*, 19993-20000.
42. Yoon, W.-S.; Balasubramanian, M.; Chung, K. Y.; Yang, X.-Q.; McBreen, J.; Grey, C. P.; Fischer, D. A., Investigation of the Charge Compensation Mechanism on the Electrochemically Li-Ion Deintercalated Li1-X Co1/3ni1/3mn1/3o2 Electrode System by Combination of Soft and Hard X-Ray Absorption Spectroscopy. *Journal of the American Chemical Society* **2005**, *127*, 17479-17487.
43. Goncharuk, N. A.; Kučera, J.; Smrčka, L., Pre-Edge Xanes Structure of Mn in (Ga, Mn) as from the First Principles. *Chemistry of metals and alloys* **2009**, 34-38.
44. Wang, L.; Li, J.; He, X.; Pu, W.; Wan, C.; Jiang, C., Recent Advances in Layered Lini X Coymn1- X- Y O2 Cathode Materials for Lithium Ion Batteries. *Journal of Solid State Electrochemistry* **2009**, *13*, 1157-1164.
45. Herstedt, M.; Abraham, D. P.; Kerr, J. B.; Edström, K., X-Ray Photoelectron Spectroscopy of Negative Electrodes from High-Power Lithium-Ion Cells Showing Various Levels of Power Fade. *Electrochimica Acta* **2004**, *49*, 5097-5110.
46. Arora, P.; White, R. E.; Doyle, M., Capacity Fade Mechanisms and Side Reactions in Lithium-Ion Batteries. *Journal of The Electrochemical Society* **1998**, *145*, 3647-3667.
47. Shizuka, K.; Kobayashi, T.; Okahara, K.; Okamoto, K.; Kanzaki, S.; Kanno, R., Characterization of Li 1+ Y Ni X Co 1- 2x Mn X O 2 Positive Active Materials for Lithium Ion Batteries. *Journal of Power Sources* **2005**, *146*, 589-593.

48. Pham, H. Q.; Nam, K.-M.; Hwang, E.-H.; Kwon, Y.-G.; Jung, H. M.; Song, S.-W., Performance Enhancement of 4.8 V Li<sub>1.2</sub>Mn<sub>0.525</sub>Ni<sub>0.175</sub>Co<sub>0.1</sub>O<sub>2</sub> Battery Cathode Using Fluorinated Linear Carbonate as a High-Voltage Additive. *Journal of The Electrochemical Society* **2014**, *161*, A2002-A2011.
49. Xu, M.; Zhou, L.; Hao, L.; Xing, L.; Li, W.; Lucht, B. L., Investigation and Application of Lithium Difluoro (Oxalate) Borate (LiDFOB) as Additive to Improve the Thermal Stability of Electrolyte for Lithium-Ion Batteries. *Journal of Power Sources* **2011**, *196*, 6794-6801.

## Chapter 5 Mechanistic Insight in the Function of Phosphite Additives for Protection of $\text{LiNi}_{0.5}\text{Co}_{0.2}\text{Mn}_{0.3}\text{O}_2$ Cathode in High Voltage Li-ion Cells

### Abstract

Triethylphosphite (TEP) and tris(2,2,2-trifluoroethyl) phosphite (TTFP) have been evaluated as electrolyte additives for high-voltage Li-ion battery cells using a Ni-rich layered cathode material  $\text{LiNi}_{0.5}\text{Co}_{0.2}\text{Mn}_{0.3}\text{O}_2$  (NCM523) and the common carbonate electrolyte. The repeated charge/discharge cycling was performed using an NCM523/graphite full cell operated at the cutoff voltage of 4.6 V vs  $\text{Li}^+/\text{Li}$ . During the initial charging, these additives decompose on the cathode surface at a significantly lower potential than the electrolyte. Impedance spectroscopy and post-test analyses indicate the formation of protective coatings on the cathode surface that prevent rapid oxidative breakdown of the electrolyte. Only TTFP containing cells demonstrate the improved capacity retention and Coulombic efficiency. For TEP, the protective coating is also formed, but low  $\text{Li}^+$  ion mobility through the interphase layer results in inferior performance. These observations are rationalized mechanistically through the inhibition of electrocatalytic centers present on the cathode surface and the formation of organophosphate deposits isolating the cathode surface from the electrolyte.

**Keywords:** electrolyte additive; oxidation stability; Triethylphosphite (TEP); tris(2,2,2-trifluoroethyl) phosphite (TTFP);  $\text{LiNi}_{0.5}\text{Co}_{0.2}\text{Mn}_{0.3}\text{O}_2$  cathode; high voltage lithium-ion batteries

## 5.1. Introduction

Lithium-ion batteries have developed into a state-of-the-art power source for portable electronics and also a promising candidate for powering electric vehicles.<sup>1-5</sup> These batteries involve three major components: a cathode, an anode, and an electrolyte.<sup>6</sup> Due to the high costs of cathode materials in commercial cells and the need to increase the operation voltage for automotive applications, many researchers are focusing on the development of new cathode materials.<sup>7</sup> The first lithium nickel manganese cobalt oxide,  $\text{LiNi}_{1/3}\text{Co}_{1/3}\text{Mn}_{1/3}\text{O}_2$  (NCM333), was synthesized by Ohzuku's group in 2000.<sup>8</sup> Extensive research on the development and improvement of new Ni-rich layered  $\text{LiNi}_x\text{Co}_y\text{Mn}_z\text{O}_2$  materials has been conducted thereafter.<sup>1-10</sup> Among these cathode materials,  $\text{LiNi}_{0.5}\text{Co}_{0.2}\text{Mn}_{0.3}\text{O}_2$  (known as NCM523) has attracted much attention due to its excellent electrochemical performance and high specific capacity under high voltage.<sup>3, 9, 11-13</sup> However, several inherent issues associated with NCM523, especially rapid capacity fading when this material is cycled at voltages in excess of 4.4 V vs  $\text{Li}^+/\text{Li}$ , must be addressed before this material can be adopted for applications.

Several explanations for performance deterioration in NCM523 cells have been suggested, including: (i) the structural change from multiple-layer to spinel structure upon cycling,<sup>4, 12</sup> (ii) the formation of thick solid-electrolyte-interphase (SEI) deposits, isolating the cathode surface from the electrolyte,<sup>9</sup> and (iii) the anodic instability of the conventional carbonate electrolytes at voltages exceeding 4.3 V vs  $\text{Li}^+/\text{Li}$ .<sup>14-16</sup> Approaches to circumvent these challenges include surface coating of the cathode particles,<sup>17-19</sup> the design and synthesis of intrinsically stable electrolytes to tolerate high voltages,<sup>1, 14, 20</sup> and the development of electrolyte additives to

stabilize the electrode/electrolyte interphase. The latter approach is particularly appealing from the techno-economic perspective, as it is cost efficient and maximally conservative.

The discovery of a suitable electrolyte additive for NCM cathodes has long been pursued. Lee *et al.*<sup>15</sup> reported that the addition of 5 wt% methyl(2,2,2-trifluoroethyl) carbonate to the conventional carbonate electrolyte can significantly improve cycling performance. Dahn and co-workers<sup>21</sup> and others<sup>22, 23</sup> obtained much improved electrolyte stability when tris(trimethylsilyl)phosphate and/or tris(trimethylsilyl) phosphite were used as electrolyte additives in NCM333/graphite cell operated at 4.2 V cutoff voltage at 40°C. Zhang *et al.*<sup>20</sup> proposed a fluorinated electrolyte consisting of a mixture of fluorinated carbonates with a fluorinated ether for 5 V operation of LiNi<sub>0.5</sub>Mn<sub>1.5</sub>O<sub>4</sub> spinel cathode coupled with lithium titanate anode. Zuo *et al.*<sup>24</sup> showed that the addition of 1.0 wt% LiBF<sub>4</sub> enhanced cycling performance for 4.5 V cycling of LiNi<sub>0.5</sub>Co<sub>0.2</sub>Mn<sub>0.3</sub>O<sub>2</sub> /graphite cell.

On the general note, an electrolyte additive for cathode passivation acts as a sacrificial agent that is oxidized prior to the decomposition of solvent molecules.<sup>1, 24, 25</sup> While the specific way in which the oxidation of the additive subsequently inhibits the electrolyte breakdown of the solvent is not understood well, inactivation of catalytic centers occurring on the surface of the electrode is the most likely cause. This inactivation can result either via chemical modification of these reaction centers and/or through the formation of protective coatings (also known as “surface reaction layers”<sup>4</sup> consisting of the insoluble products of additive decomposition and cathode corrosion). These layers physically block solvent access to reactive centers on the surface (preventing its oxidation) while allowing Li<sup>+</sup> ion conduction through their bulk.

It is noteworthy that many of the battery additives reported in the literature involve fluorinated compounds. Examples of the fluorinated compounds studied as electrolyte additives include fluoroethylene carbonate,<sup>26, 27</sup> fluorinated ether substituted propylene carbonate,<sup>28</sup> lithium difluorobis(oxalato)borate<sup>29</sup>, tris(hexafluoro-*iso*-propyl)phosphate,<sup>30</sup> and (4-(trifluoromethyl)-1,3-dioxolan-2-one, 4-(perfluorobutyl)-1,3-dioxolan-2-one, 4-(perfluorohexyl)-1,3-dioxolan-2-one, and 4-(perfluorooctyl)-1,3-dioxolan-2-one.<sup>31</sup> This fluoro substitution typically makes molecules more resistant to anodic decomposition by increasing their oxidation potential due to the electron withdrawing effect of the fluorinated alkyl groups; however, the role of this substitution in the improved performance attained through the use of fluorinated additives remains unknown. In this study, we examine and contrast non-fluorinated triethylphosphite (TEP) and fluorinated tris(2,2,2-trifluoroethyl) phosphite (TTFP) (Figure 5.1) as electrolyte additives for NCM523/graphite cells. Pries *et al.*<sup>32</sup> already demonstrated that the cycling performance of Li-rich-Mn-rich materials  $x\text{Li}_2\text{MnO}_3 \cdot (1-x)\text{LiMO}_2$  (M=Ni, Co, Mn) can be improved by incorporating 5.0 wt% TTFP. Here we demonstrate that this improvement can be traced to the modification of the cathode surface during the initial charging of the cell. We demonstrate that the fluorinated phosphite additive passivates the transition metal oxide surface resulting in a slower oxidation of the organic solvent during the subsequent cycling. Blocking of (electro) catalytically active reaction centers on the oxide surface is suggested as the likely cause for this beneficial action.

## 5.2. Material and methods

All measurements were carried out at 30 °C in an inert atmosphere. Electrochemical cycling stability was evaluated using 2032 coin cells. The cathode was composed of 90.0 wt%  $\text{LiNi}_{0.5}\text{Co}_{0.2}\text{Mn}_{0.3}\text{O}_2$ , 5.0 wt% C45 carbon black, and 5.0 wt% Solvay 5130 polyvinylidene fluoride (PVDF) binder coated on aluminum foil. The active material loading was 9.15 mg/cm<sup>2</sup>. The graphite anode consisted of 89.8 wt% ConocoPhillips CGPA12, 4.0 wt% Super P-Li, 6.0 wt% Kureha 9300 PVDF binder, and 0.2 wt% oxalic acid that were coated on copper foil. The active material loading was 5.3 mg/cm<sup>2</sup>. Celgard 2325 was used as the separator. The effective diameters of the cathode, anode and separator were 14, 15, and 16 mm, respectively. Gen2 electrolyte containing 1.2 M  $\text{LiPF}_6$  in 3:7 v/v mixture of ethylene carbonate (EC) and ethyl methyl carbonate (EMC) was used as a “baseline” electrolyte. TEP was purchased from Sigma-Aldrich and TTFP was obtained from Halocarbon Products Corporation and purified before use. Both additives are colorless liquids that are readily miscible with the electrolyte. Below, all potentials are given vs  $\text{Li}^+/\text{Li}$  couple.

Galvanostatic charge/discharge cycling was conducted between 4.6 and 3.0 V cutoff voltages at C/3 rate following the two initial (“formation”) cycles carried out at C/10 rate. Cell voltage profiles and capacity were recorded using a MACCOR Electrochemical Analyzer (MIMSciEnt). The impedance spectra were obtained using a Solartron analyzer operated between 0.01 Hz and 1 MHz with the amplitude of 10 mV. Linear sweep voltammetry was performed using a Bio-Logic VMP3 station in a three-electrode configuration with Pt electrode (100  $\mu\text{m}$  in diameter) as a working electrode and lithium metal as counter and reference electrodes; the scan rate was 10 mV/s.

For post-test analysis, the cycled cells were disassembled in an argon-filled glovebox, and the cycled electrolyte was collected by dipping the electrodes and the separator in small amount of chloroform-*d* for NMR analysis. The electrodes were thoroughly rinsed with anhydrous dimethyl carbonate and dried in a vacuum oven. The morphologies of the harvested electrodes were examined with scanning electron microscopy (SEM) using a Hitachi S-4700-II microscope in the Electron Microscopy Center of Argonne National Laboratory. X-ray photoelectron spectroscopy (XPS) measurements were carried out at the Electrochemical Discovery Laboratory of the Joint Center for Energy Storage Research at Argonne National Laboratory using an Omicron ESCA probe with Al K $\alpha$  source. A low-energy electron flood gun was used to compensate for x-ray beam induced surface charging. C<sub>1s</sub> line (284.8 eV) was used for energy calibrations. Samples for proton nuclear magnetic resonance (<sup>1</sup>H NMR) were prepared by rinsing of the disassembled cell with chloroform-*d*. These NMR spectra were obtained using a Bruker Avance III HD 300 MHz spectrometer. The chemical shifts in parts per million (ppm) are given vs tetramethylsilane standard.

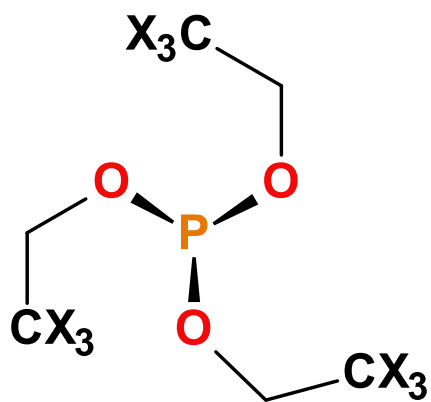
### **5.3. Results and discussion**

#### **5.3.1. Oxidative decomposition of additives**

To determine the oxidation stability of P(OR)<sub>3</sub> additives shown in Figure 5.1, linear sweep voltammetry measurements were performed and the results are shown in Figure 5.2a. For Gen 2 electrolyte, the anodic current increases drastically at 6.5 V, indicating the onset of solvent decomposition. When 1.0 wt% TEP was added to this electrolyte, an additional anodic current from TEP oxidation was observed at 4.2 V; this current increased slowly between 4.2 to 4.6 V

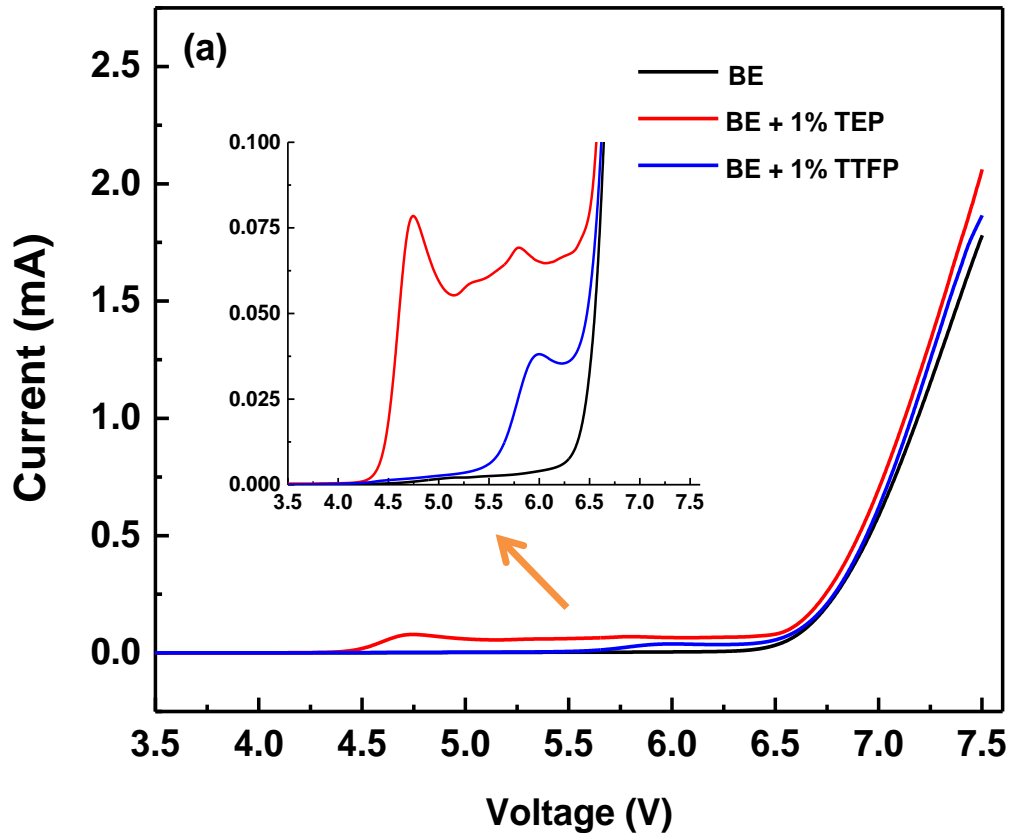
and then abruptly increased between 4.6 and 6.5 V. For electrolyte containing 1.0 wt% TTFP, the oxidation occurred at 5.5 V, which is significantly higher than for TEP. As was observed in the Introduction Section, this increase in the potential is due to the electron withdrawing effect of the fluorinated groups in TTFP.<sup>21</sup>

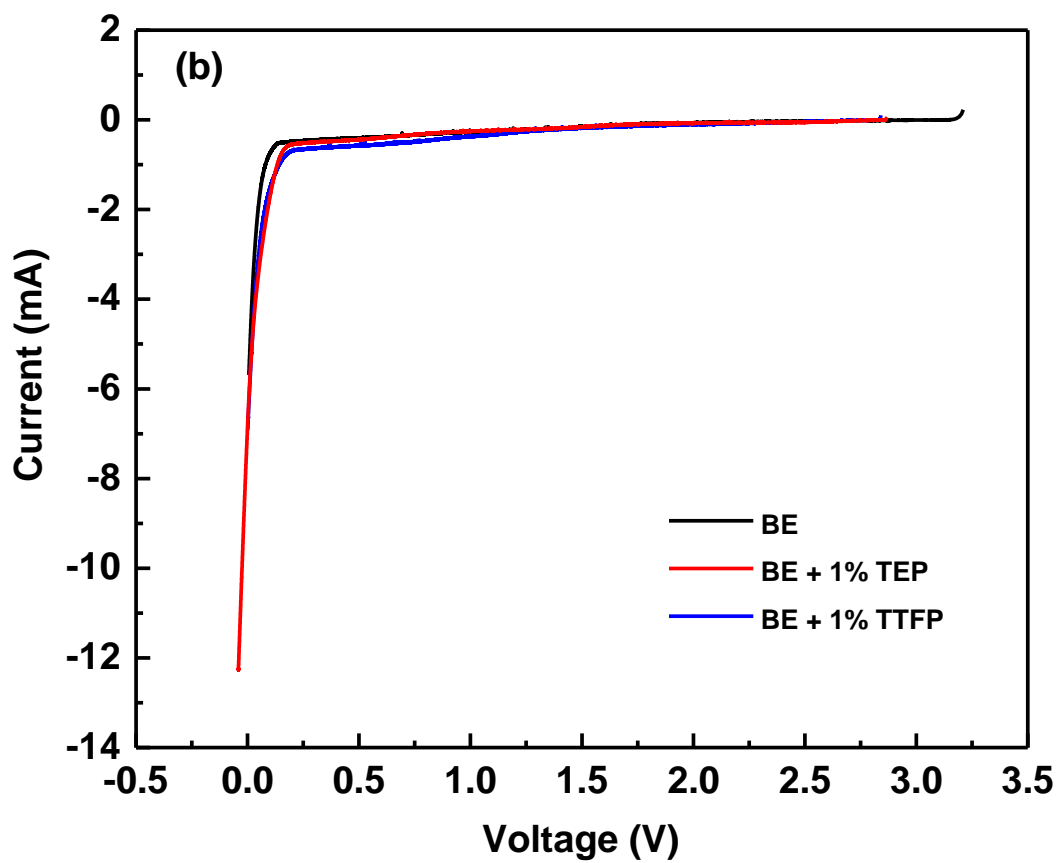
From previous studies, the most likely reaction for oxidation of the phosphite additives in the solvent bulk is the deprotonation of their alpha-methylene groups yielding an alkyl radical species.<sup>33, 34</sup> Our measurements indicate that TEP and TTFP are oxidized prior the solvent molecules, implying that both of these compounds can be considered for high voltage cells.<sup>25</sup> The electrochemical reduction of these two additives was also examined (Figure 5.2b). Except for the Li deposition peak at 0.12 V, no obvious features were observed, suggesting that TEP and TTFP did not interfere with SEI formation on the graphite electrode. This is in contradiction to the organophosphate additives ( $\text{OP}(\text{OR})_3$ ) used by others,<sup>35</sup> for which there is irreversible decomposition in the reduced state due to elimination of a substituting group (such as an  $\text{R}\cdot$  radical) and the formation of  $\text{Li}^+$  binding anions  $^-\text{O}_2\text{P}(\text{OR})_2$  (see<sup>36</sup> and references therein).



**X=H: TEP**  
**X=F: TTFP**

**Figure 5.1.** Structural formulas for TEP and TTFP additives.

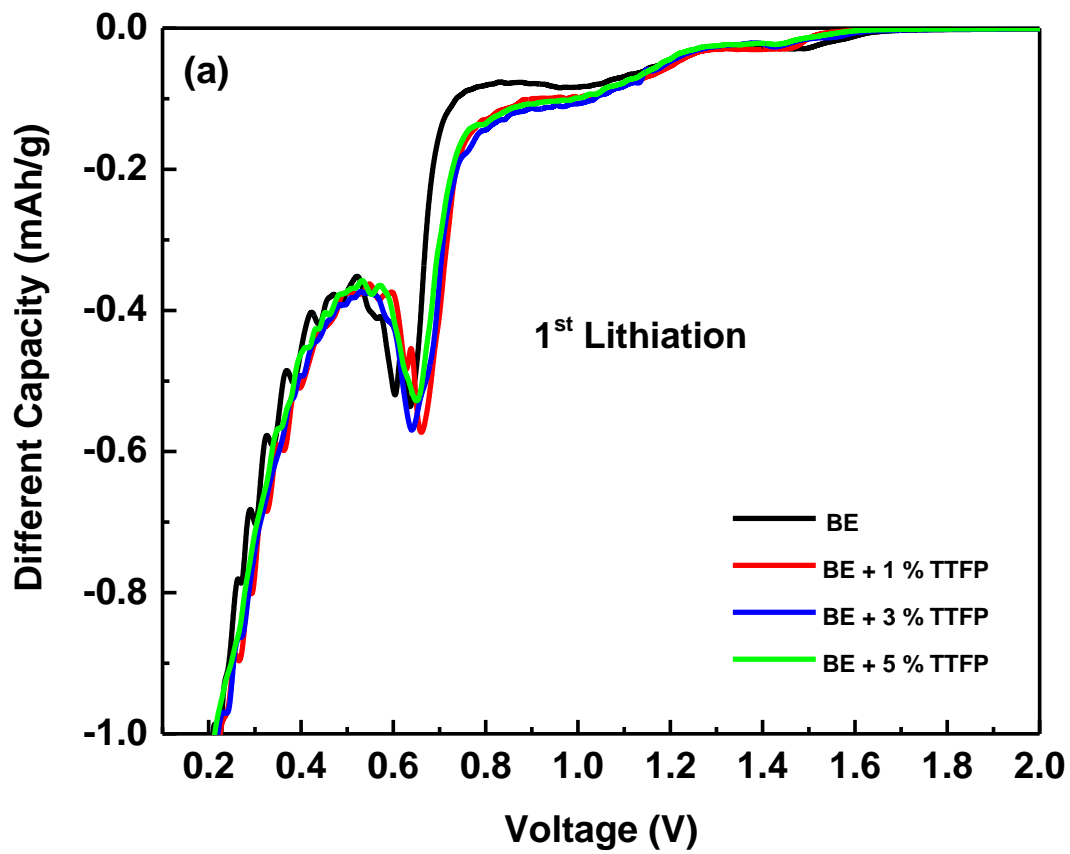




**Figure 5.2.** Linear sweep voltammograms of baseline electrolyte and electrolyte containing 1.0% TEP and 1.0% TTFP additives. (a) Oxidation sweep and (b) reduction sweep. (Pt/Li/Li three-electrode cell with a scan rate of 10 mV/s; Insets in (a) is expansion of the electrolyte oxidation region).

### 5.3.2. Differential capacity ( $dQ/dV$ ) measurements of graphite anode

To further assess the effect of these two additives on electrolyte reduction, graphite/Li half cells were assembled. Differential capacity ( $dQ/dV$ ) as a function of voltage for the first cycle of baseline cell and two additive cells is shown in Figure 5.3. The 0.65 V peak indicates the formation of SEI on the lithiated graphite surface from reductive decomposition of baseline electrolyte.<sup>1</sup> This peak does not change when TEP or TTFP additive was added to the baseline electrolyte with concentration of 1%, 3% and 5% and no new peaks emerged. The same was observed for the second charge/discharge cycle (not shown). These results indicate little or no interference of the phosphite additive with the electrochemical processes taking place on the graphite electrode.



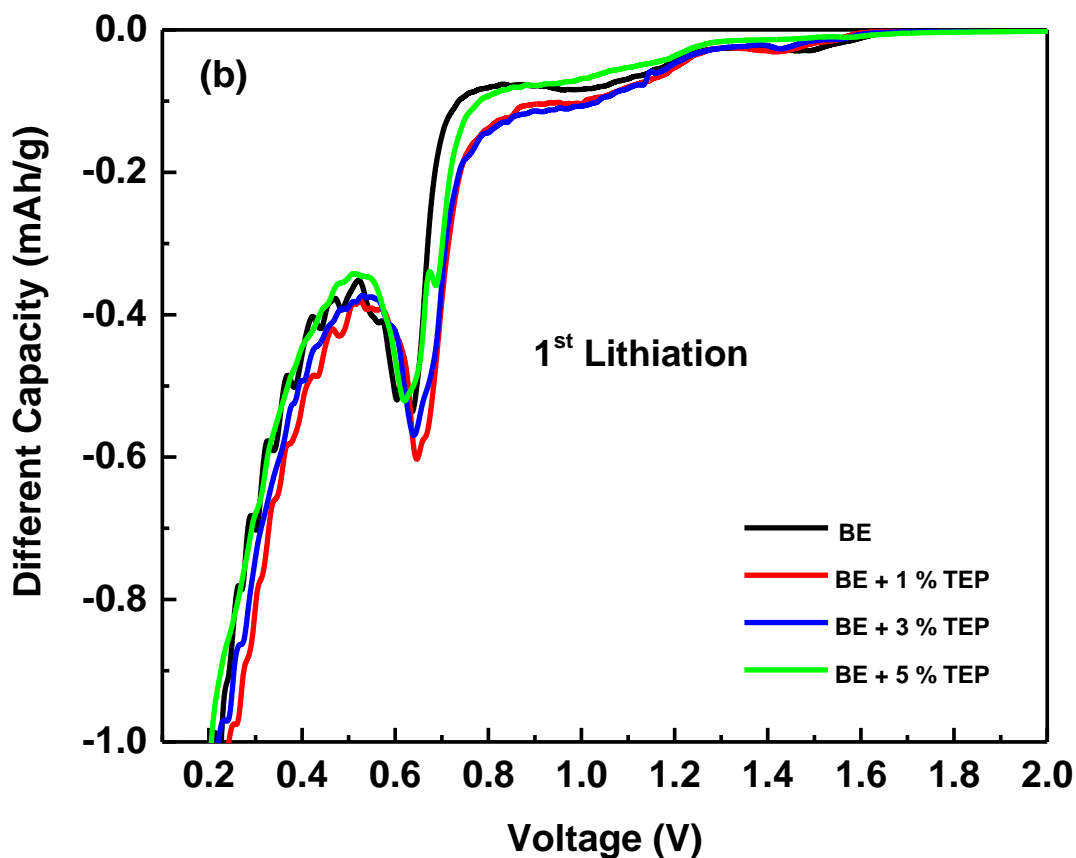


**Figure 5.3.** Differential capacity  $dQ/dV$  plotted as a function of cell voltage for the initial charge/discharge cycle of graphite/Li cells containing 0, 1, 3, and 5 wt% (a) TEP and (b) TTFP.

### 5.3.3. NCM523/graphite cell performance

$\text{LiNi}_{0.5}\text{Co}_{0.2}\text{Mn}_{0.3}\text{O}_2$ /graphite cells were subjected to charge-discharge cycling at a rate of  $C/3$  with the cutoff voltage between 4.6 V and 3.0 V. The voltage profiles for Gen2 cells, with and without 1.0 wt% additive, are shown in Figure 5.4a-4c. For the baseline cell containing no

additives, large voltage polarization was observed during the cycling test,<sup>22</sup> while the extent of this polarization was reduced when TTFP was added to the electrolyte.

Figure 5.4d shows the cycling performance of these cells. For the baseline cell (which exhibits rapid capacity fading) the initial charge and discharge capacities are 254 and 216 mAh/g, respectively (that corresponds to 84.9% Coulombic efficiency). The capacity retention is 76.9% after 50 cycles, and the Coulombic efficiency is maintained at 99.4% over 50 cycles. With 1.0 wt% TEP, the cell shows slightly improved performance. The initial charge and discharge capacities are 250 and 204 mAh/g, respectively, resulting in a Coulombic efficiency of 81.9%. The capacity retention is 82%, and the Coulombic efficiency is maintained at 98.5% over 50 cycles. In contrast, the cell containing 1.0 wt% TTFP shows significantly improved cycling performance. The first cycle charge and discharge capacities are 260 and 222 mAh/g, respectively, with 85.5% initial Coulombic efficiency that is maintained at 99.7% over 50 cycles.

It is well known that SEI formation on graphite electrode leads to loss of  $\text{Li}^+$  inventory causing irreversible capacity decrease. Additionally, oxidative decomposition of organic solvent/additive on the cathode surface causes further lithiation and/or Li plating on the graphite electrode in the closed circuit. This process depletes the lithium salt and changes the bulk properties of the electrolyte. The Coulombic efficiency during the high voltage cycling is always lower than for normal voltage cycling. The cell containing 1.0 wt% TEP exhibits the lowest Coulombic efficiency and the observed capacity fading is thought to result from the decomposition of the electrolyte<sup>1, 2</sup> and/or the accompanied corrosion<sup>4, 5</sup> of the cathode material. The improved cycling performance and Coulombic efficiency for the cell containing 1.0 wt% TTFP suggests

that the electrolyte decomposition is suppressed due to the passivation of the cathode surface during the initial oxidation of TTFP.

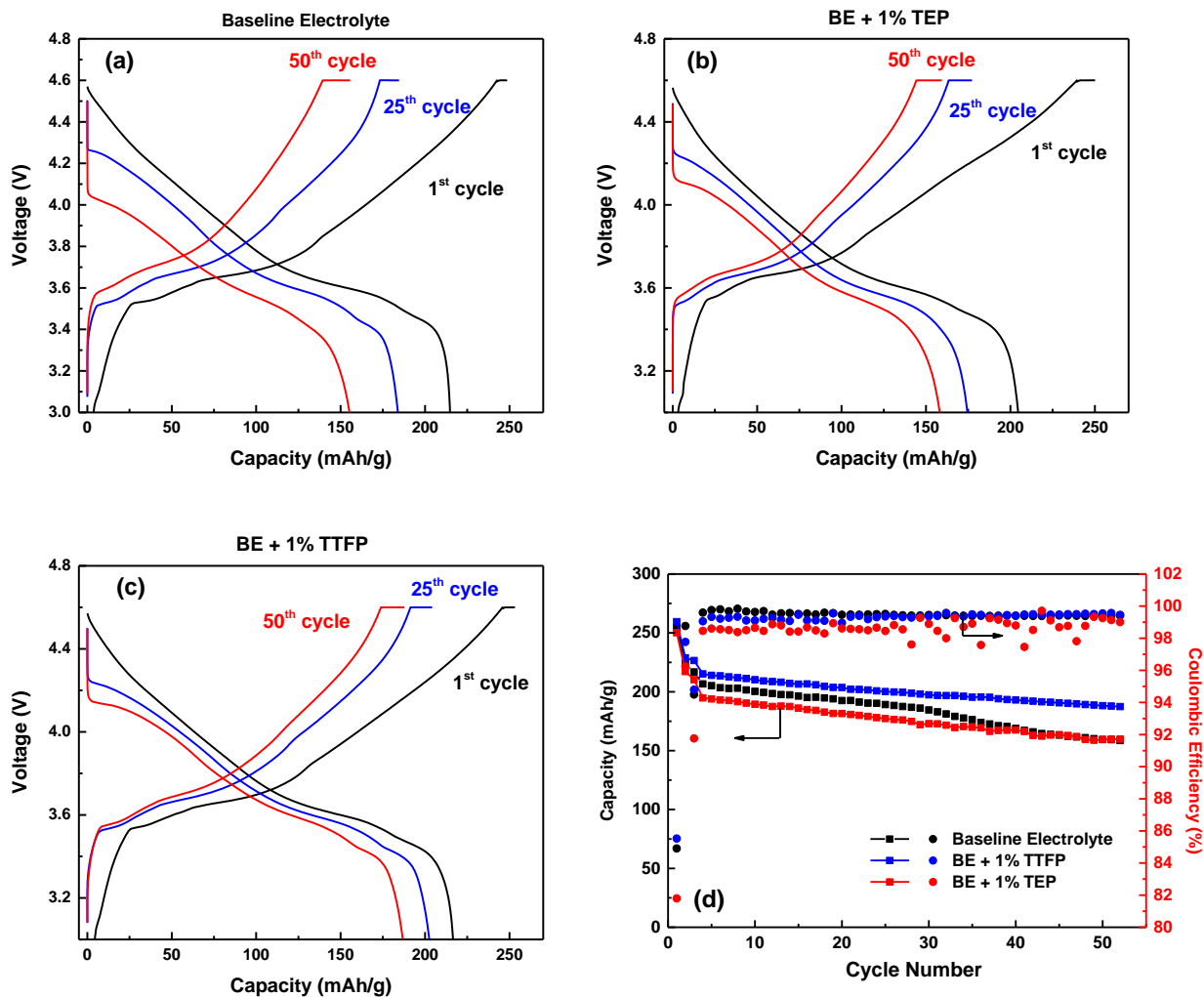


**Figure 5.4.** Voltage profiles for  $\text{LiNi}_{0.5}\text{Co}_{0.2}\text{Mn}_{0.3}\text{O}_2/\text{graphite}$  cells containing (a) BE, (b) BE + 1% TEP, and (c) BE + 1 wt% TTFP at the 1<sup>st</sup>, 25<sup>th</sup> and 50<sup>th</sup> cycle. Panel (d) indicates the capacity retention and Coulombic efficiency for these cells as a function of the cycle number.

#### 5.3.4. Electrochemical impedance spectroscopy.

Impedance spectroscopy was used to probe the nature of the cathode surface layer. The impedance spectra obtained after the first cycle and the subsequent cycling are shown in Figures 5.5a and 5b, respectively. These impedance spectra consist of two semi-cycles, with the one in the high frequency range associated with the interfacial impedance of the SEI layer ( $R_{SEI}$ ), and the one in the low frequency region representing the charge transfer resistance ( $R_{ct}$ ).<sup>3</sup> These resistances were estimated by fitting of the impedance spectra using the equivalent circuits shown in the insets. These estimates are given in Table 5.1. After the two initial (formation) cycles, the cells with and without TTFP showed similar interfacial and charge transfer resistances, while the cell containing TEP showed changed resistances. After the subsequent 50 cycles, TTFP cells displayed significantly lower cathode charge transfer resistances, suggesting that TTFP-derived coating efficiently suppressed electrolyte breakdown (that ordinarily results in the formation of thick, insulating deposits with large resistance). In contrast, the cells containing TEP exhibited higher cathode charge transfer resistance already after the initial cycling, and this resistance became still greater upon the subsequent cycling, suggesting that TEP-derived interphase acted as an insulator for  $Li^+$  ions.

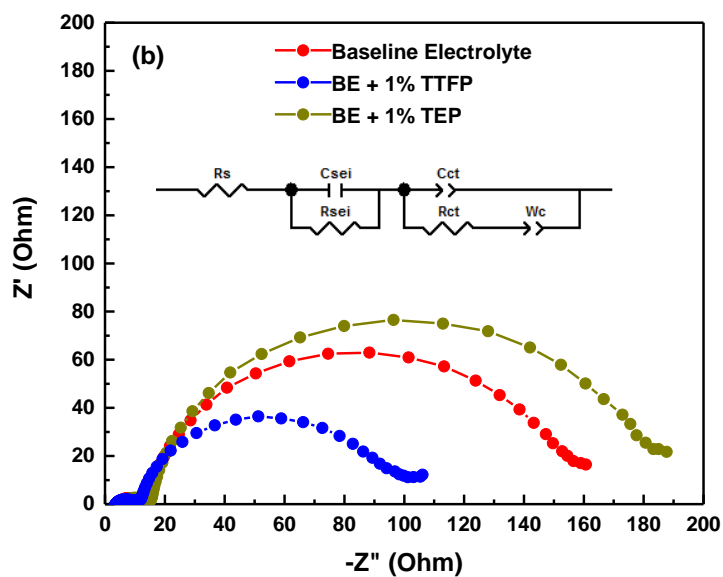
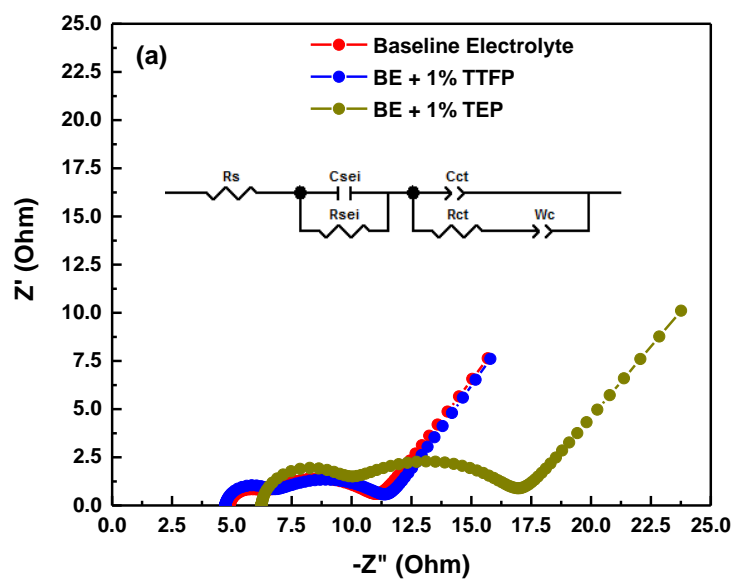


**Figure 5.5.** Electrochemical impedance spectra for  $\text{LiNi}_{0.5}\text{Co}_{0.2}\text{Mn}_{0.3}\text{O}_2/\text{graphite}$  cells (a) after the two initial cycles and (b) after 50 cycles.

**Table 5.1.** Estimates for interfacial and charge transfer resistances obtained from the model shown in Figure 5.

Cell	After 1 <sup>st</sup> cycle			After 50 <sup>th</sup> cycle		
	$R_I$	$R_{SEI}$	$R_{CT}$	$R_I$	$R_{SEI}$	$R_{CT}$
<b>Gen 2</b>	<b>4.8</b>	<b>1.75</b>	<b>5.3</b>	<b>4.9</b>	<b>10.2</b>	<b>140.2</b>
<b>1.0 wt% TEP</b>	<b>6.2</b>	<b>5.42</b>	<b>10.8</b>	<b>7.3</b>	<b>13.5</b>	<b>175.3</b>
<b>1.0 wt% TTFP</b>	<b>4.7</b>	<b>1.78</b>	<b>5.4</b>	<b>4.8</b>	<b>9.6</b>	<b>80.3</b>

$R_I$ : initial resistance;  $R_{SEI}$ : interfacial resistance;  $R_{CT}$ : charge transfer resistance (all resistances are given in the unit of Ohm)

### 5.3.5. Post mortem analyses of harvested electrodes and electrolytes

Figure 5.6 shows SEM images of the pristine NCM523 cathode and the same electrode after 50 cycles. In the pristine cathode, the secondary particle surface is clean and unobstructed. In the baseline electrolyte, the surface of a cycled cathode becomes covered with thick deposits (indicated with the red arrow in Figure 5.6b), suggesting extensive electrolyte decomposition and material corrosion. The electrodes cycled in the presence of TEP or TTFP instead exhibited compact layers and no thick deposits due to electrolyte decomposition were observed (Figures 5.6c and 6d). Thus, according to SEM, both additives were able to form the protective coating that inhibited electrolyte breakdown after prolonged cycling. In this sense, the two additives behaved in the same way. However, as suggested by the impedance spectra discussed in section

3.4, the protective layer derived from TEP hinders  $\text{Li}^+$  ion transport, causing inferior performance.

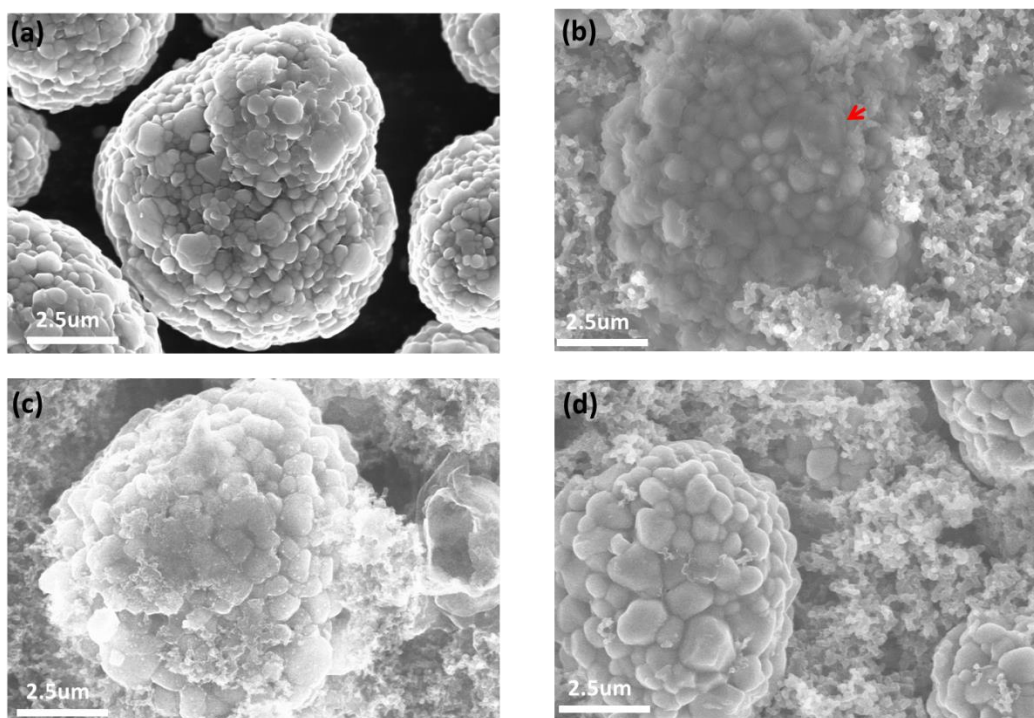


**Figure 5.6.** SEM images of (a) NCM523 particles prior to the test, (b) the same material from a cycled cell containing Gen2 electrolyte, (c) Gen 2 containing 1.0 wt% TEP and (d) Gen2 containing 1.0 wt% TTFP.

### 5.3.6. X-ray photoelectron spectra of cycled cathodes

Figure 5.7 presents XPS spectra of the pristine and cycled electrodes. Figure 5.7a gives the expanded  $C_{1s}$  region. In both cycled cathodes, the  $C_{1s}$  peak at 284.8 eV originates from the C-C bond in carbon black,<sup>37</sup> while the peaks at 286.5 and 288 eV arise from the C-O and C=O bonds, respectively. These peaks are attributed to  $ROCO_2Li$ ,  $ROLi$  and  $Li_2CO_3$  materials that are the known products of electrolyte decomposition.<sup>15</sup> The peak at 291.5 eV corresponds to a  $CF_2$  group from PVDF binder.<sup>15</sup> Importantly, a peak at 292.8 eV appears on the electrode in the cycled cell containing 1.0 wt% TTFP. This peak originates from the trifluoromethyl groups,<sup>38</sup> suggesting the presence of a TTFP-derived product bound to the surface, as was previously noticed by Pires *et al.*<sup>32</sup>

Figure 5.7b presents the  $O_{1s}$  spectra. The peaks at 529.5 and 531.8 eV are attributed to lattice  $MO_2$  (where M is a transition metal) and  $M_2O_3$  oxide in the layered  $LiNi_{0.5}Co_{0.2}Mn_{0.3}O_2$ .<sup>37</sup> A new peak at 533.5 eV is observed in the cycled electrode that originates from the C-O bonds in the products of electrolyte decomposition. Compared to the electrode harvested from the cell containing 1.0 wt% TTFP, the electrode from the control cell shows a lower MO and  $M_2O_3$  peak intensity. That is caused by a thicker electrolyte deposit on the latter (Figure 5.6b). Comparison of  $F_{1s}$  spectra is shown in Figure 5.7c. The strongest peak at 687.5 eV is from the PVDF binder. The LiF peak at 685 eV in the cycled electrodes is due to the decomposition of  $LiPF_6$ .<sup>32</sup> For the electrode from a cell containing 1.0 wt% TTFP, a small peak at 689 eV is observed that we attribute to the trifluoromethyl group<sup>38</sup> in the decomposition product of TTFP.

In the  $P_{2p}$  region, no photoelectron peaks were observed from the pristine electrode. The cycled electrodes showed a strong peak at 135 eV, which can be attributed to the species containing a (fluoro)phosphate group.<sup>32</sup> This group can originate from the decomposition of TTFP additive and/or  $LiPF_6$  salt. To identify the contribution of TTFP on the surface layer formation on cathode, new electrolyte with a non-phosphorous containing lithium salt  $LiBF_4$  was prepared (1.0 M  $LiBF_4$  EC/EMC (3/7 in weight ratio)+5% TTFP). The cycled cathode with this electrolyte was analyzed by SEM/EDS and XPS (data not shown). The presence of (fluoro)phosphate group confirmed the decomposition of TTFP on the surface of cathode. Taken together, these XPS results support our assertion that decomposition of the phosphite additives during the first charging cycle impedes the subsequent electrolyte breakdown. Interestingly, they also suggest that the substituting trifluoromethyl groups in TTFP are still present on the surface as these phosphite additives are oxidized to the phosphates.

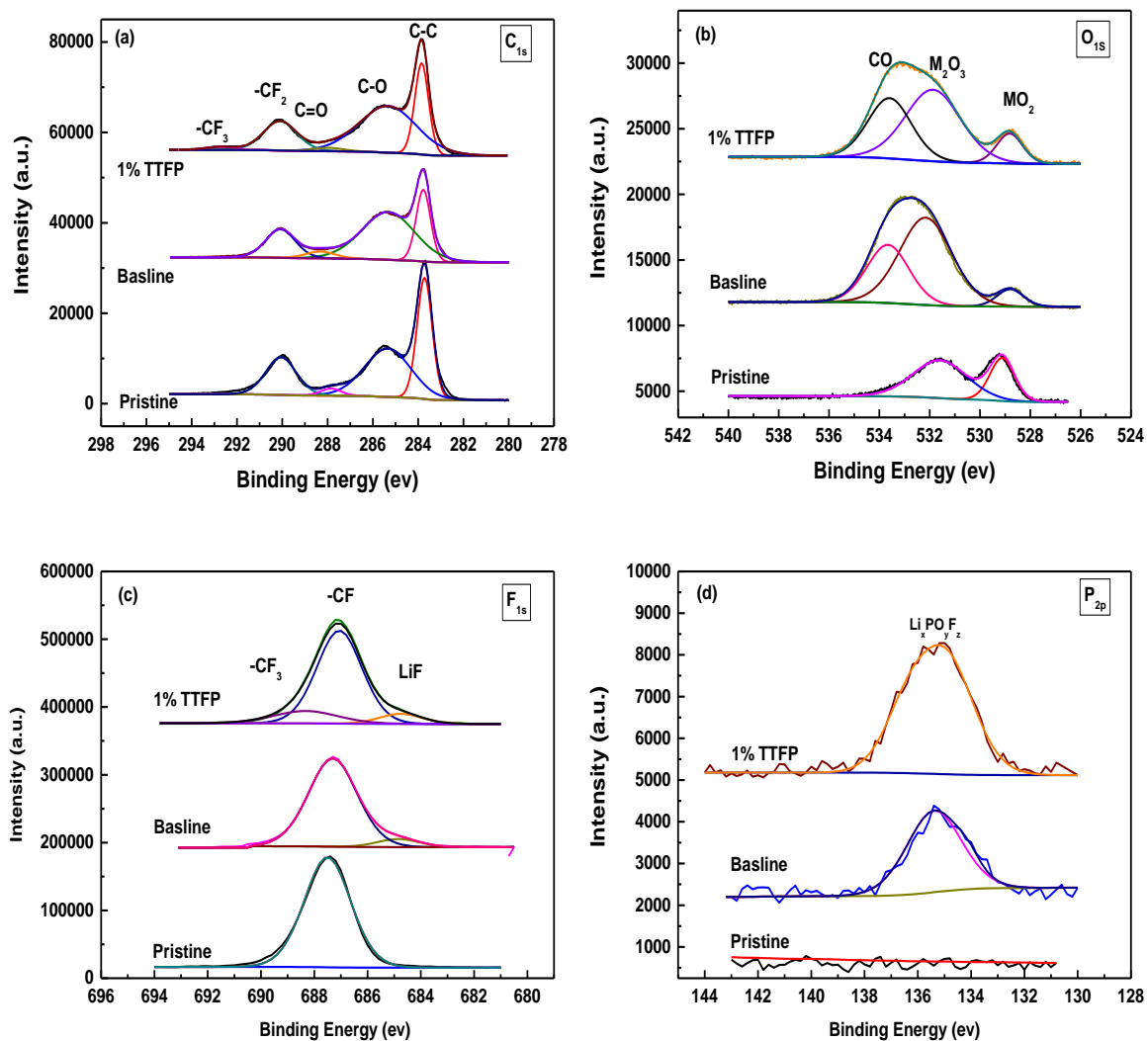


**Figure 5.7.** Photoelectron spectra of cycled  $\text{LiNi}_{0.5}\text{Co}_{0.2}\text{Mn}_{0.3}\text{O}_2$  electrodes in the (a)  $\text{C}_{1s}$ , (b)  $\text{O}_{1s}$ , (c)  $\text{F}_{1s}$ , and (d)  $\text{P}_{2p}$  regions.

### 5.3.7. Decomposition products

Proton NMR spectra of the cell fluid were obtained after 50 cycles and compared to the original electrolyte (Figure 5.8). Figure 5.8a shows the expanded section (3.6 to 4.4 ppm) of the  $^1\text{H}$  NMR spectrum from Gen2 electrolyte prior to the cycling tests. This range was chosen as it shows the greatest differences in the NMR spectra before and after cycling. The quartet at 4.20 ppm and the singlet at 3.78 ppm correspond to the methylene and methoxy protons in EMC component. After 50 cycles (Figure 5.8b), the  $^1\text{H}$  NMR spectrum from the cell containing Gen2 electrolyte exhibits new species whose resonance lines correspond to the diethyl carbonate (DEC), which is observed as a quartet at 4.21 ppm (for methylene protons) and dimethyl carbonate (DMC), which is observed as a singlet at 3.79 ppm (from methyl protons); these new resonance lines are superimposed on the resonance lines from EMC. In the cycled cell containing 1.0 wt% TTFP, these additional resonance lines were greatly reduced (Figure 5.8c). Since DEC and DMC are the products of transesterification of EMC, we surmise that catalytic centers on the cathode are involved in such reactions. Thus, the absence of these products in TTFP solutions can be interpreted as inactivation of such catalytic centers and/or the formation of a thin protective coating on the electrode.

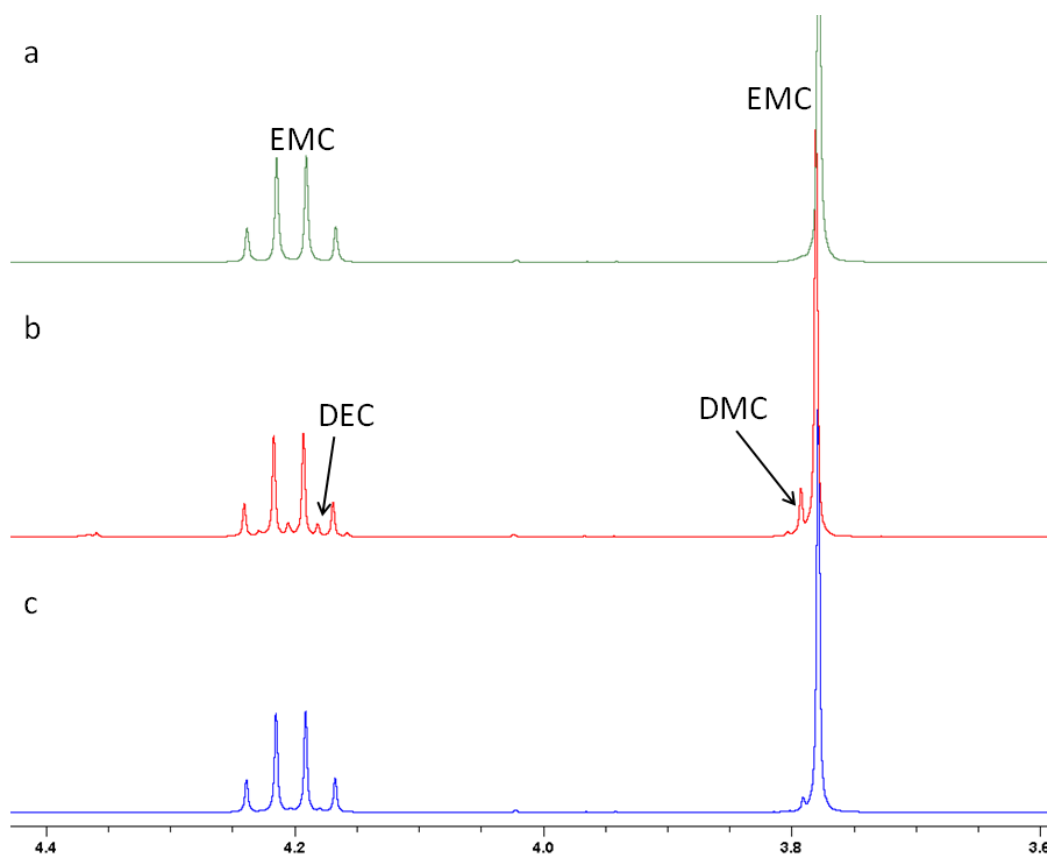


**Figure 5.8.** An excerpt of the  $^1\text{H}$  NMR spectra from (a) Gen2 electrolyte before cell cycling and (b,c) collected cell fluids from the (b) Gen2 and (c) Gen2 + 1.0 wt% TTFP cells after 50 cycles.

### 5.3.8. Mechanism for the protective action

To account for these observations, we suggest the existence of catalytically active centers at the surface of the electrode that accelerate the oxidation of solvent molecules in the electrolyte. From previous studies of photo(electro)catalysis on transition metal oxides (e.g., <sup>39-41</sup>), the most likely candidate for such a reaction center is a bound hydroxyl group, M-OH, that commonly terminates these oxide surfaces. When the cell is energized, this group becomes oxidized, deprotonates, and yields the M-O $\cdot$  radical that readily abstracts hydrogen from the solvent

molecule (LH), in the process converting back to the M-OH form (Figure 5.9). The latter becomes oxidized again, completing the catalytic cycle. The resulting solvent radical L• initiates reactions that result in irreversible loss of the solvent. Oxidation of P(OR)<sub>3</sub> molecules in the bulk is known to yield [P(OR)<sub>3</sub>]<sub>2</sub><sup>+</sup> cations that preferentially deprotonate from α-carbon, yielding the corresponding alpha-carbon radical.<sup>33, 34</sup> We suggest that P(OR)<sub>3</sub> additives react differently on the surface than in the bulk: instead of H atom abstraction, radical addition takes place with the formation of a phosphoranyl radical (Figure 5.9). Shortly thereafter, this radical undergoes β-scission with the release of R• radical and forms the phosphate shown in Figure 5.9. These reactions (for oxygen-centered organic radicals) are well known in radical chemistry.<sup>42</sup> The reason the addition is preferred over the abstraction is the favorable energetics of P-O bond formation (see below). The resulting organophosphate ligand permanently inactivates the reaction center and prevents catalytic oxidation of the solvent. The breakdown of the latter either slows down, or requires a higher potential to occur. Thus, even a relatively low concentration of the additive can have dramatic impact on the electrocatalytic activity of the oxide surface.

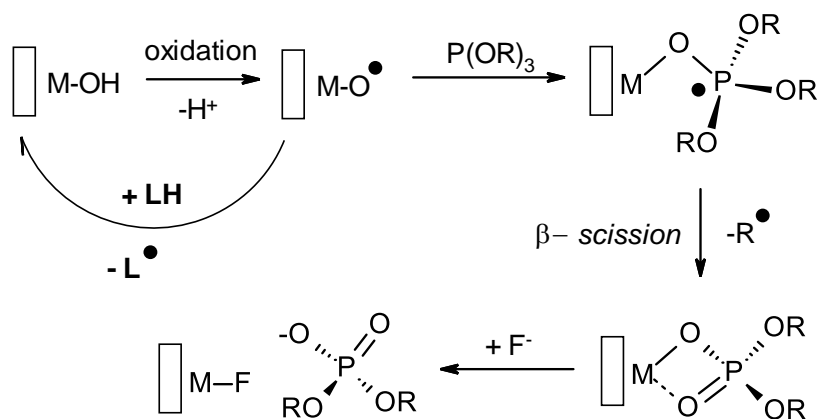


**Figure 5.9.** The proposed electrocatalytic cycle.

To ascertain the suggested mechanism we turned to density functional theory (DFT) modeling using B3LYP/6-31+G(d,p) functional. The simplest phosphite molecule, trimethylphosphite, represented the additive, while MO• center was represented by (HO)<sup>2</sup>Al<sup>III</sup>O• species (aluminum hole center), as shown in Figure 5.10. According to our gas phase calculation, the H abstraction from trimethylphosphite by this reactive center is exergonic by 0.62 eV, whereas the addition of the same molecule to the non-bridging oxygen is exergonic by 2.11 eV. The elimination of RO- arm (with the formation of the hydroxymethyl radical) is considerably less favored energetically than the postulated  $\beta$ -scission, which is exergonic by 1.01 eV. These estimates indicate that the formation of M[O<sub>2</sub>P(OR)<sub>2</sub>] phosphate and elimination of R• radical is the favored reaction path, as can be expected by analogy to reactions of alkoxy radicals.<sup>42</sup> Somewhat similar reactions with triplet oxygen and/or superoxide radicals (derived via the oxygen reduction)<sup>43, 44</sup> were suggested by Pires *et al.*,<sup>32</sup> but our mechanism obviates the need to postulate the formation of oxygen, for which there is scant experimental evidence.

The reactions shown in Figures 5.9 and 5.10 rationalize our XPS results, as they account for (i) the retention of the substituting RO- groups in the reaction product (that are observed through the C<sub>1s</sub> and F<sub>1s</sub> lines in XPS spectra shown in Figure 5.7) and (ii) the concurrent appearance of the phosphate group (observed through P<sub>2p</sub> lines). This scheme also explains how the phosphite additive becomes covalently attached to the electrode surface. However, by itself, this scheme does not explain the difference in Li<sup>+</sup> ion transport that was observed between TEP and TTFP. A possible rationale is that the phosphate groups eventually become exchanged with other anions, yielding thin LiOP(O)(OR)<sub>2</sub> deposits that serve as “protective coatings” inferred in our studies.

This exchange is possible, for example, through electrochemical generation of HF and  $\text{HPOF}_2$  (which are the known products of  $\text{LiPF}_6$  decomposition/hydrolysis near the cathode surface, e.g. 4, 23, 45). Aggregation of these organophosphate salts and the products of their further oxidation (that involves H abstraction from the substituting groups and the ensuing polymerization) can create a thin barrier impeding  $\text{Li}^+$  migration into the solvent bulk. The formation of such deposits may be difficult to distinguish by XPS from the presence of  $\text{MO}_2\text{P(OR)}_2$  centers in Figure 5.9. As the mobility of  $\text{Li}^+$  ions is very sensitive to the composition of such deposits, the performance of the cells can also be very sensitive to variations in the additive structure.

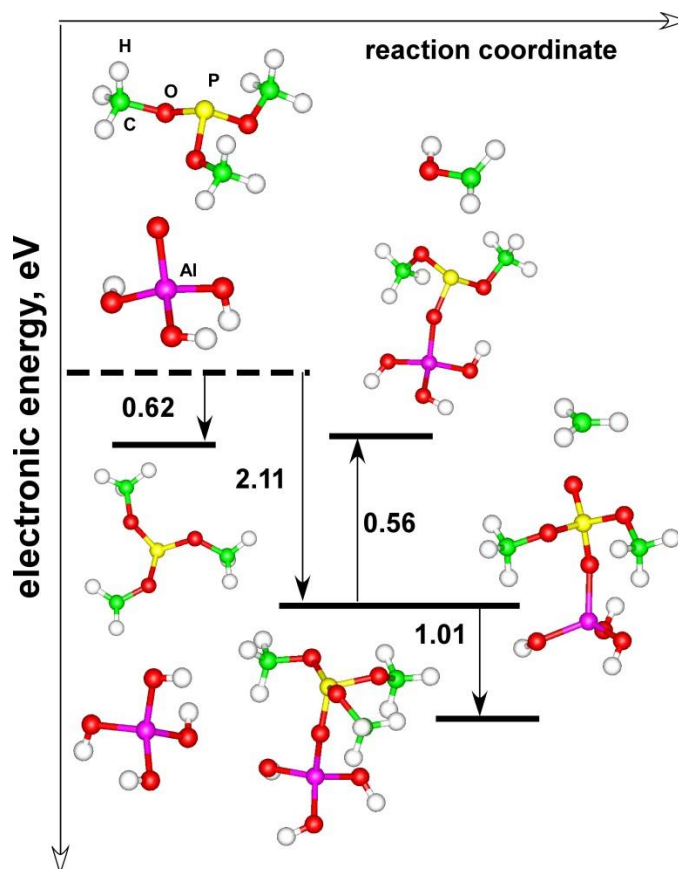


**Figure 5.10.** Energetics of reactions between  $\text{P(OMe)}_3$  and a model Al oxygen hole center according to our DFT calculations. The insets in the plot demonstrate optimized structures in the gas phase. All energies are given in the units of eV.

Recently, Han *et al.*<sup>23</sup> speculated that the entire benefit of tris(trimethylsilyl)phosphite  $\text{P}[\text{OSi}(\text{CH}_3)_3]$  derives from the reaction with HF acid that is generated near the cathode surface (through the decomposition of  $\text{PF}_6^-$  anions); this reaction yields  $\text{HOP}(\text{OR})_2$  acid and RF fluoro-compound. Through this reaction, the additive consumes HF acid preventing the corrosion of the cathode.<sup>4</sup> For trimethylsilyl derivative, this reaction is strongly exergonic, whereas for TEP and TTFP, it is almost thermoneutral. Since TTFP exhibits the same beneficial effect as the tris(trimethylsilyl)phosphite, we believe that the phosphite compounds act in a more subtle way than envisioned by Han *et al.*<sup>23</sup>

## 5.4 Conclusion

In this study, we compared the effectiveness of TEP and TTFP as cathode protecting electrolyte additive in  $\text{LiNi}_{0.5}\text{Co}_{0.2}\text{Mn}_{0.3}\text{O}_2/\text{graphite}$  4.6 V cells. Both of these molecules have a lower oxidation potential than the solvent molecules in the carbonate electrolyte. The electrochemical performance of cells containing 1.0 wt% TTFP was significantly improved as compared to the baseline system. This improvement is attributed to selective decomposition of TTFP during the initial charging cycle, which results in a modification of the cathode surface that prevents subsequent rapid oxidation of the solvent. This modification can be the inhibition of catalytic centers on the electrode surface (Figures 5.9 and 5.10) and/or the formation of a protective coating consisting of decomposition products derived from the additive (most likely, the organophosphates). The prevention of oxidation and transesterification of the carbonate molecules can be rationalized either way. For the cell containing 1.0 wt% TEP, the decomposition of the additive also takes place, but the resulting coating blocks  $\text{Li}^+$  ion transport,

resulting in low Coulombic efficiency and high interfacial resistance. Thus, it appears that the role of the fluorination may be less in the manner of chemical changes involving the surface active centers than in the different rates for  $\text{Li}^+$  migration through the resulting layer. The presence of the trifluoromethyl groups at the surface (as suggested by XPS) indicates that the oxidation/decomposition of TTFP does not result in complete mineralization. We suggest that the phosphite additives react with the catalytic centers inactivating them through the formation of phosphates as shown in Figure 5.9. The phosphates eventually form a protective coating on the surface, but even such a thin coating can hinder  $\text{Li}^+$  ion transport which appears to be the case for TEP. The role of fluorination may be in preventing the complete mineralization of the organophosphate deposits through their progressive oxidation, as the  $\text{RO}_2\text{P}(\text{OR})_2$  phosphates bind  $\text{Li}^+$  ions less strongly than  $\text{PO}_4^{3-}$  anions, allowing a modicum of  $\text{Li}^+$  mobility through the electrode/electrolyte interphase.

## References

- (1) Xu, K. Nonaqueous Liquid Electrolytes for Lithium-Based Rechargeable Batteries. *Chem. Rev.* **2004**, *104*, 4303-4418.
- (2) Zhang, S.; Ding, M. S.; Xu, K.; Allen, J.; Jow, T. R. Understanding Solid Electrolyte Interface Film Formation on Graphite Electrodes. *Electrochem. Solid State Lett.* **2001**, *4*, A206-A208.
- (3) Xu, B.; Qian, D.; Wang, Z.; Meng, Y. S. Recent Progress in Cathode Materials Research for Advanced Lithium Ion Batteries. *Mater. Sci. Eng. Reports* **2012**, *73*, 51-65.
- (4) Lin, F.; Markus, I. M.; Nordlund, D.; Weng, T.-C.; Asta, M. D.; Xin, H. L.; Doeff, M. M. Surface Reconstruction and Chemical Evolution of Stoichiometric Layered Cathode Materials for Lithium-Ion Batteries. *Nat. Commun.* **2014**, *5*, 3529 (9 pages).
- (5) Mohanty, D.; Kalnaus, S.; Meisner, R. A.; Rhodes, K. J.; Li, J.; Payzant, E. A.; Wood III, D. L.; Daniel, C. Structural Transformation of a Lithium-Rich  $\text{Li}_{1.2}\text{Co}_{0.1}\text{Mn}_{0.55}\text{Ni}_{0.15}\text{O}_2$  Cathode During High Voltage Cycling Resolved by in Situ X-Ray Diffraction. *J. Power Sources* **2013**, *229*, 239-248.
- (6) Abe, K.; Yoshitake, H.; Kitakura, T.; Hattori, T.; Wang, H.; Yoshio, M. Additives-Containing Functional Electrolytes for Suppressing Electrolyte Decomposition in Lithium-Ion Batteries. *Electrochim. Acta* **2004**, *49*, 4613-4622.
- (7) Sa, Q.; Gratz, E.; He, M.; Lu, W.; Apelian, D.; Wang, Y. Synthesis of High Performance  $\text{LiNi}_{1/3}\text{Mn}_{1/3}\text{Co}_{1/3}\text{O}_2$  from Lithium Ion Battery Recovery Stream. *J. Power Sources* **2015**, *282*, 140-145.
- (8) Ohzuku, T.; Makimura, Y. Layered Lithium Insertion Material of  $\text{LiCo}_{1/3}\text{Ni}_{1/3}\text{Mn}_{1/3}\text{O}_2$  for Lithium-Ion Batteries. *Chem. Lett.* **2001**, *7*, 642-643.
- (9) Chikkannanavar, S. B.; Bernardi, D. M.; Liu, L. A Review of Blended Cathode Materials for Use in Li-Ion Batteries. *J. Power Sources* **2014**, *248*, 91-100.
- (10) Huang, Z.-D.; Liu, X.-M.; Oh, S.-W.; Zhang, B.; Ma, P.-C.; Kim, J.-K. Microscopically Porous, Interconnected Single Crystal  $\text{LiNi}_{1/3}\text{Co}_{1/3}\text{Mn}_{1/3}\text{O}_2$  Cathode Material for Lithium Ion Batteries. *J. Mater. Chem.* **2011**, *21*, 10777-10784.
- (11) Le, A. V.; Wang, M.; Shi, Y.; Noelle, D.; Qiao, Y.; Lu, W. Effects of Additional Multiwall Carbon Nanotubes on Impact Behaviors of  $\text{LiNi}_{0.5}\text{Mn}_{0.3}\text{Co}_{0.2}\text{O}_2$  Battery Electrodes. *J. Appl. Phys.* **2015**, *118*, 085312 (5 pages).
- (12) Jung, S.-K.; Gwon, H.; Hong, J.; Park, K.-Y.; Seo, D.-H.; Kim, H.; Hyun, J.; Yang, W.; Kang, K. Understanding the Degradation Mechanisms of  $\text{LiNi}_{0.5}\text{Co}_{0.2}\text{Mn}_{0.3}\text{O}_2$  Cathode Material in Lithium Ion Batteries. *Adv. Energy Mater.* **2014**, *4*, 1-7.
- (13) Sun, X.; Zhang, X.; Huang, B.; Zhang, H.; Zhang, D.; Ma, Y. ( $\text{LiNi}_{0.5}\text{Co}_{0.2}\text{Mn}_{0.3}\text{O}_2$  + Ac)/Graphite Hybrid Energy Storage Device with High Specific Energy and High Rate Capability. *J. Power Sources* **2013**, *243*, 361-368.
- (14) He, M.; Hu, L.; Xue, Z.; Su, C. C.; Redfern, P.; Curtiss, L. A.; Polzin, B.; von Cresce, A.; Xu, K.; Zhang, Z. Fluorinated Electrolytes for 5-V Li-Ion Chemistry: Probing Voltage Stability of Electrolytes with Electrochemical Floating Test. *J. Electrochem. Soc.* **2015**, *162*, A1725-A1729.
- (15) Lee, Y.-M.; Nam, K.-M.; Hwang, E.-H.; Kwon, Y.-G.; Kang, D.-H.; Kim, S.-S.; Song, S.-W. Interfacial Origin of Performance Improvement and Fade for 4.6 V  $\text{LiNi}_{0.5}\text{Co}_{0.2}\text{Mn}_{0.3}\text{O}_2$  Battery Cathodes. *J. Phys. Chem. C* **2014**, *118*, 10631-10639.

- (16) Song, M.-K.; Cho, J.-Y.; Cho, B. W.; Rhee, H.-W. Characterization of UV-Cured Gel Polymer Electrolytes for Rechargeable Lithium Batteries. *J. Power Sources* **2002**, *110*, 209-215.
- (17) Kong, J.-Z.; Ren, C.; Tai, G.-A.; Zhang, X.; Li, A.-D.; Wu, D.; Li, H.; Zhou, F. Ultrathin ZnO Coating for Improved Electrochemical Performance of  $\text{LiNi}_{0.5}\text{Co}_{0.2}\text{Mn}_{0.3}\text{O}_2$  Cathode Material. *J. Power Sources* **2014**, *266*, 433-439.
- (18) Qiu, B.; Wang, J.; Xia, Y.; Wei, Z.; Han, S.; Liu, Z. Enhanced Electrochemical Performance with Surface Coating by Reactive Magnetron Sputtering on Lithium-Rich Layered Oxide Electrodes. *ACS Appl. Mater. & Interfaces*, **2014**, *6*, 9185-9193.
- (19) Cho, W.; Kim, S.-M.; Song, J. H.; Yim, T.; Woo, S.-G.; Lee, K.-W.; Kim, J.-S.; Kim, Y.-J. Improved Electrochemical and Thermal Properties of Nickel Rich  $\text{LiNi}_{0.6}\text{Co}_{0.2}\text{Mn}_{0.2}\text{O}_2$  Cathode Materials by  $\text{SiO}_2$  Coating. *J. Power Sources* **2015**, *282*, 45-50.
- (20) Zhang, Z.; Hu, L.; Wu, H.; Weng, W.; Koh, M.; Redfern, P. C.; Curtiss, L. A.; Amine, K. Fluorinated Electrolytes for 5 V Lithium-Ion Battery Chemistry. *Energy Environ. Sci.* **2013**, *6*, 1806-1810.
- (21) Sinha, N. N.; Burns, J. C.; Dahn, J. R. Comparative Study of Tris(Trimethylsilyl)Phosphate and Tris(Trimethylsilyl)Phosphite as Electrolyte Additives for Li-Ion Cells. *J. Electrochem. Soc.* **2014**, *161*, A1084-A1089.
- (22) Mai, S.; Xu, M.; Liao, X.; Hu, J.; Lin, H.; Xing, L.; Liao, Y.; Li, X.; Li, W. Tris(Trimethylsilyl)Phosphite as Electrolyte Additive for High Voltage Layered Lithium Nickel Cobalt Manganese Oxide Cathode of Lithium Ion Battery. *Electrochim. Acta* **2014**, *147*, 565-571.
- (23) Han, Y.-K.; Yoo, J.; Yim, T. Why Is Tris(Trimethylsilyl) Phosphite Effective as an Additive for High-Voltage Lithium-Ion Batteries? *J. Mater. Chem.* **2015**, *3*, 10900-10909.
- (24) Zuo, X.; Fan, C.; Liu, J.; Xiao, X.; Wu, J.; Nan, J. Lithium Tetrafluoroborate as an Electrolyte Additive to Improve the High Voltage Performance of Lithium-Ion Battery. *J. Electrochem. Soc.* **2013**, *160*, A1199-A1204.
- (25) Abe, K.; Ushigoe, Y.; Yoshitake, H.; Yoshio, M. Functional Electrolytes: Novel Type Additives for Cathode Materials, Providing High Cycleability Performance. *J. Power Sources* **2006**, *153*, 328-335.
- (26) Shin, H.; Park, J.; Sastry, A. M.; Lu, W. Effects of Fluoroethylene Carbonate (FEC) on Anode and Cathode Interfaces at Elevated Temperatures Batteries and Energy Storage. *J. Electrochem. Soc.* **2015**, *162*, A1683-A1692.
- (27) Shkrob, I. A.; Wishart, J. F.; Abraham, D. P. What Makes Fluoroethylene Carbonate Different? *J. Phys. Chem. C* **2015**, *119*, 14954-14964.
- (28) Hu, L.; Xue, Z.; Amine, K.; Zhang, Z. Fluorinated Electrolytes for 5-V Li-Ion Chemistry: Synthesis and Evaluation of an Additive for High-Voltage  $\text{LiNi}_{0.5}\text{Mn}_{1.5}\text{O}_4$ /Graphite Cell. *J. Electrochem. Soc.* **2014**, *161*, A1777-A1781.
- (29) Shkrob, I. A.; Zhu, Y.; Marin, T. W.; Abraham, D. P. Mechanistic Insight into the Protective Action of Bis(Oxalato)Borate and Difluoro(Oxalato)Borate Anions in Li-Ion Batteries. *J. Phys. Chem. C* **2013**, *117*, 23750-23756.
- (30) von Cresce, A.; Xu, K. Electrolyte Additive in Support of 5 V Li Ion Chemistry. *J. Electrochem. Soc.* **2011**, *158*, A337-A342.
- (31) Zhu, Y.; Casselman, M. D.; Li, Y.; Wei, A.; Abraham, D. P. Perfluoroalkyl-Substituted Ethylene Carbonates: Novel Electrolyte Additives for High-Voltage Lithium-Ion Batteries. *J. Power Sources* **2014**, *246*, 184 – 191.
- (32) Pires, J.; Castets, A.; Timperman, L.; Santos-Peña, J.; Dumont, E.; Levasseur, S.; Tessier, C.; Dedryvère, R.; Anouti, M. Tris(2,2,2-Trifluoroethyl)Phosphite as an Electrolyte Additive for

High-Voltage Lithium-Ion Batteries Using Lithium-Rich Layered Oxide Cathode. *J. Power Sources* **2015**, 296, 413-425.

(33) Symons, M. C. R. Electron Spin Resonance Spectrum of Radicals in  $\Gamma$ -Irradiated Trimethyl Phosphite:  $\text{P(OMe)}_4$ ,  $\text{Hp(OMe)}_3$ ,  $\text{P(OMe)}_2$ ,  $(\text{MeO})_3\text{p-P(OMe)}_3^+$  and  $\text{H}_2\text{cop(OMe)}_2$ . *Molec. Phys.* **1972**, 24, 885-887.

(34) Gillbro, T.; Kerr, C. M. L.; Williams, F. Electron Spin Resonance Identification of the Dimer Radical Cation  $(\text{CH}_3\text{O})_3\text{p-P(OCH}_3)_3^+$  in Gamma-Irradiated Trimethyl Phosphite from Second-Order Hyperfine Structure. *Molec. Phys.* **1974**, 28, 1225-1232.

(35) von Cresce, A.; Xu, K. Electrolyte Additive in Support of 5 V Li Ion Chemistry Batteries and Energy Storage. *J. Electrochem. Soc.* **2011**, 158, A337.

(36) Shkrob, I. A.; Marin, T. W. Electron Solvation by Clustered H-Bond Complexes of Water with Tri-*N*-Butylphosphate. *Chem. Phys. Lett.* **2008**, 465, 234-237.

(37) Gong, Z.; Wang, E. G.; Xu, G. C.; Chen, Y. Influence of Deposition Condition and Hydrogen on Amorphous-to-Polycrystalline SiC Films. *Thin Solid Films* **1999**, 348, 114-121.

(38) Jiang, L.; Cheung, R.; Brown, R.; Mount, A. Inductively Coupled Plasma Etching of SiC in  $\text{SF}_6/\text{O}_2$  and Etch-Induced Surface Chemical Bonding Modifications. *J. Appl. Phys.* **2003**, 93, 1376-1383.

(39) Wang, D.; Wang, H.; Hu, P. Identifying the Distinct Features of Geometric Structures for Hole Trapping to Generate Radicals on Rutile  $\text{TiO}_2(110)$  in Photooxidation Using Density Functional Theory Calculations with Hybrid Functional. *Phys. Chem. Chem. Phys.* **2015**, 17, 1549-1555.

(40) Rajh, T.; Poluektov, O. G.; Thurnauer, M. C., Charge Separation in Titanium Oxide Nanocrystalline Semiconductors Revealed by Magnetic Resonance. In *Chemical Physics of Nanostructured Semiconductors*, Kokorin, A. I.; Bahnmann, D., Eds. NOVA Science Publ., Inc.: New York, 2003; pp 1-34.

(41) Howe, R. F.; Gratzel, M. EPR Study of Hydrated Anatase under UV Irradiation. *J. Phys. Chem.* **1987**, 91, 3906-3909.

(42) Bentrude, W. G. Phosphoranyl Radicals: Their Structure, Formation, and Reactions. *Acc. Chem. Res.* **1982**, 15, 117-125.

(43) Hong, J.; Lim, H.-D.; Lee, M.; Kim, S.-W.; Kim, H.; Oh, S.-T.; Chung, G.-C.; Kang, K. Critical Role of Oxygen Evolved from Layered Li-Excess Metal Oxides in Lithium Rechargeable Batteries. *Chem. Mater.* **2012**, 24, 2692-2697.

(44) Freunberger, S. A.; Chen, Y.; Peng, Z.; Griffin, J. M.; Hardwick, L. J.; Barde, F.; Novak, P.; Bruce, P. G. Reactions in the Rechargeable Lithium  $\text{O}_2$  Battery with Alkyl Carbonate Electrolytes. *J. Am. Chem. Soc.* **2011**, 133, 8040-8047.

(45) Markovsky, B.; Amalraj, F.; Gottlieb, H. E.; Gofer, Y.; Martha, S. K.; Aurbach, D. On the Electrochemical Behavior of Aluminum Electrodes in Nonaqueous Electrolyte Solutions of Lithium Salts. *J. Electrochem. Soc.* **2010**, 157, A423-A429.

## **Chapter 6 *De Novo* Fluorinated Phosphate Additives for High Voltage Lithium-ion Battery: Molecular Engineering and Synthesis**

### **Abstract**

Fluorinated cyclic phosphates were introduced as novel additives for high voltage Li-ion batteries using graphite/LiNi<sub>0.5</sub>Co<sub>0.2</sub>Mn<sub>0.3</sub>O<sub>2</sub> (NCM523) cell. Cyclic fluorinated phosphates with various chemical structures were designed, synthesized and characterized by different analytical methods including NMR, GC-MS and FT-IR. Full cells (graphite/ NCM523) using the state-of-the-art electrolyte with 1 wt% phosphate additive demonstrated significant improvement in the cycling performance compared to the cell without additive. The ineffectiveness of the corresponding non-fluorinated cyclic phosphate and non-cyclic fluorinated phosphate as additives indicate both the fluorinated substituents and the cyclic ring are crucial for the improvement of cycling performance. Ex situ surface analysis such as X-ray photoelectron spectroscopy (XPS) and scanning electron microscope (SEM) confirms the formation of modified films on the electrode surface. Our data indicate that the cyclic fluorinated phosphates can sacrificially decompose on cathode surface, leading to the formation of passivation layers on the electrode surfaces which suppress electrolyte decomposition.

### **6.1 Introduction**

Undoubtedly, lithium-ion (Li-ion) batteries have become the most widely used power source for portable electronic devices and electric vehicles.<sup>1-3</sup> To massively commercialize electric vehicles, the development of lithium-ion batteries with higher energy and power density is essential.<sup>3-8</sup> As a result, extensive research on pioneering new cathode materials with elevated operating voltage

(> 4.5V vs Li/Li<sup>+</sup>) and improved specific capacity has been carried out.<sup>9-12</sup> Since the first synthesis of lithium nickel manganese cobalt oxide (LiNi<sub>0.33</sub>Co<sub>0.33</sub>Mn<sub>0.33</sub>O<sub>2</sub> NCM333) by Ohzuku et al. in 2000<sup>13</sup>, tremendous effort has been given to the development of Ni-rich layer-structured lithium nickel cobalt manganese oxide (NCM) materials because of its high specific capacity under high voltage.<sup>14-15</sup> However, the high voltage instability of the state-of-the-art electrolyte, which contains 1.2 M lithium hexafluorophosphate (LiPF<sub>6</sub>) dissolved in a mixture of ethylene carbonate (EC) and dimethyl carbonate (DMC)/ethyl methyl carbonate (EMC), hinders the extensive application of these new high voltage cathode materials.<sup>16-18</sup> Electrolytes with enhanced voltage stability such as fluorinated carbonates, sulfones, dinitriles and diisocyanates have been actively pursued.<sup>19-25</sup> Several electrolyte additives, which can improve the cell performance drastically with the addition of only a small quantity (1-5 %), have also been developed. It is believed that the additives can sacrificially decompose to form a protective layer on the cathode surface that can kinetically suppress the oxidative decomposition of electrolyte.<sup>26-27</sup> Because the additive approach is a more cost effective solution compared to electrode coating or new electrolyte formulation, it is important to obtain promising additives for the application of high voltage cathodes.

Recently, the investigation of electrolyte additives for NCM cathodes has been actively implemented by many researchers all over the world. In 2013, Nan et al. reported the addition of 1% lithium tetrafluoroborate into the conventional electrolyte could enhance the cycling performance of a graphite/ LiNi<sub>0.5</sub>Co<sub>0.3</sub>Mn<sub>0.2</sub>O<sub>2</sub> cell.<sup>28</sup> Later, Dahn and coworkers demonstrated the effectiveness of various additives including vinylene carbonate (VC), trimethylene sulfone (TMS), ethylene sulfone (DTD), methylene methanedisulfonate (MMDS), prop-1-ene-1,3-sultone (PES) and tris(trimethylsilyl) phosphate (TTSP) in improving the performance of NCM cathodes.

<sup>29-32</sup> Moreover, Song et al. showed that the use of 5% methyl (2,2,2-trifluoroethyl) carbonate (FEMC) as electrolyte additive could effectively enhance the cycling retention of a Li/ NCM cell. <sup>33</sup> More recently, Anouti and coworkers suggested the use of tris(2,2,2-trifluoroethyl) phosphite (TTFP) as an electrolyte additive for a lithium-rich NCM cathode, <sup>34</sup> while Xiang and coworkers reported the use of 2-Ethoxy-1,3,2-dioxaphospholane 2-oxide (EDP) displayed beneficial effect on a Li/NCM cell. <sup>35</sup>[ref X] All the additives above were believed to form a passivation layer on the cathode surface that can suppress electrolyte oxidation which can lead to rapid capacity fading.

In an effort to design new additives, the general features of the above additives were first summarized (Figure 6.1) to provide valuable structural clues about these additives. As shown in Figure 6.1, DTD contains dioxolane-type five-member ring which can be polymerized readily during electrochemical process, <sup>26, 30</sup> while organophosphorus compounds such as EDP, THFPP and TTFP were proven to be effective additives for high voltage cathodes, plausibly by forming protective films on the cathode surface. <sup>26-27, 34, 36-37</sup> Attempting to include the structural property of DTD, TTFP, THFPP and EDP, a new class of cyclic fluorinated phosphates, TFEOP, PFPOP and HFiPOP were designed and synthesized. All of the synthesized phosphates contain dioxolane-type five-member ring which can be easily polymerized to protect the anode surface, while their fluorinated alkyl phosphate group was evidenced forming passivation layer on the cathode surface. Improved cycling performance was observed for the graphite/ NCM523 full cells with the cyclic fluorinated phosphates added as additive. Interfacial analysis showed that the new additives polymerized on the surfaces of both anode and cathode, resulting in less electrolyte decomposition on both electrodes for the full cell utilizing the new phosphate-based additives.

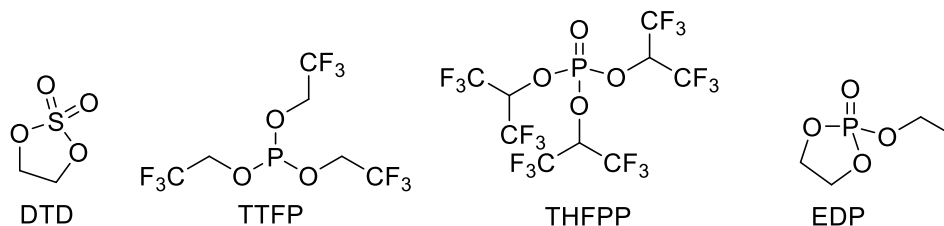


**Figure 6.1.** Chemical Structure of additives DTD, TTFP, THFPP and MDP.

## 6.2 Experimental section

### 6.2.1 Synthesis of 2-(2,2,2-trifluoroethoxy)-1,3,2-dioxaphospholane 2-oxide (TFEOP).

2-Chloro-2-oxo-1,3,2-dioxaphospholane (10.0 g, 0.0702 mol) dissolved in 20 mL anhydrous tetrahydrofuran (THF) was added drop wise to a solution of 2,2,2-trifluoroethanol (8.78 g, 0.0877 mol) and trimethylamine (12.2 mL, 0.0875 mol) in 160 mL anhydrous THF at 0 °C. The reaction mixture was allowed to warm up to room temperature and stirred overnight. The resulting mixture was then subjected to vacuum filtration and the solvent of the filtrate collected was then removed by rotary evaporation. The crude product was dried over 4 Å molecular sieves and purified by vacuum distillation. The final product (b.p. 97 °C, 4 mmHg) is a colorless liquid (6.94 g, 0.0337 mmol) obtained with a yield of 48 %. <sup>1</sup>H NMR (CDCl<sub>3</sub>, 300 MHz): δ 4.52-4.32 (m, 7H); <sup>13</sup>C NMR (CDCl<sub>3</sub>, 75 MHz): δ 122.4 (quartet of doublets (qd), J = 276, 8.2 Hz) 66.3 (d, J = 2.8 Hz), 66.1 (qd, J = 37.8, 4.6 Hz); <sup>19</sup>F NMR (CDCl<sub>3</sub>, 282 MHz): δ -75.7; MS-EI m/z: 205.0 [M - H]: 186.0, 161.0, 137.0, 107.0, 81.0, 64.0.

### 6.2.2 Synthesis of 2-(2,2,3,3,3-pentafluoropropoxy)-1,3,2-dioxaphospholane 2-oxide (PFPOP).

2-Chloro-2-oxo-1,3,2-dioxaphospholane (10.0 g, 0.0702 mol) dissolved in 20 mL anhydrous THF was added drop wise to a solution of 2,2,3,3,3-Pentafluoro-1-propanol (13.17 g, 0.0878 mol) and trimethylamine (12.2 mL, 0.0875 mol) in 160 mL anhydrous THF at 0 °C. The reaction mixture was allowed to warm up to room temperature and stirred overnight. The

resulting mixture was then subjected to vacuum filtration and the solvent of the filtrate collected was then removed by rotary evaporation. The crude product was dried over 4 Å molecular sieves and purified by vacuum distillation. The final product (b.p. 107 °C, 4 mmHg) is a colorless liquid (9.13 g, 0.0357 mmol) obtained with a yield of 51 %. <sup>1</sup>H NMR (CDCl<sub>3</sub>, 300 MHz): δ 4.56-4.34 (m, 6H); <sup>13</sup>C NMR (CDCl<sub>3</sub>, 75 MHz): δ 118.3 (quartet of triplets (qt), J = 286, 35 Hz), 111.6 (triplet of quartets (tq) 254, 37.5 Hz), 66.3 (d, J = 2.6 Hz), 63.3 (triplet of doublets (td), J = 28.4, 5.0 Hz); <sup>19</sup>F NMR (CDCl<sub>3</sub>, 282 MHz): δ -83.7, -125.0; MS-EI m/z: 257.0 [M + H]<sup>+</sup>: 236.0, 211.0, 137.0, 107.0, 81.0, 64.0.

**6.2.3 Synthesis of 2-((1,1,1,3,3,3-hexafluoropropan-2-yl)oxy)-1,3,2-dioxaphospholane 2-oxide (HF<sub>6</sub>POP).** 2-Chloro-2-oxo-1,3,2-dioxaphospholane (15.0 g, 0.105 mol) dissolved in 30 mL anhydrous THF was added drop wise to a solution of 1,1,1,3,3,3-Hexafluoro-2-propanol (22.9 g, 0.137 mol) and trimethylamine (19.1 mL, 0.137 mol) in 200 mL anhydrous THF at 0 °C. The reaction mixture was allowed to warm up to room temperature and stirred overnight. The resulting mixture was then subjected to vacuum filtration and the solvent of the filtrate collected was then removed by rotary evaporation. The crude product was dried over 4 Å molecular sieves and purified by vacuum distillation. The final product (b.p. 93 °C, 4 mmHg) is a colorless liquid (13.04 g, 0.0476 mmol) obtained with a yield of 45 %. <sup>1</sup>H NMR (CDCl<sub>3</sub>, 300 MHz): δ 5.30-5.11 (m, 1H), 4.57-4.44 (m, 4H); <sup>13</sup>C NMR (CDCl<sub>3</sub>, 75 MHz): δ 120.1 (q, J = 278 Hz) 72.1 (septet of doublets (sd), J = 35.3, 4.5 Hz), 66.8 (d, J = 3.4 Hz); <sup>19</sup>F NMR (CDCl<sub>3</sub>, 282 MHz): δ -74.6; MS-EI m/z: 274.1 [M]<sup>+</sup>: 254.0, 228.9, 144.9, 106.9, 80.9, 68.9.

**6.2.4 Characterization of synthesized cyclic fluorinated phosphates.** All newly reported synthetic cyclic fluorinated phosphates were characterized by both NMR spectroscopy and gas chromatography – mass spectrometry (GC-MS) to confirm the structure and purity. All NMR

spectra were acquired on a 300 MHz Bruker spectrometer.  $^1\text{H}$  chemical shifts were referenced to chloroform-*d* at 7.27 ppm and  $^{13}\text{C}$  chemical shifts were referenced to 77.0 ppm. All GC spectra were acquired on an Agilent Technologies 7890B GC System and all MS spectra were acquired on an Agilent Technologies 5977A MSD System.

**6.2.5 Materials and methods.** All measurements were carried out at 30 °C in an inert atmosphere. Electrochemical cycling stability was evaluated using 2032 coin cells. The cathode was composed of 90.0 wt%  $\text{LiNi}_{0.5}\text{Co}_{0.2}\text{Mn}_{0.3}\text{O}_2$ , 5.0 wt% C45 carbon black, and 5.0 wt% Solvay 5130 polyvinylidene fluoride (PVDF) binder coated on aluminum foil. The active material loading was 9.15 mg/cm<sup>2</sup>. The graphite anode consisted of 89.8 wt% ConocoPhillips CGPA12, 4.0 wt% Super P-Li, 6.0 wt% Kureha 9300 PVDF binder, and 0.2 wt% oxalic acid that were coated on copper foil. The active material loading was 5.3 mg/cm<sup>2</sup>. Celgard 2325 was used as the separator. The effective diameters of the cathode, anode and separator were 14, 15, and 16 mm, respectively. Gen2 electrolyte containing 1.2 M  $\text{LiPF}_6$  in 3:7 w/w mixture of ethylene carbonate (EC) and ethyl methyl carbonate (EMC) was used as a “baseline” electrolyte. DTD, TTFP, tris(1,1,1,3,3,3-hexafluoropropan-2-yl) phosphate (THFPP) was purchased from Sigma-Aldrich and purified before use. 2-Ethoxy-1,3,2-dioxaphospholane 2-oxide (EDP) was synthesized following the reported procedure. Below, all potentials are given vs  $\text{Li}^+/\text{Li}$  couple.

**6.2.6 Electrochemical measurements.** Galvanostatic charge/discharge cycling was conducted between 4.6 and 3.0 V cutoff voltages at C/3 rate following two initial “formation” cycles carried out at a C/10 rate. Cell voltage profiles and capacity were recorded using a MACCOR Electrochemical Analyzer (MIMSciEnt). The impedance spectra were obtained using a Solartron analyzer operated between 0.01 Hz and 1 MHz with the amplitude of 10 mV. Linear sweep voltammetry was performed using a Bio-Logic VMP3 station in a three-electrode configuration

with NCM523 (100  $\mu\text{m}$  in diameter) as a working electrode and lithium metal as counter and reference electrodes; the scan rate was 0.1 mV/s.

**6.2.7 Post-test analysis.** For post-test analysis, the cycled cells were disassembled in an argon-filled glove box, and the cycled electrolyte was collected by dipping the electrodes and the separator in small amount of chloroform-*d* for NMR analysis. The electrodes were thoroughly rinsed with anhydrous dimethyl carbonate and dried in a vacuum oven. The morphologies of the harvested electrodes were examined with scanning electron microscopy (SEM) using a Hitachi S-4700-II microscope in the Electron Microscopy Center of Argonne National Laboratory. X-ray photoelectron spectroscopy (XPS) measurements were carried out by using an Omicron ESCA probe with Al  $K\alpha$  source. A low-energy electron flood gun was used to compensate for x-ray beam induced surface charging.  $C_{1s}$  line (284.8 eV) was used for energy calibrations. Samples for proton nuclear magnetic resonance ( $^1\text{H}$  NMR) were prepared by rinsing of the disassembled cell with chloroform-*d*. These NMR spectra were obtained using a Bruker Avance III HD 300 MHz spectrometer. The chemical shifts in parts per million (ppm) are given vs a tetramethylsilane standard.

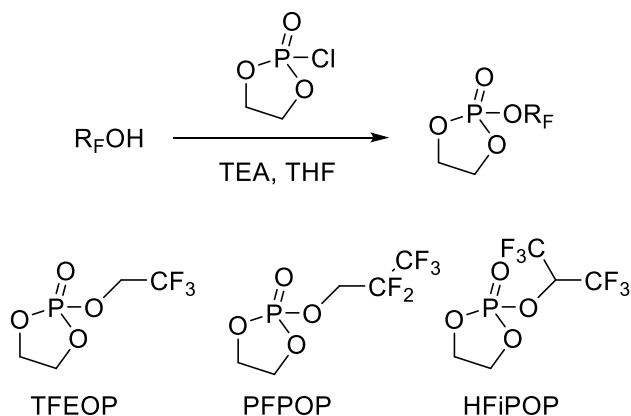
## 6.3 Results and Discussion

### 6.3.1. Synthesis and Characterization of *De Nova* Cyclic Fluorinated Phosphates

Cyclic fluorinated phosphates including 2-(2,2,2-trifluoroethoxy)-1,3,2-dioxaphospholane 2-oxide (TFEOP), 2-(2,2,3,3,3-pentafluoropropoxy)-1,3,2-dioxaphospholane 2-oxide (PFPOP) and 2-((1,1,1,3,3,3-hexafluoropropan-2-yl)oxy)-1,3,2-dioxaphospholane 2-oxide (HFiPOP) were prepared *via* the reaction of fluorinated alcohol with 2-chloro-1,3,2-dioxaphospholane-2-oxide in THF as depicted in Scheme 1. Triethylamine was added to scavenge the hydrogen chloride

produced by the reaction of alcohol and 2-chloro-1,3,2-dioxaphospholane-2-oxide in order to facilitate the formation of the cyclic fluorinated phosphate. Moreover, the precipitated ammonium chloride salt can be easily filtered out and the crude intermediates purified via vacuum distillation to yield colorless liquids as products. The compounds were characterized by  $^1\text{H}$ ,  $^{13}\text{C}$  and  $^{19}\text{F}$  NMR, as well as GC-MS. Representative  $^1\text{H}$ ,  $^{13}\text{C}$  and  $^{19}\text{F}$  NMR spectra of PFPOP are displayed in Figure 6.2. The signal of methylene protons within the five-membered ring overlaps with the signal of the methylene protons adjacent to the  $\text{CF}_2\text{CF}_3$  group, resulting in one multiplet in the proton NMR. The  $^{19}\text{F}$  NMR spectrum clearly shows two peaks corresponding to the  $\text{CF}_2$  and  $\text{CF}_3$  fluorine groups. The  $^{13}\text{C}$  spectrum further supports the structure of this single pure compound PFPOP with the triplet of doublets at 63.3 ppm corresponding to the methylene carbon adjacent to the  $\text{CF}_2\text{CF}_3$  group, the doublet at 66.3 ppm corresponding to the methylene carbons within the five-membered ring, the triplet of quartets at 111.6 ppm correlating with the  $\text{CF}_2$  carbon and the quartet of triplets at 118.3 ppm correlating with the  $\text{CF}_3$  carbon. The  $^1\text{H}$ ,  $^{13}\text{C}$  and  $^{19}\text{F}$  NMR spectra undoubtedly confirm the structures of the cyclic fluorinated phosphates shown in Scheme 1. The synthesis and spectral details of all cyclic fluorinated phosphates are summarized in the experimental section.

### Scheme 1



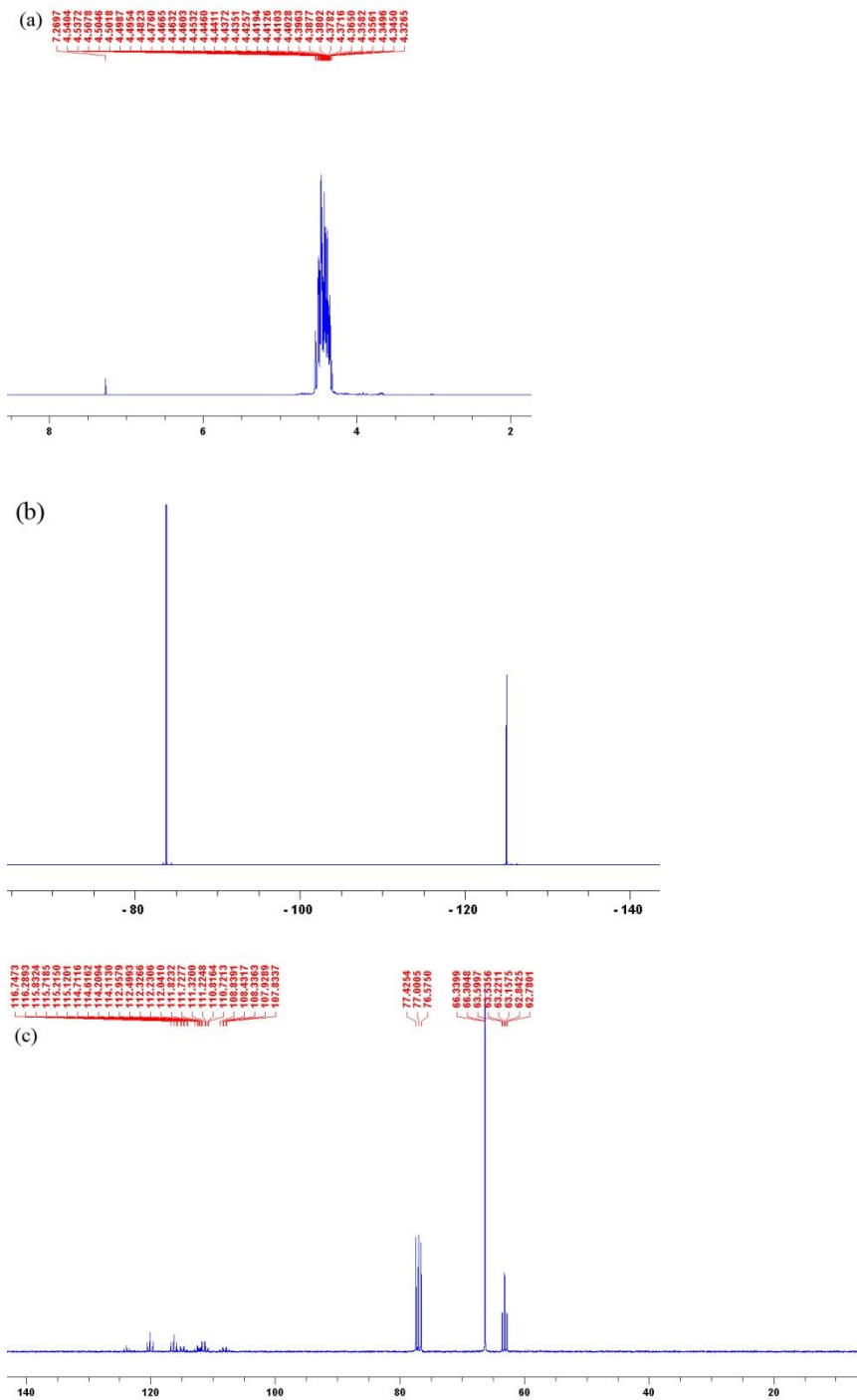


Figure 6.2. NMR spectra of PFPOP in  $\text{CDCl}_3$ : a)  $^1\text{H}$  NMR; b)  $^{19}\text{F}$  NMR and c)  $^{13}\text{C}$  NMR.

### 6.3.2. Electrochemical Measurement

### **The performance of graphite/ LiNi<sub>0.5</sub>Co<sub>0.2</sub>Mn<sub>0.3</sub>O<sub>2</sub> (NCM523) full cell with known additives.**

Figure 6.3 shows the capacity retention of the graphite/NCM523 full cells employing the baseline Gen2 (1.2 M LiPF<sub>6</sub> in EC/EMC 3/7 wt%) electrolyte and Gen2 with 1 wt% of various additives including DTD, TTFP, THFPP and EDP at room temperature. And Table 6.1 shows the detail. The current rate of the full cells was C/10 for the first 2 cycles and C/3 for the subsequent 100 cycles. The initial capacity and capacity retention after 100 cycles for the full cell using Gen2 electrolyte are 214.8 mAhg<sup>-1</sup> and 67.5%, respectively. Meanwhile, the cycling performance of the full cell with 1% DTD, which also has a polymerizable five-member ring, was significantly improved compared to the baseline cell showing an initial capacity of 212.7 mAhg<sup>-1</sup> and capacity retention of 74.0%. While the initial capacity was only 198.6 mAhg<sup>-1</sup> for the full cell with 1% THFPP, a fluorinated phosphate additive, the capacity retention was 76.6% which was significantly higher than the 64.9% capacity retention shown by the full cell with the addition of a fluorinated phosphite additive, TTFP. Although the initial capacity of the cell employing 1% EDP, which is a cyclic phosphate, was as low as 131.9 mAhg<sup>-1</sup>, the 100th cycle capacity was 155.3 mAhg<sup>-1</sup> and was the highest among all the cells tested. These results demonstrate the potentially beneficial effect of introducing a five-member ring, fluorinated substitution group and phosphate into the additive molecules.

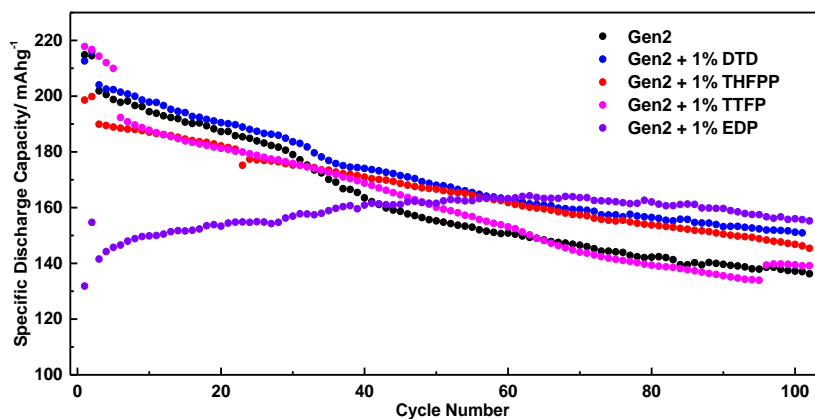


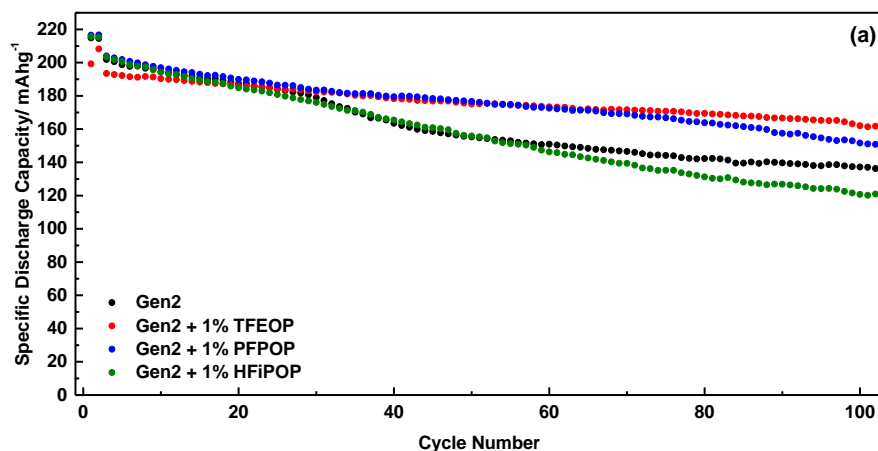
Figure 6.3. Capacity retention of NCM523/graphite cells using Gen2 and Gen2 with 1% additives at room temperature.

Table 6.1

Electrolyte	Initial discharge capacity mAh/g	100 <sup>th</sup> cycle discharge capacity mAh/g	Capacity retention after 50 cycles %	Capacity retention after 100 cycles %
BE	214.8	136.2	77.1	67.5
BE+1% DTD	212.7	150.9	81.8	74.0
BE+1% THFPP	198.6	146.2	87.8	76.6
BE+1% TTFP	217.8	140	74.2	64.9
BE+1% EDP	131.86	155	114	85.6

**Cycling of graphite/LiNi<sub>0.5</sub>Co<sub>0.2</sub>Mn<sub>0.3</sub>O<sub>2</sub> (NCM523) full cells with cyclic fluorinated phosphates as additives.** In light of the above results, cyclic fluorinated phosphates including TFEOP, PFPOP and HFiPOP were designed and synthesized. The graphite/NCM523 full cells using Gen2 with 1% cyclic fluorinated phosphates were subjected to the same cycling test mentioned above and the capacity retention is depicted in Figure 6.4a. Details are shown in Table 6.2. All of the fluorinated phosphate additives showed improvement on the cycling performance of graphite/NCM full cell except HFiPOP, which is the hexafluoroisopropyl version of the cyclic phosphate additives. The initial capacity of the full cell using Gen2 with 1% TFEOP was 199.3 mAhg<sup>-1</sup>, which was lower than the initial capacity 216.5 mAhg<sup>-1</sup> shown by Gen2 with 1%

PFPOP. However, the capacity retention and 100<sup>th</sup> cycle capacity of TFEOP added cell were 83.6% and 161.8 mAhg<sup>-1</sup> respectively, and they were significantly higher than those of PFPOP added cell (73.9% and 150.8 mAhg<sup>-1</sup>) and the cell without any additive (67.5% and 136.3 mAhg<sup>-1</sup>). The Coulombic efficiency (CE) of the HFiPOP added full cell system was significantly lower than that of other three systems (Gen2, Gen2 with 1% TFEOP and Gen2 with 1% PFPOP) as presented in Figure 6.4b and this low CE could probably account in part for the low capacity retention of the HFiPOP added cell. The TFEOP and PFPOP added cells displayed relatively high CE (> 99.6%) and the coulombic efficiencies were much steadier than that of baseline cell. Overall, the graphite/NCM full cell system using Gen2 with 1% TFEOP demonstrated the highest capacity retention and 100<sup>th</sup> cycle capacity among the cell systems mentioned above.



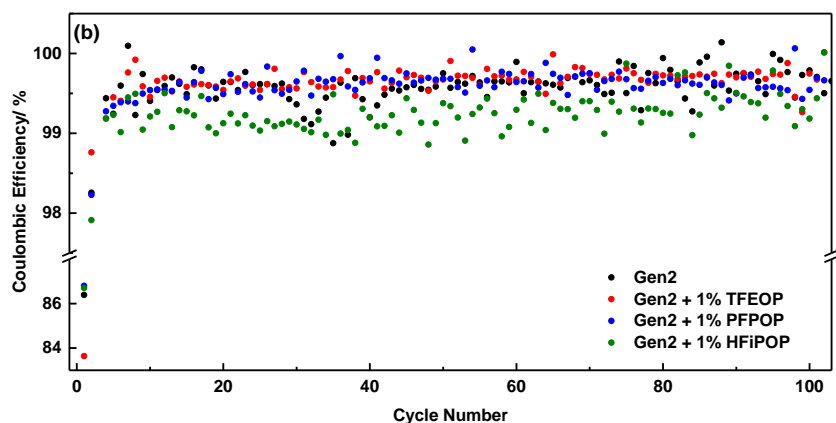


Figure 6.4. (a) Capacity retention and (b) coulombic efficiency of NCM523/graphite cells using Gen2 and Gen2 with 1% cyclic phosphate additives at room temperature.

Table 6.2

Electrolyte	Initial discharge capacity mAh/g	1st Coulombic efficiency %	100 <sup>th</sup> cycle discharge capacity mAh/g	Capacity retention after 50 cycles %	Capacity retention after 100 cycles %
BE	214.8	86.4	136.2	77.1	67.5
BE+1% TFEOP	199.3	83.8	161.8	91.1	83.6
BE+1% PFPOP	216.5	86.8	150.8	86.6	74.7
BE+1% HFiPOP	215.7	86.7	120.9	77.6	59.1

**Electrochemical Impedance Spectroscopy and Linear Sweep Voltammetry.** Impedance spectroscopy was carried out to probe the electrical properties of electrodes and their interfaces.

Figure 6.5 presents the impedance spectra obtained after 100 charge/discharge cycles of

graphite/NCM full cells using Gen2, Gen2 with 1% TFEOP, Gen2 with 1% PFPOP and Gen2 with 1% HFiPOP electrolytes. These impedance spectra consist of two partially overlapped semi-circles. The EIS can be fitted by the equivalent circuit shown in the inset of Figure 6.5<sup>38-39</sup>. The  $R_b$  is the bulk resistance of the whole battery that represents the electric conductivity of the electrolyte, separator and electrodes. The semicircle at high frequencies is related to  $R_{sei}$  and  $C_{sei}$ , which are resistance and capacitance of the solid electrolyte interface on the electrodes, respectively.  $R_{ct}$  and  $C_{ct}$  are faradic charge-transfer resistance and its relative double-layer capacitance, which correspond to the semicircle at medium frequencies. And the estimated values are shown in Table 6.3. While the surface film resistance  $R_{sei}$  of the baseline cell is slightly higher than that of the other cells with additive, the charge transfer resistance  $R_{ct}$  of the baseline cell is almost three times the  $R_{ct}$  of cells with TFEOP and PFPOP, indicating a significant decomposition of electrolyte on the electrode surface for the baseline cell. The cycling and impedance results suggest that cyclic phosphates TFEOP and PFPOP are effective in mitigating the side reactions on the surface of either the anode or the cathode.

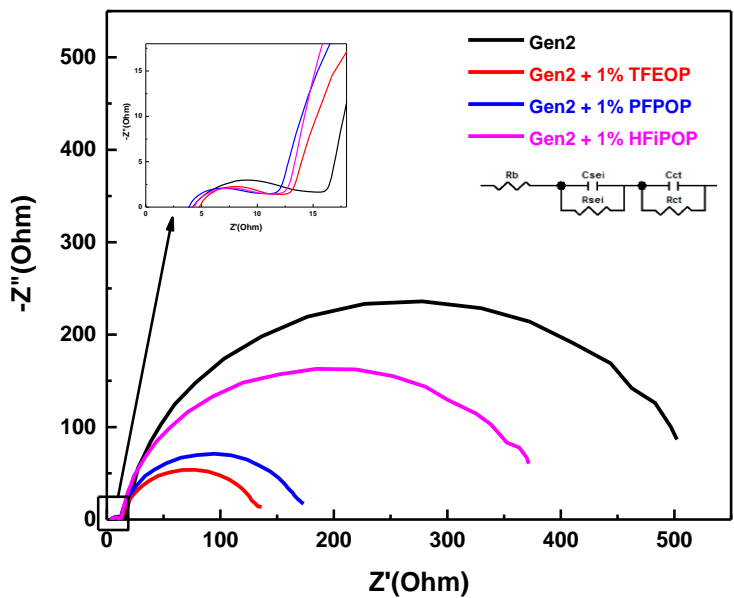


Figure 6.5. Electrochemical impedance spectra for graphite/NCM full cells using Gen2 and Gen2 with 1% cyclic phosphate additives after 100 cycles. Inset: the R<sub>sei</sub> area

Table 6.3. Estimates for surface film and charge transfer resistances for the graphite/NCM full cells

Cell	R <sub>b</sub> (Ω)	R <sub>sei</sub> (Ω)	R <sub>ct</sub> (Ω)
Gen2	3.41	10.2	475
Gen2 with 1% TFEOP	3.85	6.18	133
Gen2 with 1% PFPOP	3.07	7.24	164
Gen2 with 1% HFiPOP	3.47	7.89	356

Because TFEOP shows the best performance among the three as synthesized additives, it is selected as the representative additive for post analysis.

Linear sweep voltammetry (LSV) measurements were carried out to probe the nature of the cathode surface. In this experiment, NCM523 electrode was used as the working electrode while lithium metal was used as both counter and reference electrodes. The scan rate of the LSV was set to be as low as 0.1 mV/s in order for the electrode reaction to reach equilibrium. The results of baseline Gen2 electrolyte and Gen2 electrolyte with 1% TFEOP, which gave the best cycling performance, are compared in Figure 6.6. For the 3-electrode cell employing the baseline electrolyte, an oxidation peak occurs at 3.86 V, which is 0.08 V smaller than the oxidation peak 3.94 V observed with 1% TFEOP electrolyte. This cathodic peak delay is consistent with the formation of a kinetic barrier on the NCM surface.

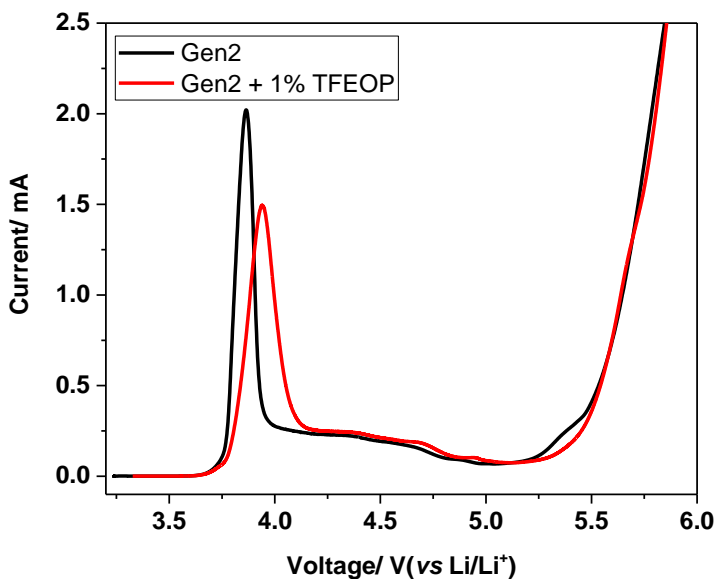


Figure 6.6. Linear sweep voltammogram of Gen2 electrolyte and Gen2 electrolyte containing 1% TFEOP.

### 6.3. Post-test Analysis

#### Scanning electron microscope (SEM).

The SEM images of the pristine cathode, the harvested cathode from the baseline cell and the harvested cathode from the TFEOP added cell are depicted in Figure 6.7a, 6.7b and 6.7c respectively. In the baseline electrolyte, the surface of the aged cathode was covered with thick deposits (Figure 6.7b), suggesting severe electrolyte oxidation of the baseline electrolyte on the cathode surface. The cathode cycled in Gen2+1%TFEOP electrolyte (Figure 6.7c) exhibits a comparatively much cleaner surface; there is no indication of thick deposits due to electrolyte decomposition.

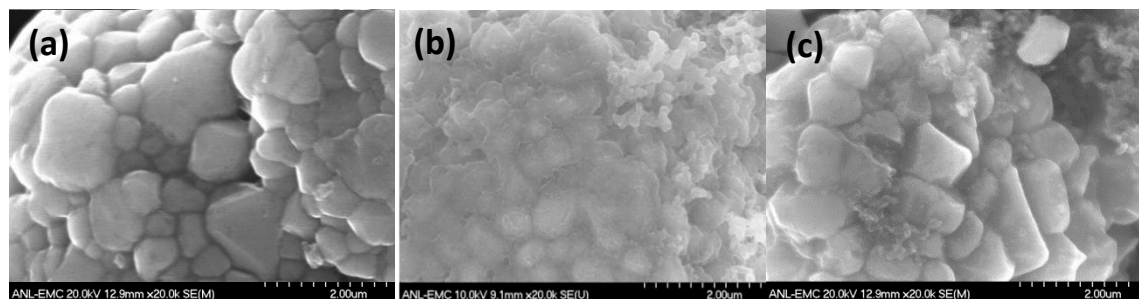


Figure 7. SEM images of (a) pristine cathode, and harvested cathode from cells with (b) Gen2 electrolyte and (c) Gen2 with 1% TFEOP electrolyte.

**XPS.** Figure 6.8 presents XPS spectra of the cycled cathodes in the baseline electrolyte with/without 1% TFEOP as additive. Figure 6.8a gives the expanded  $C_{1s}$  region. In both cycled cathodes, the  $C_{1s}$  peak at 284.8 eV originates from the C-C bond in carbon black, while the peaks at 286.5 and 288 eV arise from the C-O and C=O bonds, respectively. These peaks are attributed to  $ROCO_2Li$ ,  $ROLi$  and  $Li_2CO_3$  crystallites that are the known products of electrolyte decomposition.<sup>40</sup> The peak at 291.5 eV corresponds to a  $CF_2$  group from PVDF binder.<sup>40</sup>

Importantly, a peak at 293 eV appears on the electrode in the cycled cell containing 1 wt% TFEOP. This peak originates from the trifluoromethyl groups, suggesting the presence of a TFEOP-derived product bound to the cathode surface.

Figure 6.8b shows the F1s spectra of the cycled cathodes. Four peaks are observed in the baseline aged cathode F 1s spectrum, LiF (684.5 eV), MF<sub>2</sub> (Metal fluoride) (~685.4eV), Li<sub>x</sub>PO<sub>y</sub>F<sub>z</sub> (~686 eV) and CF<sub>2</sub> (~687.8eV). For the baseline with 1 wt % TFEOP cycled cathode, one more peak was identified on 689.2eV, which indicate the CF<sub>3</sub> group from the decomposition of TFEOP. This corroborates the CF<sub>3</sub> groups identified on the C1s spectra previously discussed.

Figure 6.8c presents the O<sub>1s</sub> spectra. The peak at 530.1eV is attributed to lattice transition metal oxide in the layered LiNi<sub>0.5</sub>Co<sub>0.2</sub>Mn<sub>0.3</sub>O<sub>2</sub>.<sup>41</sup> A peak at 531.5eV is observed in the cycled electrode that originates from the C-O bonds in the products of electrolyte decomposition. A peak at 533.3eV can be attributed to the species containing a (fluoro)phosphate group.

In the P<sub>2p</sub> region, the cycled electrodes shows strong peaks at 133.6, 135 and 136.4eV, which can be attributed to the species containing a (fluoro)phosphate group.<sup>42</sup> This group can originate from the decomposition of TFEOP additive and/or LiPF<sub>6</sub> salt.

Taken together, these XPS results support our assertion that TFEOP reacts on the cathode surface and forms a surface film different from the baseline electrolyte.

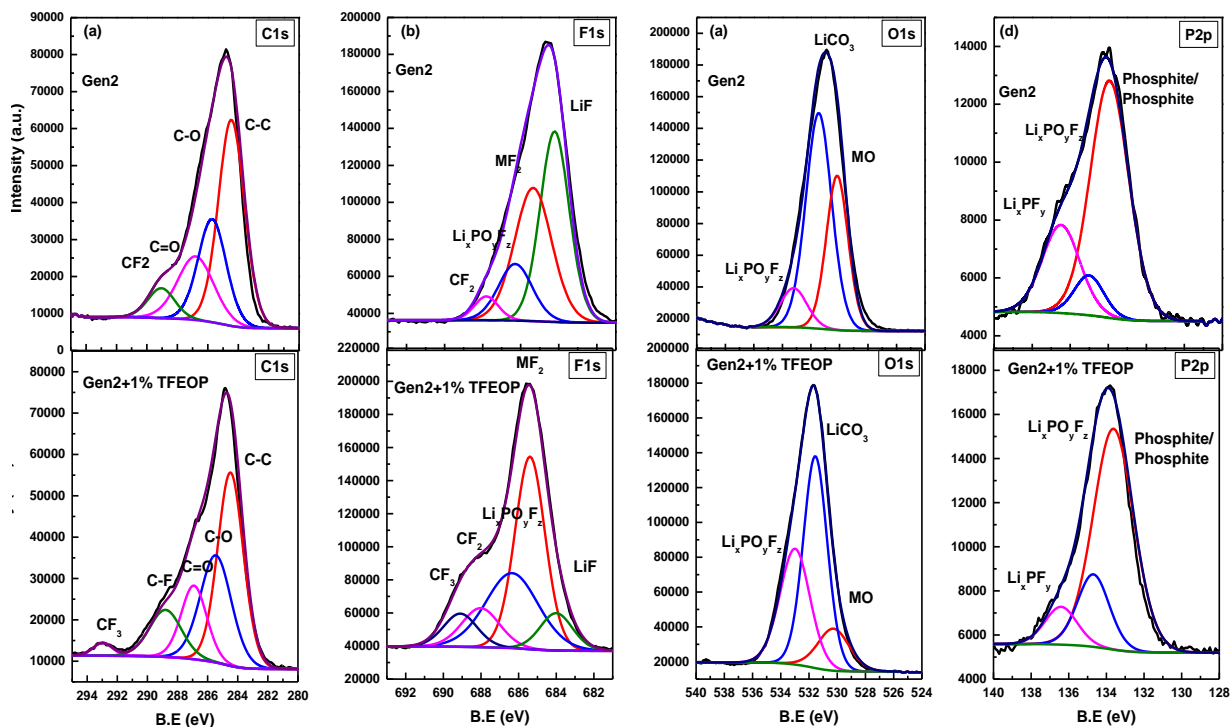


Figure 6.9. X ray Photoelectron spectra of aged  $\text{LiNi}_{0.5}\text{Co}_{0.23}\text{Mn}_{0.3}\text{O}_2$  electrodes in the baseline electrolyte with/without 1% TFEOP as additive the (a) C1s, (b) F1s, (c) O1s, and (d) P2p regions.

**Nuclear Magnetic Resonance (NMR).** Proton NMR was used to probe the extent of the transesterification side reaction of EMC, which can be alleviated by the formation of a protective coating on cathode surface<sup>43</sup>. Figures 6.9a and 6.9b present the proton NMR spectra of the cell

fluid collected after 100 cycles from the baseline cell and the TFEOP added cell, respectively. Apparently, a noticeable amount of diethyl carbonate (DEC) and dimethyl carbonate (DMC) generated by the transesterification reaction of EMC can be observed from the baseline cell; however, the amount of transesterification by-products was greatly reduced and can hardly be observed in the proton NMR spectra for the cells with cyclic fluorinated phosphate additive added. Again, this result supports the formation of a coating layer on the cathode surface by the polymerization of cyclic fluorinated phosphates.

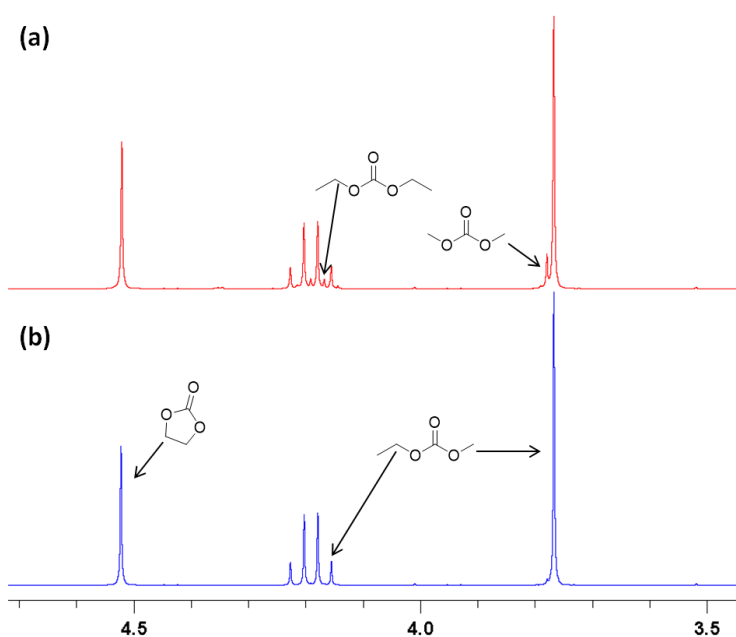
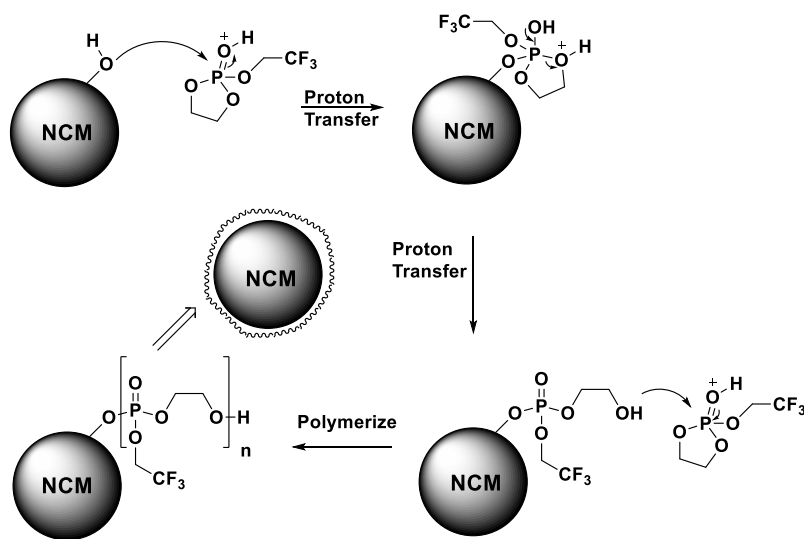


Figure 6.9. An excerpt of the <sup>1</sup>H NMR spectra from collected cell fluids from the (a) Gen2, and (b) Gen2 with 1% TFEOP cells after 100 cycles.

#### 6.4 Proposed mechanism.

Taking the electrochemical data and post test analysis results together, we speculate that TFEOP

can form a kinetic barrier on the cathode surface and prevent the conventional electrolyte from severe oxidation side reactions on the electrode surface. The protective layer could possibly be formed by the polymerization of the cyclic fluorinated phosphate additives, which can react with a hydroxyl (-OH) group<sup>44</sup> on the surface of the NCM surface as described in Scheme 2. (Schöttler, 2016 #88) [Ref 37, Y, Z] Presumably, the cyclic phosphates can be protonated by the acid generated from Gen2 or the oxidation decomposition of the electrolyte solvents on the cathode surface, rendering the cyclic phosphates prone to nucleophilic attack by the hydroxyl residue on the surface of the NCM particles. Eventually, the cyclic phosphates may polymerize and form a protective layer on the NCM surface. Due to the electron withdrawing effect of the fluorinated substituent in the fluorinated cyclic phosphate, the P=O double bond is more prone to nucleophilic addition than that of non-fluorinated cyclic phosphate. Thus, the cathode protective layer could form readily with the use of fluorinated cyclic phosphate, rendering the cell using fluorinated cyclic phosphate additives better cycling performance.



Scheme 2. Proposed mechanism of the TFEOP polymerization.

## Conclusion

In summary, *de novo* cyclic fluorinated phosphates were designed by combining the beneficial structural features of various known additives including a five-member ring, fluorinated substituents and phosphate functional groups. The designed additives were successfully synthesized and applied as additives in a graphite/NCM523 full cell system. The cycling performance is significantly improved with the use of 1% TFEOP or PFPOP as additive in Gen2 electrolyte. The results of EIS and LSV suggest the formation of a protective layer which can reduce the electrolyte oxidative decomposition was formed on the surface of the cathode when cyclic fluorinated phosphate additive was used. Presumably the protective layer was generated by the polymerization of the cyclic fluorinated phosphates. Post-test analyses including SEM, EDS and NMR were performed to probe the nature of the electrodes and electrolyte system. The SEM and EDS results showed that the addition of TFEOP additive could reduce the morphology changes of electrodes and the transition metal dissolution from the cathode. Transesterification side reaction was also mitigated by the addition of TFEOP additive as illustrated by the proton NMR spectra. All results of the post-test analyses are also consistent with the formation of a protective layer which mitigates electrolyte oxidation and transition metal dissolution on the cathode surface. Extensive work on the synthesis of more diversified cyclic phosphate molecules and further mechanistic studies are currently being carried out.

## References

1. Tarascon, J.-M.; Armand, M., Issues and Challenges Facing Rechargeable Lithium Batteries. *Nature* **2001**, *414*, 359-367.
2. Armand, M.; Tarascon, J.-M., Building Better Batteries. *Nature* **2008**, *451*, 652-657.
3. Goodenough, J. B.; Park, K.-S., The Li-Ion Rechargeable Battery: A Perspective. *Journal of the American Chemical Society* **2013**, *135*, 1167-1176.
4. Thackeray, M. M.; Kang, S.-H.; Johnson, C. S.; Vaughey, J. T.; Benedek, R.; Hackney, S., Li<sub>2</sub>MnO<sub>3</sub>-Stabilized LiMO<sub>2</sub> (M= Mn, Ni, Co) Electrodes for Lithium-Ion Batteries. *Journal of Materials Chemistry* **2007**, *17*, 3112-3125.
5. Wu, Y.; Murugan, A. V.; Manthiram, A., Surface Modification of High Capacity Layered Li [Li<sub>0.2</sub>Mn<sub>0.54</sub>Ni<sub>0.13</sub>Co<sub>0.13</sub>]O<sub>2</sub> Cathodes by AlPO<sub>4</sub>. *Journal of The Electrochemical Society* **2008**, *155*, A635-A641.
6. Ito, A.; Li, D.; Sato, Y.; Arao, M.; Watanabe, M.; Hatano, M.; Horie, H.; Ohsawa, Y., Cyclic Deterioration and Its Improvement for Li-Rich Layered Cathode Material Li [Ni<sub>0.17</sub>Li<sub>0.2</sub>Co<sub>0.07</sub>Mn<sub>0.56</sub>]O<sub>2</sub>. *Journal of Power Sources* **2010**, *195*, 567-573.
7. Sun, Y. K.; Lee, M. J.; Yoon, C. S.; Hassoun, J.; Amine, K.; Scrosati, B., The Role of AlF<sub>3</sub> Coatings in Improving Electrochemical Cycling of Li-Enriched Nickel-Manganese Oxide Electrodes for Li-Ion Batteries. *Advanced Materials* **2012**, *24*, 1192-1196.
8. Lin, F.; Markus, I. M.; Nordlund, D.; Weng, T.-C.; Asta, M. D.; Xin, H. L.; Doeff, M. M., Surface Reconstruction and Chemical Evolution of Stoichiometric Layered Cathode Materials for Lithium-Ion Batteries. *Nature communications* **2014**, *5*.
9. Nyttén, A.; Abouimrane, A.; Armand, M.; Gustafsson, T.; Thomas, J. O., Electrochemical Performance of Li<sub>2</sub>Fesio<sub>4</sub> as a New Li-Battery Cathode Material. *Electrochemistry communications* **2005**, *7*, 156-160.
10. Ellis, B.; Makahnouk, W.; Makimura, Y.; Toghill, K.; Nazar, L., A Multifunctional 3.5 V Iron-Based Phosphate Cathode for Rechargeable Batteries. *Nature materials* **2007**, *6*, 749-753.
11. Santhanam, R.; Rambabu, B., Research Progress in High Voltage Spinel Lini<sub>0.5</sub>Mn<sub>1.5</sub>O<sub>4</sub> Material. *Journal of Power Sources* **2010**, *195*, 5442-5451.
12. Hu, M.; Pang, X.; Zhou, Z., Recent Progress in High-Voltage Lithium Ion Batteries. *Journal of Power Sources* **2013**, *237*, 229-242.
13. Ohzuku, T.; Makimura, Y., Layered Lithium Insertion Material of Lico<sub>1/3</sub>ni<sub>1/3</sub>mn<sub>1/3</sub>o<sub>2</sub> for Lithium-Ion Batteries. *Chemistry Letters* **2001**, 642-643.
14. Chikkannanavar, S. B.; Bernardi, D. M.; Liu, L., A Review of Blended Cathode Materials for Use in Li-Ion Batteries. *Journal of Power Sources* **2014**, *248*, 91-100.
15. Huang, Z.-D.; Liu, X.-M.; Oh, S.-W.; Zhang, B.; Ma, P.-C.; Kim, J.-K., Microscopically Porous, Interconnected Single Crystal Lini<sub>1/3</sub>Co<sub>1/3</sub>Mn<sub>1/3</sub>O<sub>2</sub> Cathode Material for Lithium Ion Batteries. *Journal of Materials Chemistry* **2011**, *21*, 10777-10784.
16. Hu, L.; Zhang, Z.; Amine, K., Electrochemical Investigation of Carbonate-Based Electrolytes for High Voltage Lithium-Ion Cells. *Journal of Power Sources* **2013**, *236*, 175-180.
17. He, M.; Hu, L.; Xue, Z.; Su, C. C.; Redfern, P.; Curtiss, L. A.; Polzin, B.; von Cresce, A.; Xu, K.; Zhang, Z., Fluorinated Electrolytes for 5-V Li-Ion Chemistry: Probing Voltage Stability of Electrolytes with Electrochemical Floating Test. *Journal of The Electrochemical Society* **2015**, *162*, A1725-A1729.

18. Kunduraci, M.; Amatucci, G., Synthesis and Characterization of Nanostructured 4.7 V Li<sub>x</sub>Mn<sub>1-5x</sub>O<sub>4</sub> Spinel for High-Power Lithium-Ion Batteries. *Journal of The Electrochemical Society* **2006**, *153*, A1345-A1352.
19. Hu, L.; Zhang, Z.; Amine, K., Fluorinated Electrolytes for Li-Ion Battery: An Fec-Based Electrolyte for High Voltage Lini<sub>0.5</sub>Mn<sub>1.5</sub>O<sub>4</sub>/Graphite Couple. *Electrochemistry Communications* **2013**, *35*, 76-79.
20. Zhang, Z.; Hu, L.; Wu, H.; Weng, W.; Koh, M.; Redfern, P. C.; Curtiss, L. A.; Amine, K., Fluorinated Electrolytes for 5 V Lithium-Ion Battery Chemistry. *Energy & Environmental Science* **2013**, *6*, 1806-1810.
21. Hu, L.; Xue, Z.; Amine, K.; Zhang, Z., Fluorinated Electrolytes for 5-V Li-Ion Chemistry: Synthesis and Evaluation of an Additive for High-Voltage Lini<sub>0.5</sub>Mn<sub>1.5</sub>O<sub>4</sub>/Graphite Cell. *Journal of The Electrochemical Society* **2014**, *161*, A1777-A1781.
22. Xu, K.; Angell, C., High Anodic Stability of a New Electrolyte Solvent: Unsymmetric Noncyclic Aliphatic Sulfone. *Journal of The Electrochemical Society* **1998**, *145*, L70-L72.
23. Sun, X.; Angell, C. A., Doped Sulfone Electrolytes for High Voltage Li-Ion Cell Applications. *Electrochemistry Communications* **2009**, *11*, 1418-1421.
24. Abu-Lebdeh, Y.; Davidson, I., High-Voltage Electrolytes Based on Adiponitrile for Li-Ion Batteries. *Journal of The Electrochemical Society* **2009**, *156*, A60-A65.
25. Gmitter, A. J.; Plitz, I.; Amatucci, G. G., High Concentration Dinitrile, 3-Alkoxypropionitrile, and Linear Carbonate Electrolytes Enabled by Vinylene and Monofluoroethylene Carbonate Additives. *Journal of The Electrochemical Society* **2012**, *159*, A370-A379.
26. Xu, K., Nonaqueous Liquid Electrolytes for Lithium-Based Rechargeable Batteries. *Chemical reviews* **2004**, *104*, 4303-4418.
27. Xu, K., Electrolytes and Interphases in Li-Ion Batteries and Beyond. *Chemical reviews* **2014**, *114*, 11503-11618.
28. Zuo, X.; Fan, C.; Liu, J.; Xiao, X.; Wu, J.; Nan, J., Lithium Tetrafluoroborate as an Electrolyte Additive to Improve the High Voltage Performance of Lithium-Ion Battery. *Journal of The Electrochemical Society* **2013**, *160*, A1199-A1204.
29. Sinha, N. N.; Burns, J.; Dahn, J., Comparative Study of Tris (Trimethylsilyl) Phosphate and Tris (Trimethylsilyl) Phosphite as Electrolyte Additives for Li-Ion Cells. *Journal of The Electrochemical Society* **2014**, *161*, A1084-A1089.
30. Madec, L. n.; Xia, J.; Petibon, R. m.; Nelson, K. J.; Sun, J.-P.; Hill, I. G.; Dahn, J. R., Effect of Sulfate Electrolyte Additives on Lini<sub>1/3</sub>Mn<sub>1/3</sub>Co<sub>1/3</sub>O<sub>2</sub>/Graphite Pouch Cell Lifetime: Correlation between Xps Surface Studies and Electrochemical Test Results. *The Journal of Physical Chemistry C* **2014**, *118*, 29608-29622.
31. Ma, L.; Xia, J.; Dahn, J., Ternary Electrolyte Additive Mixtures for Li-Ion Cells That Promote Long Lifetime and Less Reactivity with Charged Electrodes at Elevated Temperatures. *Journal of The Electrochemical Society* **2015**, *162*, A1170-A1174.
32. Madec, L.; Petibon, R.; Tasaki, K.; Xia, J.; Sun, J.-P.; Hill, I.; Dahn, J., Mechanism of Action of Ethylene Sulfite and Vinylene Carbonate Electrolyte Additives in Lini<sub>1/3</sub>Mn<sub>1/3</sub>Co<sub>1/3</sub>O<sub>2</sub>/Graphite Pouch Cells: Electrochemical, Gc-Ms and Xps Analysis. *Physical Chemistry Chemical Physics* **2015**, *17*, 27062-27076.
33. Lee, Y.-M.; Nam, K.-M.; Hwang, E.-H.; Kwon, Y.-G.; Kang, D.-H.; Kim, S.-S.; Song, S.-W., Interfacial Origin of Performance Improvement and Fade for 4.6 V Lini<sub>0.5</sub>Co<sub>0.2</sub>Mn<sub>0.3</sub>O<sub>2</sub> Battery Cathodes. *The Journal of Physical Chemistry C* **2014**, *118*, 10631-10639.

34. Pires, J.; Castets, A.; Timperman, L.; Santos-Peña, J.; Dumont, E.; Levasseur, S.; Tessier, C.; Dedryvère, R.; Anouti, M., Tris (2, 2, 2-Trifluoroethyl) Phosphite as an Electrolyte Additive for High-Voltage Lithium-Ion Batteries Using Lithium-Rich Layered Oxide Cathode. *Journal of Power Sources* **2015**, *296*, 413-425.
35. Gao, Y.; Li, Q.; Li, H.-B.; Lia, W.; Chenga, J., Rsc Advances. *molecules*, *29*, 30.
36. Xu, M.; Zhou, L.; Dong, Y.; Chen, Y.; DEMEAUX, J.; MacIntosh, A. D.; Garsuch, A.; Lucht, B. L., Development of Novel Lithium Borate Additives for Designed Surface Modification of High Voltage Lini<sub>0.5</sub>mn<sub>1.5</sub>o<sub>4</sub> Cathodes. *Energy & Environmental Science* **2016**.
37. von Cresce, A.; Xu, K., Electrolyte Additive in Support of 5 V Li Ion Chemistry. *Journal of The Electrochemical Society* **2011**, *158*, A337-A342.
38. Xu, K.; Zhang, S.; Jow, R., Electrochemical Impedance Study of Graphite/Electrolyte Interface Formed in Libob/Pc Electrolyte. *Journal of power sources* **2005**, *143*, 197-202.
39. Zhang, S.; Ding, M. S.; Xu, K.; Allen, J.; Jow, T. R., Understanding Solid Electrolyte Interface Film Formation on Graphite Electrodes. *Electrochemical and Solid-State Letters* **2001**, *4*, A206-A208.
40. Lee, Y.-M.; Nam, K.-M.; Hwang, E.-H.; Kwon, Y.-G.; Kang, D.-H.; Kim, S.-S.; Song, S.-W., Interfacial Origin of Performance Improvement and Fade for 4.6 V Lini<sub>0.5</sub>Co<sub>0.2</sub>Mn<sub>0.3</sub>O<sub>2</sub> Battery Cathodes. *J. Phys. Chem. C* **2014**, *118*, 10631-10639.
41. Gong, Z.; Wang, E. G.; Xu, G. C.; Chen, Y., Influence of Deposition Condition and Hydrogen on Amorphous-to-Polycrystalline Sicn Films. *Thin Solid Films* **1999**, *348*, 114-121.
42. Pires, J.; Castets, A.; Timperman, L.; Santos-Peña, J.; Dumont, E.; Levasseur, S.; Tessier, C.; Dedryvère, R.; Anouti, M., Tris(2,2,2-Trifluoroethyl)Phosphite as an Electrolyte Additive for High-Voltage Lithium-Ion Batteries Using Lithium-Rich Layered Oxide Cathode. *J. Power Sources* **2015**, *296*, 413-425.
43. He, M.; Su, C.-C.; Peebles, C.; Feng, Z.; Connell, J. G.; Liao, C.; Wang, Y.; Shkrob, I. A.; Zhang, Z., Mechanistic Insight in the Function of Phosphite Additives for Protection of Lini<sub>0.5</sub>Co<sub>0.2</sub>Mn<sub>0.3</sub>O<sub>2</sub> Cathode in High Voltage Li-Ion Cells. *ACS applied materials & interfaces* **2016**, *8*, 11450-11458.
44. Mohanty, D.; Dahlberg, K.; King, D. M.; David, L. A.; Sefat, A. S.; Wood, D. L.; Daniel, C.; Dhar, S.; Mahajan, V.; Lee, M., Modification of Ni-Rich Fcg Nmc and Nca Cathodes by Atomic Layer Deposition: Preventing Surface Phase Transitions for High-Voltage Lithium-Ion Batteries. *Scientific reports* **2016**, *6*.

## Chapter 7 Research Conclusions and Future Work

In this thesis project, the goal of this research was to study new electrolytes for next generation Li ion batteries, with emphasis on its performance at high voltage and elevated temperatures. This has been accomplished using a combination of electrochemical and material analysis techniques. Furthermore, following conclusions are drawn corresponding to the research objectives presented in Chapter 1.

**First of all, a screening method for oxidation stability of the synthesized F-solvents has been developed.** Electrochemical floating tests have been used as an evaluation tool for voltage stability of electrolyte solvents. Of the cyclic carbonates screened, FEC is the most stable solvent, followed by TFPC, EC and TFP-PC-E. The differences of voltage stability are much more pronounced at elevated temperature than at RT. In the case of diluent solvents such as linear carbonates and ethers, only F-EMC, EMC and DMC showed stable current upon overcharge at high temperature, all the other solvents tested gave different degree of instability when exposed to high voltage and high temperature simultaneously. Among the three tested DMC gave the smallest residue current. Mixtures of FEC and DMC by various ratios have demonstrated that cyclic carbonates are the more stable component in the formulations although the beneficial effect is insignificant after concentration of cyclic carbonate is increased over 50%. Test of various salt concentrations did not result in great variation of the electrolyte stability which implies that the effect of salt on electrolyte voltage stability is minimal. Finally, an electrolyte formulated based on the screening results of the electrochemical floating tests have showed

slightly improved performance over our previously reported best formulations of fluorinated electrolyte.

**Secondly, different fluorinated cyclic carbonates were studied systematically by different electrochemical method.** Fluorinated cyclic carbonates with different substituents including fluoroethylene carbonate (FEC), difluoroethylene carbonate (DFEC), trifluoropropylene carbonate (TFPC), 4-((2,2,3,3-tetrafluoropropoxy)methyl)-1,3-dioxolan-2-one (HFEEC) and 4-(2,2,3,3,4,4,5,5,5-nonafluoropentyl)-1,3-dioxolan-2-one (NFPEC) was designed, synthesized and evaluated. Combining the electrochemical results and bulk material post analysis results, the electrolyte with DFEC as the SEI former shows the best performance. When introduce the DFEC based electrolyte in to the HEHV system, it will not only shows a stable interphase due to its high anodic stability, but also can prevent the cathode from loss active Li.

**Thirdly, by using different post analysis techniques, we also gained a fundamental understanding of the interaction between electrolyte and electrode materials.**i) The transition metal dissolution is not detected by EDS and XPS on the fluorinated electrolyte cycled graphite anode, suggesting the enhanced voltage stability on the cathode side and the robust SEI formation on the graphite anode. ii) XAS experiment confirm the Ni and also Co could be charged to higher oxidation state ( $\text{Ni}^{3+}/\text{Ni}^{4+}$ ) with fluorinated electrolyte due to its enhanced oxidation stability. iii) fluorinated electrolyte was proved to assist the preservation of the crystal structure of NCM523 cathode by SXRD results. The lattice structure of NCM523 is almost intact while significant shrinkage in its unit cell for Gen 2 electrolyte cycled cathode. All results converge to the conclusion that fluorinated electrolyte is intrinsic ally stable towards oxidation and is suitable high voltage electrolyte for high voltage high energy density lithium ion cell.

**Fourthly, additives with different substitutional group were systematically studied. Moreover, by taking together the advantages of different additives we tested, a new additive, 2-(2,2,2-trifluoroethoxy)-1,3,2-dioxaphospholane 2-oxide (TFEOP), was designed, synthesized and introduced in to the HEHV system.** Other than change the carbonated based conventional electrolyte into the fluorinated carbonate system, adding the additive to passivate the electrode surface is one of the most efficient way to stabilize the electrode interphase. In the additive study, the function that have been found from our selected and synthesized additives include :(i) it cooperates to SEI formation and stabilizes SEI, (ii) it reduces dissolution of the cathode materials, (iii) it provides excellent kinetic barrier on the cathode .

Taken together in this project, we formulated, designed and synthesized different fluorinated based solvent and additive for the HEHV battery system. New electrolytes have been evaluated by comparison with the conventional EC-based Gen 2 electrolytes. The new electrolytes showed much better cycle performance at both room temperature and 55 °C. In post-test analysis, it indicates that the new electrolytes can realize a stable interface and maintain the cathode structure. The extraordinary electrochemical stability of our new electrolytes makes it a suitable candidate for next generation high energy high voltage Li ion batteries system.

In the future, both coin cell and pouch cell will be fabricated to test the electrochemical performance of the new electrolyte.

Moreover, more In-Situ techniques could be involved in to the fundamental study. i). In-situ X-ray absorption spectroscopy will be carried out to examine the change of the electronic transitions and local structure at the Mn, Co and Ni K-edge for the NCM523 electrode during charging and discharging process in different electrolyte system. ii). In-situ X-ray diffraction

could be involved to test the thermostability of the electrode in different electrolyte system and account the losing of Li ion during high voltage charging and discharging. iii) In-situ impedance testing also could be involved to investigate the surface change under different state of charge (SOC) and state of discharge (SOD).

## Appendices

### Select Publications

#### ❖ Published

1. *Caramel Popcorn Shaped Silicon Particle with Carbon Coating as a High Performance Anode Material for Li-Ion Batteries*, **He, M.**, Sa, Q., Liu, G., & Wang, Y, ACS applied materials & interfaces **5**, no. 21 (2013): 11152-11158.
2. *Pure Inorganic Separator for Lithium Ion Batteries*, **He, M.**, Zhang, X., Jiang, K., Wang, J., & Wang, Y, ACS applied materials & interfaces **7**, no. 1 (2014): 738-742.
3. *Fluorinated Electrolytes for 5-V Li-Ion Chemistry: Probing Voltage Stability of Electrolytes with Electrochemical Floating Test*, **He, M.**, Hu, L., Xue, Z., Su, C. C., Redfern, P., Curtiss, L. A., & Zhang, Z. Journal of The Electrochemical Society **162**, no. 9 (2015): A1725-A1729.
4. *Mechanistic Insight in the Function of Phosphite Additives for Protection of LiNi<sub>0.5</sub>Co<sub>0.2</sub>Mn<sub>0.3</sub>O<sub>2</sub> Cathode in High Voltage Li-ion Cells*, **He, M.**, Su, C.C., Peebles, C., Feng, Z., Connell, J., Wang, Y., Zhang, Z. ACS applied materials & interfaces **8**.no. 18 (2016): 11450-11458.
5. *Synthesis of high performance LiNi<sub>1/3</sub> Mn<sub>1/3</sub>Co<sub>1/3</sub>O<sub>2</sub> from lithium ion battery recovery stream*, Sa, Q., Gratz, E., **He, M.**, Lu, W., Apelian, D., & Wang, Y, Journal of Power Sources **282** (2015): 140-145.
6. *Advanced electrolyte/additive for lithium-ion batteries with silicon anode*. Zhang, S., **He, M.**, Su, C. C., & Zhang, Z. Current Opinion in Chemical Engineering, **13**, (2016). 24-35.
7. *Direct observation of reversible magnesium ion intercalation into a spinel oxide host*. Kim, C., Phillips, P.J., Key, B., Yi, T., Nordlund, D., Yu, Y.S., Bayliss, R.D., Han, S.D., **He, M.**, Zhang, Z. and Burrell, A.K., 2015. Advanced Materials, **27(22)**, pp.3377-3384.
8. *The Role of MgCl<sub>2</sub> as a Lewis Base in ROMgCl–MgCl<sub>2</sub> Electrolytes for Magnesium-Ion Batteries*. Pan B, Huang J, **He M**, Brombosz SM, Vaughey JT, Zhang L, Burrell AK, Zhang Z, Liao C.. ChemSusChem (2016).
9. *Alkyl Substitution Effect on Oxidation Stability of Sulfone Based Electrolytes*. Su CC, **He M**, Redfern P, Curtiss LA, Liao C, Zhang L, Burrell AK, Zhang Z. ChemElectroChem. 2016 Jan 1.

❖ **To be submitted**

1. *Mechanism Study of Fluorinated Electrolyte for High Voltage  $\text{LiNi}_{0.5}\text{Co}_{0.2}\text{Mn}_{0.3}\text{O}_2$  Cathode of Lithium ion Batteries*, **He, M.**, Su, C.C., Peebles, C., Feng, Z., Connell, J., Wang, Y., Zhang, Z. To be submitted
2. *Comparative Study of Fluorinated Cyclic Carbonate as Electrolyte Cosolvent for High Voltage Lithium ion Batteries*, **He, M.**, Su, C.C., Peebles, C., Feng, Z., Connell, J., Wang, Y., Zhang, Z. To be submitted
3. *Synthesis and Characterization of Novel Sulfone Electrolytes for High Voltage Li-ion Battery*", Su, C.; **He, M.**; Peebles, C.; Wang, Y.; Zhang, Z. To be submitted
4. *Design and Synthesis of Novel Phosphates Additives for High Voltage Lithium-ion Battery*" ", Su, C.; **He, M.**; Peebles, C.; Wang, Y.; Zhang, Z. To be submitted
5. *Synthesis and Characterization of Novel Fluorinated Ether Electrolytes for Lithium Sulfur Battery*", ", Su, C.; **He, M.**; Peebles, C.; Wang, Y.; Zhang, Z. *Manuscript in preparation.*
6. *Synthesis and Characterization of Novel Sulfone Electrolytes for High Voltage Li-ion Battery*", Su, C.; **He, M.**; Peebles, C.; Wang, Y.; Zhang, Z. To be submitted
7. *Design and Synthesis of Novel Phosphates Additives for High Voltage Lithium-ion Battery*" ", Su, C.; **He, M.**; Peebles, C.; Wang, Y.; Zhang, Z. To be submitted
8. *Synthesis and Characterization of Novel Fluorinated Ether Electrolytes for Lithium Sulfur Battery*", ", Su, C.; **He, M.**; Peebles, C.; Wang, Y.; Zhang, Z. *Manuscript in preparation.*

